POLITECNICO DI MILANO
DEPARTMENT of ENERGY
DOCTORAL PROGRAMME IN ENERGY AND NUCLEAR SCIENCE AND TECHNOLOGY

FLASHING FLOW MODEL FOR INDUSTRIAL ENERGY APPLICATIONS

Doctoral Dissertation of:
Quang Dang Le

Supervisor:
Prof. Fabio Inzoli
Prof. Vincenzo Dossena

Chair of the Doctoral Program:
Prof. Carlo Enrico Bottani

June 2017

DEDICATION

To my family

Acknowledgements

I would like to thank Politecnico di Milano which has been the place that gave me a chance to work on this interesting project. Especially, I am extremely grateful as well to Parcol company which sponsors the whole project.

I am deeply indebted to my supervisors who have always supported and helped me with their technical and personal advices: Prof. Fabio Inzoli, Prof. Vincenzo Dossena and Dr. Riccardo Mereu. Besides, I would like to thank to Prof. Luigi Pietro Maria Colombo who teaches me course "Heat and Mass Transfer" which becomes my background on this PhD thesis.

Finally, most of all I want to thank, with a few words in both in Vietnamese and in English, to my family

In Vietnamese:

"Con cám ơn ba má đã luôn ủng hộ con để hoàn thành luận án Tiến Sĩ này"

In English:

"Many thanks to my father and my mother for always supporting me to accomplish this PhD thesis"

CONTENTS

LIST OF FIGURES

LIST OF TABLES

1. INTRODUCTION

Flashing flow phenomenon in control valves plays a significant role in numerous industrial fields and applications, such as oil and gas industry, nuclear power plants and chemical plants. The control of flashing flow inside the valves is fundamental for granting safety and efficiency of the whole system.

However, the understanding of this phenomenon is still limited and the modern measurement techniques cannot capture all the local flow characteristics inside the device, such as nucleation, bubble departure and bubble growth processes.

Furthermore, the main tools used for designing the control valves in industrial field are sizing equations, which help engineers and experts to predict the flow coefficient of the device. At this time, sizing equations for control valves in case of two phase flashing flow, developed and applied by companies, are only based on semi-empirical method. These semi-empirical correlations have a limitation when using to design new products.

As a result, a reliable numerical CFD (Computational Fluid Dynamics) model can help to increase the knowledge about flashing flow phenomenon that supports for design and application of devices. Besides, reliable numerical data could be used, indeed, to develop and validate more accurate sizing equations in case of flashing flow inside control valves.

In order to face and overcome these limits, the goal of this thesis is to provide a reliable CFD modeling approach which is able to better predict and describe the flashing flow phenomenon. Then, development of a sizing equation for two-phase control valve, based on numerical results, will be performed.

The first part of the study is focused on the development and validation of the CFD modeling approach with mixture phase change model in ANSYS-FLUENT 16.0.

The modeling approach is first validated with a benchmark case study without phase change (air-water flow) and then with a complete benchmark including the flashing flow. The main validation of the flashing flow is performed by using available experimental data of both global and local quantities for a circular convergent-divergent nozzle.

In the second part, the information and data provided by CFD model are used to develop a new sizing equation for control valves with the presence of the flashing flow. Results of both literature and new sizing equation are validated to confirm their applicability and accuracy.

The thesis is structured in order to initially provide a description of control valves and the traditional sizing tools used in industrial applications (Chapter 2).

Chapter 3 presents physical phenomenon of evaporation and flashing boiling including explanation of non-equilibrium effect as boiling delay.

Chapter 4 is devoted for the state of the art with scientific background of experimental method for flashing flow, valve sizing equation of two-phase and CFD model of flashing flow.

Chapter 5 presents the theoretical background of physical phenomena under investigation in this thesis, such as fluid dynamics, turbulence modelling, two-phase flow and phase change process.

Chapter 6 yields the CFD model used in this work and validation.

Chapter 7 presents proposed sizing equation and validation.

Finally, chapter 8 presents the conclusion and future work to be done in the future for better accuracy of both proposed CFD model and sizing equation.

2. CONTROL VALVE DESIGN

In this chapter, control valve, components and terminologies are described. Moreover, traditional sizing equations for single phase and how to use these equations in industrial applications are presented.

2.1. Definition and terminology

Control valve is a device used to change the fluid flow rate in a process of control system. An actuator will be connected to control valve to move closure component corresponding to a controlling system signal.

In this section, some terminologies referring to functions and group of valve components in field of control valve are presented in **Table 2-1** and **Table 2-2**. Following parts are the most representative of the valve, as shown in **Figure 2.1**.

Valve body: The valve body is an envelope to retain pressure with closure member inside throttling the fluid flow.

Bonnet: Referring to the top closure of the valve body side extended from the valve stem.

Plug: Plug is the most important part inside valves including two main tasks: (i) to throttle mass flow rate inside valves (ii) assuring shut off of flow inside valves.

Seat: Seat is combined to plug for throttling and shut off flow inside valve.

Table 2-1: Component terminology

Valve trim	The valve body internal parts in contact to the controlled fluid are assembled together. For examples: closure member, seat ring, cage, valve plug stem, etc. are valve trim parts. The valve body, bonnet, bottom flange and gasket are not valve trim parts
Seat	The sealing surfaces of a seat ring of valve body in contact to the closure member at closed position of control valve
Seat ring	A fitted part in the valve body providing a removable seat in the port of the valve body.
Closure member	A movable part of a valve controlled by actuator to tune fluid flow rate. For examples: disc in butterfly valves and plug for other types of valves
Valve stem (shaft)	An extending rod through the bonnet assembly which moves corresponding to the motion of the actuator stem to position closure member

Table 2-2: *Functional terminology*

Closed position	A specific position presenting the closure member and the valve seat is in a continuous contact line (or surface)
Flow coefficient	A coefficient representing the flow capacity of a control valve.
Critical differential pressure ratio $(\Delta P/P_1)_{cr}$	The ratio of pressure drop between upstream and downstream to upstream pressure showing limit of sonic compressible fluid flow
Choked flow	For fixed upstream conditions, the mass flow rate cannot continue to increase when outlet pressure continue to decrease.

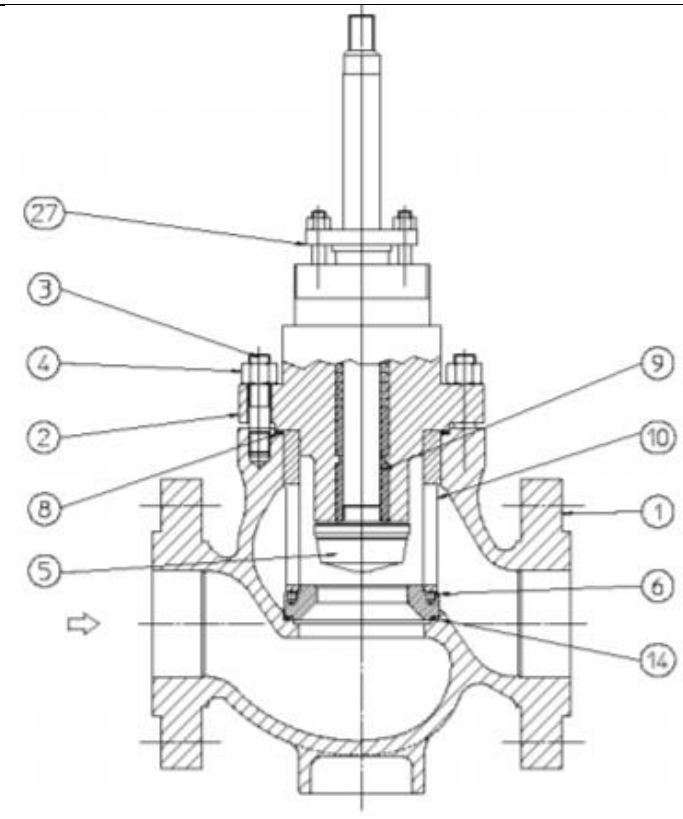

1	BODY
2	BONNET
3	BODY STUD
4	NUT
5	PLUG and STEM
6	SEAT
8-14	GASKET
9	GUIDE
10	CAGE
27	PACKING

Figure 2.1: *control valve and components*

2.2. Flow coefficients

In this section, the most important parameters for the characterization and design of a control valve are described. The definition of IEC standard [1] for the flow coefficients states:

"A coefficient used to calculate the flow rate of a control valve under given conditions. Flow coefficients normally are: A_V, K_V and C_V, depending on used units".

Practically, K_V and C_V are commonly used in industry while A_V is derived with analytical model from theory.

Typical, conversion coefficients are shown in Eq. 2-1.

$$\frac{A_V}{K_V} = 2.78 \cdot 10^{-5} \quad \frac{A_V}{C_V} = 2.40 \cdot 10^{-5} \quad \frac{K_V}{C_V} = 8.65 \cdot 10^{-1} \qquad 2\text{-}1$$

Algebraic equations to predict flow coefficient of control valves are named "sizing equations".

The geometrical characteristics and operating conditions for defining the flow coefficients through standard tests are as follow:

1. There are no cavitation and vaporization phenomena inside devices.
2. Diameter of valve and pipe at connection region is equal.
3. Pressure taps are positioned as in **Figure 2.2** to measure pressure difference between upstream and downstream.
4. Length of upstream and downstream pipes must be performed as in **Figure 2.2**.

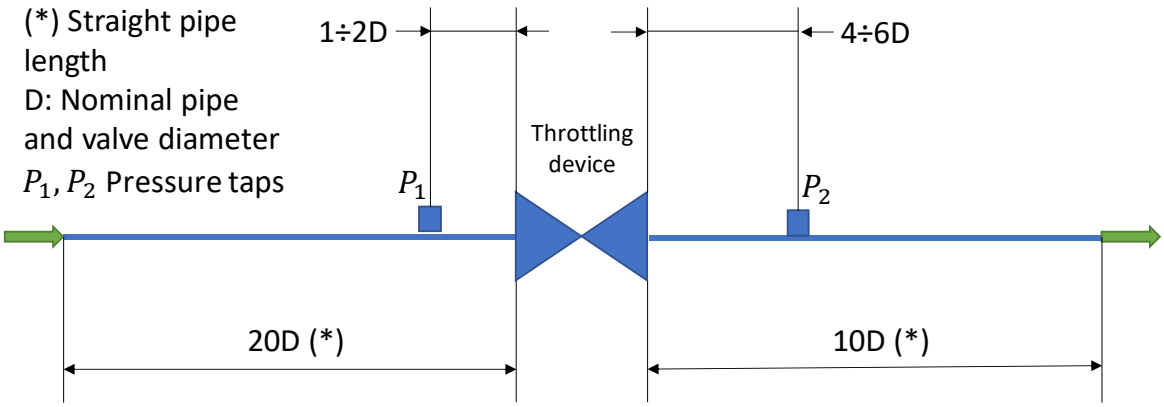

Figure 2.2: *Set-up of standard test in IEC standard* [1]

All the flow coefficients are defined and valid at standard test conditions presented here.

2.2.1. Flow coefficient A_V

The flow coefficient A_V is derived from the Bernoulli equation and it is defined as:

$$A_V \propto \dot{V}\sqrt{\frac{\rho}{\Delta P}} \quad 2\text{-}2$$

where $\dot{V}$ is volume flow rate, ρ is fluid density and ΔP is static pressure drop between upstream and downstream of valves.

2.2.2. Flow coefficient K_V

Approximation of K_V is presented by Eq. 2-3 and coefficients can be inserted into expression by experimental tests

$$K_V[m^3/h] \propto \dot{V} \cdot \sqrt{\frac{\Delta P(kv)}{\Delta P} \cdot \frac{\rho}{\rho_0}} \quad 2\text{-}3$$

where $\dot{V}$ is volumetric flow rate in $[m^3/h]$. $\Delta P(kv)$ is reference pressure drop. ΔP in [bar] is static pressure drop from upstream to downstream. ρ is fluid density [kg/m^3] and ρ_0 is reference state of water

Following IEC standard [1], The tests are conducted with range of temperature from 5^{o}C to 40^{o}C, $\Delta P(kv) = 1$ [bar] and reference state of water, ρ_0, is at 15^{o}C.

2.2.3. Flow coefficient C_V

Approximation of C_V is presented by Eq. 2-4

$$C_V[gpm] \propto \dot{V} \cdot \sqrt{\frac{\Delta P(cv)}{\Delta P} \cdot \frac{\rho}{\rho_0}} \quad 2\text{-}4$$

where $\dot{V}$ is volumetric flow rate in $[gpm]$. $\Delta P(cv)$ is reference pressure drop. ΔP is static pressure drop from upstream to downstream used in [psi]. ρ is fluid density [kg/m^3] and ρ_0 is reference state of water.

Following IEC standard [1], The tests are conducted with range of temperature from 5^{o}C to 40^{o}C, $\Delta P(cv) = 1$ psi (6895 Pa)) and reference state of water, ρ_0, is at 15^{o}C in [kg/m^3].

It should be noticed that using C_V or K_V is free because user can convert from C_V to K_V and reverse.

Following sizing equations in this thesis for single phase and two-phase flows will be presented in C_V.

2.3. Sizing equations of single-phase flow applied to control valves

In this section, sizing equations for fully developed turbulent flow $(\mathrm{Re} > 30000)$ are presented According to standards in IEC standard [1], [2]. The accuracy between theoretical and experimental flow coefficient data is in the range of $\pm 5\%$. Operating fluids are both incompressible and compressible.

2.3.1. Sizing equations for incompressible fluids

In **Figure 2.3**, incompressible mass flow rate, $\dot{M}$, versus the square root of pressure difference, $\sqrt{\Delta P}$, under fixing upstream conditions is presented.

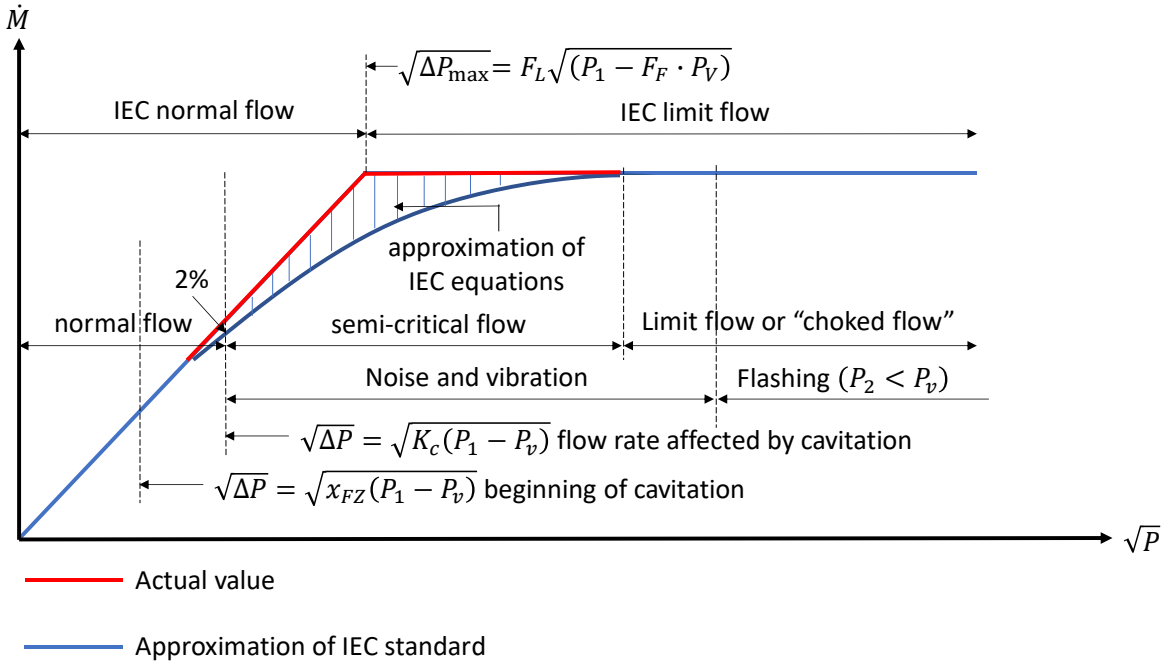

Figure 2.3: *Flow rate diagram of valve in case of incompressible fluid versus downstream pressure under constant upstream conditions, approximated following formulas and information in IEC standard [1], [2]*

There are three main regions in **Figure 2.3**.

1. **Normal flow region**: $\dot{M}$ is proportional to $\sqrt{\Delta P}$.
2. **Semi-critical flow region**: the increase of $\sqrt{\Delta P}$ still leads the increase of mass flow rate, $\dot{M}$; however, coefficient of proportionality is different from normal flow region due to effects of cavitation.
3. **Limit flow or saturation region**: the mass flow rate $\dot{M}$ becomes flat despite pressure difference, $\sqrt{\Delta P}$, continues to increase. In this region, flow operating conditions at vena contracta reaches to the maximum evaporation rate with Mach number equal to 1. Evaluation of maximum evaporation rate is based on upstream conditions of flow.

In IEC standard [1] for sizing equations, hatched area of the diagram in **Figure 2.3**, corresponding to semi-critical flow region (cavitation), is ignored. To predict cavitation phenomenon inside valve, a correction factor of C_V is imposed including onset cavitation coefficient x_{FZ} and critical cavitation coefficient K_c. Details of x_{FZ} and K_c, including (i) range of application and (ii) approximation equation, are presented in appendix A.

Sizing equations for incompressible fluids, according to IEC standard, [1], are presented as follow:

Normal flow (turbulent and non-vaporizing)

If $\Delta P < \Delta P_{max} = (F_L)^2 \cdot (P_1 - F_F \cdot P_V)$

$$\mathrm{C_V} = \frac{\dot{M}}{865 \cdot \sqrt{\Delta P \cdot \rho_r}} \quad \text{2-5}$$

$$\mathrm{C_V} = \frac{1.16 \cdot \dot{V}}{\sqrt{\frac{\Delta P}{\rho_r}}} \quad \text{2-6}$$

where $\rho_r = \rho/\rho_0$ with $\rho_0 = 999.2\ [\mathrm{kg/m^3}]$ and $\rho[\mathrm{kg/m^3}]$ is density of operating fluid, $\dot{M}[kg/h]$, $\dot{V}[\mathrm{m^3/h}]$. ΔP is pressure drop, $P_1[\mathrm{bar}]$ is static pressure at inlet. $P_V[\mathrm{bar}]$ is vaporization pressure of liquid on inlet condition. F_F and F_L are liquid critical pressure ratio factor and recovery factor, details in Appendix A. Subscripts 1, 2 are used here is for upstream and downstream. $\mathrm{C_V}$ is used in [gpm].

Limit flow

If $\Delta P \geq \Delta P_{max} = (F_L)^2 \cdot (P_1 - F_F \cdot P_V)$

$$\mathrm{C_V} = \frac{\dot{M}_{(max)}}{865 \cdot F_L \cdot \sqrt{(P_1 - F_F \cdot P_V) \cdot \rho_r}} \quad \text{2-7}$$

$$\mathrm{C_V} = \frac{1.16 \cdot \dot{V}_{(max)}}{F_L \cdot \sqrt{\frac{(P_1 - F_F \cdot P_V)}{\rho_r}}} \quad \text{2-8}$$

2.3.2. Sizing equations for compressible fluids

In case of compressible fluids, the mass flow rate, $\dot{M}$, and the square root of pressure difference, $\sqrt{\Delta P}$, are no longer proportional because of variation of fluid density inside device. From upstream to vena contracta, fluid density decreases and the flow is accelerated (expansion process).

As a result, expansion coefficient Y should be considered for expansion of compressible fluid in convergent part. From that idea, Sizing equations for compressible fluids, according to IEC standard [1], are presented as follow:

Normal flow

If $x < F_\gamma \cdot x_T$ or $2/3 < Y \leq 1$

$$\mathrm{C_V} = \frac{\dot{M}}{27.3 \cdot Y \cdot \sqrt{x \cdot p_1 \cdot \rho_r}} \quad \text{2-9}$$

$$\mathrm{C_V} = \frac{\dot{V}}{2120 \cdot p_1 \cdot Y} \cdot \sqrt{\frac{M \cdot T_1 \cdot Z}{x}} \quad 2\text{-}10$$

$$Y = 1 - \frac{x}{3 \cdot F_\gamma \cdot x_T} \quad 2\text{-}11$$

where $\mathrm{C_V}[\mathrm{gpm}]$, $\rho_1[kg/m^3]$, $\dot{M}[kg/h]$, $\dot{V}[m^3/h]$ and $P_1[bar]$. $x = \Delta P/P_1$ is pressure differential ratio factor and $x_T \cong 0.85 \cdot F_L^2$ is pressure differential ratio factor in choked condition. $F_\gamma = \gamma/1.4$ is specific heat ratio factor and $\gamma = c_p/c_v$ is specific heat ratio of operating fluid. M, T_1 and Z are Molar mass, inlet temperature and compressibility factor, respectively.

Definition of Y is presented in detail in Appendix A.

Limit flow

If $x \geq F_\gamma \cdot x_T$ or $Y = 2/3 = 0.667$

$$\mathrm{C_V} = \frac{\dot{M}_{(max)}}{18.2 \cdot \sqrt{F_\gamma \cdot x_T \cdot P_1 \cdot \rho_r}} \quad 2\text{-}12$$

$$\mathrm{C_V} = \frac{\dot{V}_{(max)}}{1414 \cdot P_1} \cdot \sqrt{\frac{M \cdot T_1 \cdot Z}{F_\gamma \cdot x_T}} \quad 2\text{-}13$$

2.4. Sizing equations of two-phase flow applied to control valves

There are some sizing equations in literature used in case of two-phase sizing with and without phase change. This section will be devoted to briefly present these equations.

SUM model This is a simple method considering assumptions of separated two-phase flow with different velocities at vena contracta in throttling devices and without exchange of energy between the two phases. SUM model is suggested in Driskell [3] and Parcol [4].

SUM method gives:

$$\mathrm{C_V} = \mathrm{C_{V_G}} + \mathrm{C_{V_L}} \quad 2\text{-}14$$

Extension of Eq. 2-14 considering subcritical condition leads to:

$$\mathrm{C_V} = \frac{\dot{M}_G\sqrt{V_{eG}} + \dot{M}_L\sqrt{V_{L1}}}{27.3 \cdot \sqrt{\Delta P}} \quad 2\text{-}15$$

$$V_{eG} = V_{G1}/Y^2 \quad (V_{G1} = 1/\rho_1) \quad 2\text{-}16$$

In Eq. 2-15, $\dot{M}[\mathrm{kg/h}]$ is mass flow rate, ΔP is pressure drop in bar. $V_{L1}[\mathrm{m^3/kg}]$ is specific volume of liquid at inlet. $V_{eG}[\mathrm{m^3/kg}]$ is specific volume of gas phase after expansion between upstream and vena contracta. Y is expansion factor of gas phase with details in appendix A. Subscripts G and L here refer to gas and liquid, respectively.

EQUIVALENCE model This method assumes two-phase passing vena contracta at the same velocity and mixing ideally Driskell [3].

Firstly, equivalent specific volume, V_e, is introduced by Eq. 2-17

$$V_e = \dot{x}_{G1} \cdot \frac{V_{G1}}{Y^2} + (1 - \dot{x}_{G1}) \cdot V_{L1} \qquad 2\text{-}17$$

where $\dot{x}_{G1}$ is gas mass fraction at inlet. V_{G1} and V_{L1} are specific volume of gas and liquid evaluated at inlet, respectively.

The sizing equation in conditions of subcritical two-phase flow gives:

$$\mathrm{C_V} = \frac{\dot{M}\sqrt{V_e}}{27.3 \cdot \sqrt{\Delta P}} \qquad 2\text{-}18$$

In general, EQUIVALENCE and SUM method do not have a clear validation for range of applicability. In some documents, EQUIVALENCE method is stated more suitable when gas mass fraction $\dot{x}_G > 0.2 \div 0.3$ while SUM method can be used with liquid mass fraction is close to one.

Above equations suggested for subcritical condition and there is no a clear indication for using in the limit flow condition. As a result, inaccuracies of sizing equations will increase close to the limit flow condition.

HNE-DS model This model is developed by Diener and Schmidt for throttling devices as control valves, orifices and nozzles Diener and Schmidt [5], is suggested in ISO 4126 part 10 [6] for safety valve.. HNE-DS modifies OMEGA model of Leung [7] with correction factors for thermodynamic non-equilibrium effect and relative motions between two phases.

Expression for calculation gives

Flow coefficient $\mathrm{C_V}$	For $\Delta P < \Delta P_{max}$
	$\mathrm{C_V} = 1.16 \sqrt{\frac{\Delta P_0}{\Delta P}} \frac{1}{\sqrt{\rho_0 \rho_1}} \dot{M} \frac{1}{Y_{DS}}$
	For $\Delta P \geq \Delta P_{max}$
	$\mathrm{C_V} = 1.16 \sqrt{\frac{\Delta P_0}{\Delta P_{max}}} \frac{1}{\sqrt{\rho_0 \rho_1}} \dot{M} \frac{1}{Y_{DS}}$

where ΔP_0 and ρ_0 are reference pressure drop and reference density, respectively. ΔP_{max} is critical pressure drop accounted for choked flow. Y_{DS} is expansion factor of two-phase flow. Details of all parameters are given in Diener and Schmidt [5].

2.5. Practical application of sizing equations

Each control valve in industry has C_V's values corresponding to different valve openings and these values are provided by producer. For example, VeGA 1-6948 Control Valve from Parcol company (http://www.parcol.com) is shown in **Figure 2.4** with values of C_V, F_L and x_T corresponding to Characteristics of valve (inner diameter, port, seat, travel). A control valve is typically sized by the expected operating conditions. Engineers from this information will predict C_V's values and suggest suitable control valves. Chosen valve should satisfy the minimum size corresponding to the expected operating conditions to compete about cost with the other valve companies.

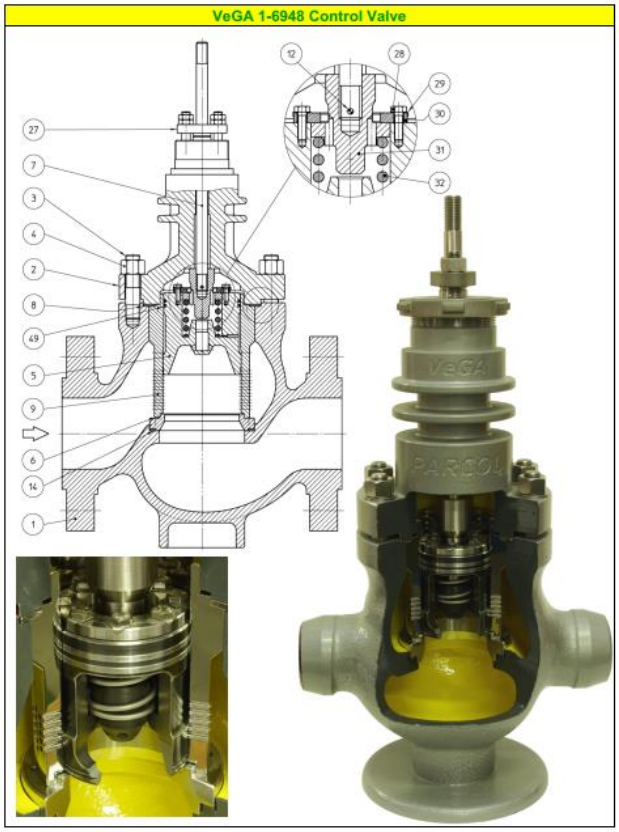

Flow coefficient $C_V[gpm]$

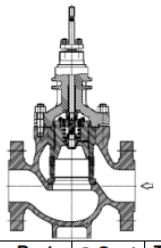

VeGA valve 1-6948 Type - Cv F_L x_T

PXLN-E Trim type: Plug with Pilot - Special Low Noise
Flow characteristic: EQUAL PERCENTAGE

DN [in]	Port [in]	Φ Seat [mm]	Travel [mm]	TRAVEL % 5% *	10% *	20%	30%	40%	50%	60%	70%	80%	90%	100%
Pressure recovery factor F_L				0.94	0.94	0.94	0.94	0.94	0.94	0.93	0.93	0.93	0.93	0.93
Press. diff. ratio factor x_T				0.78	0.78	0.78	0.78	0.77	0.77	0.76	0.76	0.75	0.75	0.74
2	2	65.5	34	0	0	1.21	2.26	4.4	8.44	13.4	18.7	25	31.6	**38.4**
3	3	83.5	45	0	0	1.57	3.87	9.36	17.6	26.7	36.8	48.7	61	**73**
4	4	105.5	60	0	2.72	3.06	9.18	18.3	29.9	43.9	61.2	80.3	99.3	**118**
6	6	127.5	60	0	0	3.46	10.5	20.5	35.6	55.1	78.4	102	125	**149**
8	8	162.5	76	0	5.75	7.33	17.7	36.4	59.3	89	125	159	195	**232**
10	10	216.5	100	0	9.45	13	30.7	63.3	112	173	239	309	376	**442**
12	12	244.5	120	0	12.4	21.1	51.9	99	166	249	341	435	530	**624**
14	14	294.5	150	0	16.5	23.8	70.3	141	240	369	510	655	796	**937**
16	16	344.5	200	0	21.7	42	116	226	378	573	792	1020	1240	**1420**
20	20	443.5	250	36.2	36.4	101	228	413	652	966	1310	1650	2000	**2310**
24	24	524.5	300	55.2	55.3	137	326	583	933	1390	1880	2390	2890	**3340**

*When Cv value is not indicated pilot plug is open and main plug is still closed.

Figure 2.4: *VeGA valve 1-6948 valve and its coefficients*

3. FLASHING PHENOMENON

Flashing phenomenon is a vaporization process driven by pressure. This process is usually encountered in throttling devices when liquid spends a rapid depressurization and reaches to saturation stage, **Figure 3.1**, for phase change. Besides, many experimental studies confirm that the flashing flow inside throttling devices possesses non-equilibrium effects which cannot be comprehended yet. For this reason, this chapter will be presented as an open discussion to explain flashing phenomenon considering previous works in literature including theoretical researches Saha [8], Wallis [9], Richter [10], Pinhasi [11] and Xi [12] and experimental researches Reocreux [13], Schrock [14], Abuaf et al. [15] and Araneo and Donde [16].

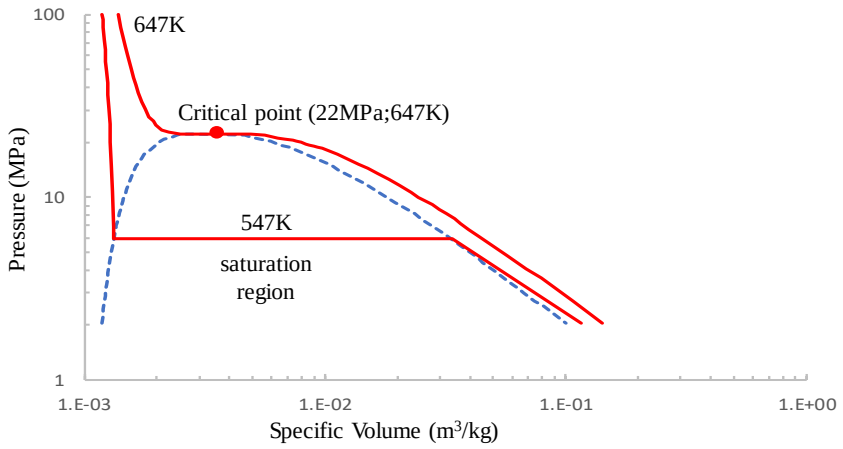

Figure 3.1: *Saturation stage of water, reference in Moran et al. [17]*

Generally, flashing phenomenon is separated into 3 stages as reported in **Figure 3.2**.

Stage 1: the small nuclei existing in non-wettable cavities of wall and in bulk flow start growing after pressure drops below saturation stage. However, bubble growth at this stage is restricted by the surface tension force (this is reason for this stage called delay period in Miyatake et al. [18] or idle in Oza and Sinnamon [19]). This boiling delay effect, accounted for thermal non-equilibrium, has an influence on global terms of flow as mass flow rate and outlet vapor fraction. Mechanisms of nucleation include (i) heterogeneous nucleation Blander and Katz [20], Page and Sear [21], Li and Peterson [22] and Jo et al. [23] and (ii) homogeneous Lau et al. [24]. Heterogeneous mode describes existence of vapor in non-wettable cavities of rough wall or dissolved impurities in superheated liquid leads to heterogeneous mode. On the other hand, homogenous mode plays a significant role when nuclei in surface and impurities does not exist.

Stage 2: This stage is the pressure-driven bubble growth stage starting when the diameter of bubble exceeds a critical value. Bubble growth rate at this stage is dominated by pressure difference between bubble surface and adjacent water and can be approximated by generalized Rayleigh-Plesset equation, Eq *5-49*, in Barbone [25], Brennen [26] and Rayleigh [27], which becomes assumption in many cavitation models if constant pressure difference is accepted.

Stage 3: the bubble growth at this stage is dominated by heat transfer around bubble surface. In this stage, a major influence to heat transfer mechanism at water-bubble interface comes from turbulence fluctuations and relative motion between bubbles and around liquid Sher et al. [28].

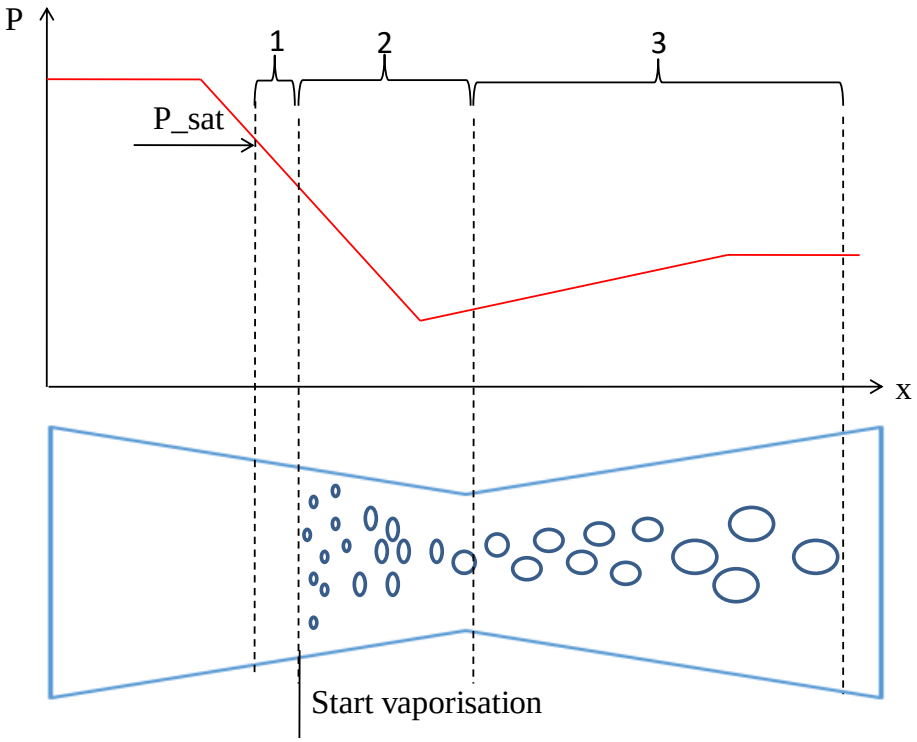

Figure 3.2: *Physical behaviour of flashing flow*

Please notice that critical bubble radius is an important term to separate stages of bubble growth from nuclei (stage 1) to the pressure-driven bubble growth (stage 2). So, an approximation for estimating this value should be presented here.

Thermodynamic equilibrium theory gives an expression of critical radius in Eq. 3-1 considering force balance across vapor-liquid interface Rayleigh [27].

$$r_{c1} = \frac{2\sigma}{\Delta P} \tag{3-1}$$

where σ is the surface tension, ΔP is the pressure difference across bubble interface.

For case of thermodynamic non-equilibrium phase change in flashing flow, according to Xi [12], the difference of the chemical potential function between two phases $(\Delta\mu)$ with constant temperature and pressure is shown in Eq. 3-2

$$\Delta\mu = (h_l - T_l \cdot s_l) - (h_v - T_{Sat} \cdot s_v) \tag{3-2}$$

$$h_l = h_{ls} + c_{pl}(T_l - T_{Sat}) \tag{3-3}$$

$$h_v = h_{vs} + c_{pv}(T_v - T_{Sat}) = h_{vs} + c_{pv}(T_l - T_{Sat}) \tag{3-4}$$

$$s_l = s_{ls} + c_{pl} \cdot ln\frac{T_l}{T_{Sat}} \tag{3-5}$$

$$s_v = s_{vs} + c_{pv} \cdot ln\frac{T_l}{T_{Sat}} - R \cdot ln\frac{P_{Sat}}{P_l} \tag{3-6}$$

where T_v is superheated vapor temperature. $T_v = T_l$ at equilibrium stage. The chemical potential difference is presented by $\Delta\mu$ with $\mu_v, \mu_l, h_v, h_l, s_v, s_l$ are chemical potential function, enthalpy and entropy of superheated vapor and liquid, respectively. Specific heat and enthalpy at constant pressure for liquid and vapor are presented by $c_{pl}, c_{pv}, h_{ls}, h_{vs}, s_l, s_v$. P_{Sat} and P_l presents saturated vapor pressure at T_l and droplet pressure, respectively.

Laplace's equation provides a relation between pressure inside and outside bubble considering surface tension and bubble radius. The force equilibrium leads to

$$P_l = P_{Sat} - \frac{2\sigma}{r} \tag{3-7}$$

Expression 3-8 is obtained by substituting from Eq. 3-3 to Eq. 3-7 into Eq. 3-2

$$\Delta\mu = \left(\frac{h_{fg}}{T_{Sat}} + c_{pl} - c_{pv}\right)\Delta T - T_l\left(c_{pl} - c_{pv}\right) \cdot ln\frac{T_l}{T_{Sat}} - R \cdot T_l \cdot ln\frac{P_{Sat}}{P_l} \tag{3-8}$$

h_{fg} defined in Eq. *3-8* is the latent heat of evaporation

Using Taylor series to expand the logarithm terms

$$ln\frac{T_l}{T_{Sat}} = \frac{\Delta T}{T_l} - \frac{\Delta T^2}{T_l^2} + o\left(\left(\frac{\Delta T}{3T_l}\right)^3\right), \quad \frac{\Delta T}{T_l} \in (-1,1] \tag{3-9}$$

$$ln\frac{P_{Sat}}{P_l} = 2\frac{P_{Sat} - P_l}{P_{Sat} + P_l} + o\left(\left(\frac{\frac{P_{Sat}}{P_l} - 1}{\frac{P_{Sat}}{P_l} + 1}\right)^3\right), \quad \frac{P_{Sat}}{P_l} \in (0, \infty] \tag{3-10}$$

According to De Groot and Mazur [29], $\Delta\mu < 0$ leads to irreversible spontaneous process (thermodynamic non-equilibrium). On the other hand, $\Delta\mu > 0$ causes collapse of bubble due to surface tension. Thus, radius of bubble will reach to critical value at $\Delta\mu = 0$ and can be approximated as in Eq. *3-11* by Xi [12].

$$r_c = \frac{2\sigma T_{Sat}}{\rho_v h_{fg} \cdot \Delta T} \tag{3-11}$$

Where

ρ_v is vapor density

$\Delta T = T_l - T_{Sat}$ is the overheat temperature

After exceeding critical radius, bubble grows rapidly under influences of pressure gradient across vapor-liquid interface. A model for this growth, expression 3-12 in [30] , is proposed by Rayleigh [27]

$$r\ddot{r} + \frac{3}{2}\dot{r}^2 = \frac{1}{\rho_l}\left(P_{Sat}(T_l) - P_a - \frac{2\sigma}{r} - \frac{4\mu}{r}\dot{r}\right) \tag{3-12}$$

Eq. 3-12 describes development of bubble radius (ρ_l is liquid density). Bubble radius, bubble growth rate and acceleration are r, ṙ and r̈, respectively. Initial conditions of Eq. 3-12, assuming the bubble growth process starts when bubble radius equals to critical radius, is presented in Eq. 3-13.

$$r(t = 0) = r_c \tag{3-13}$$

4. STATE OF THE ART OF FLASHING FLOW MODELLING

Flashing flow is a phase change phenomenon, which occurs in high speed flow inside throttling devices as control valves, nozzles and injectors, with the mechanical (i.e., the slip between the two-phases) and the thermal (i.e., boiling delay phenomenon) non-equilibrium effects. This phenomenon is of practical interest in many industrial applications; A typical example concerns the flashing flows in the control valves: the correct prediction of valve size is requested in the correct selection of valve-based systems.

This phenomenon has been widely studied during last decades by studies of experiment, analytical sizing equations and numerical model.

Experimental studies

In the last decades, experimental studies were performed by Reocreux [13], Schrock [14], Abuaf et al. [15] and Charless [31] with different throttling devices in case of flashing flow. Generally, experimental set-up in these classical measurements includes a well-controlled steady water flow going through device under controlled pressure drop. Thermodynamic conditions of water were designed for measurement of phase change rate with non-equilibrium effects. Inside device, taps were attached on inside-wall to capture local quantities as absolute pressure, averaged vapor volume fraction along device and detailed transverse vapor volume fraction distribution.

Sizing equation

One important assumption in many kinds of valve sizing equation is homogeneous assumption which considers two-phase flow as a single fluid. In this assumption, fluid properties and flow variables are evaluated by averaging the contribution of the separate phases. Basing on homogeneous assumption, there are many methods for sizing valve: The most used two approaches are equilibrium flow model and non-equilibrium flow model.

The first one, homogeneous equilibrium assumption, assumes flashing flow goes through vena contracta of control valves in equilibrium stage. This kind of valve sizing equation is suggested when vapor mass fraction (or quality) is greater than 0.14 ($\dot{x}_V > 0.14$) Giacchetta et al. [32] and Leung [33]. One of the earliest methods applying this assumption is the Omega method in Leung [7], [33]–[35] which is widely accepted in standards ISO 4126 part 10 [6], American Petroleum Institute [36] and reported in Darby [37], [38]. Calculation of Omega method depends mainly on compressibility parameter (Omega parameter) which is obtained by expansion law of two-phase flow.

Assumption of homogeneous non-equilibrium flow is proposed for the case of low quality ($\dot{x}_V < 0.14$). Phenomena happen inside device including (i) boiling delay of liquid phase accounting for thermodynamic non-equilibrium and (ii) slip phenomenon between the two phases accounting for hydrodynamic non-equilibrium. To overcome non-equilibrium effects, A model in Henry and Fauske [39] is established with a correction factor for boiling showing excellent results for approximation of the mass flow rate. However, this sizing

equation requires many fluid properties which are rarely available in industry. Besides, usage of this equation is more complicated than Omega method of Leung. For purpose of simplicity, Diener and Schmidt developed their method named Homogeneous Non-equilibrium method of Diener and Schmidt (HNE-DS). This method extends Omega method by adding correction factors for non-equilibrium effects. In Diener and Schmidt [40], their equation is applied to predict the mass flow rate of safety valve in case of steam/water flow. Sizing equation for control valves, orifices, and nozzles, is also introduced by Diener and Schmidt [5] using the same equation with a slightly difference in correction factors. Due to important contribution in valve sizing, HNE-DS for safety valves is included in standard ISO 4126 part 10 [6].

Numerical model

In recent years, the computational fluid dynamics (CFD) approach progressively becomes more attractive to researchers because modelling can provide insights in global and local fluid dynamic quantities. Derived numerical results can then help to improve the understanding of the physical behavior of flow inside devices. There are two main categories of CFD model for flashing flow: (i) CFD models considering the nucleation process: these models show a good agreement to real fluid-flow behavior but require experimental source terms for the nucleation equation in order to tune phase change process (as reported in **Table 4-1**); (ii) CFD flashing models neglecting the process of nucleation and imposing artificial coefficients for controlling the non-equilibrium effects: they are listed in **Table 4-2**.

Table 4-1: *Flashing flow simulation using nucleation models: a literature survey*

References and code	Numerical model and assumptions	Experimental benchmark and remarks
Maksic and Mewes [41] CFX 4.2	- Simplified two fluids model with 5 equations - Considering nucleation process by scalar transport equation for bubble number density with wall nucleation rate as source term. - Nucleation rate is determined by model of Jones [42]–[45]. - Mean bubble diameter and interfacial area density are functions of void fraction and bubble number density. - Not consider mass, energy and momentum transfer driven by nucleation. - Dominated conduction at interface. - Always saturated stage of vapor phase	- Flashing flows in nozzles is validated by Abuaf et al. [15]. - Relative motion of bubbles leads to dominant convective heat transfer in most cases of flashing flow

Marsh and O'Mahony [46] FLUENT 6.2.16	- 6-equation model including Mass, momentum and energy equations are performed separately for each phase - Effects of bubble nucleation and interfacial heat transfer to phase change process, momentum and energy conservation are considered. - Lift, wall lubrication and turbulent dispersion forces are ignored in momentum transfer. - A transport equation for vapor phase with only source term of heterogeneous nucleation. - Model for nucleation rate is modified from study of Blander and Katz [20] using two unphysical parameters to improve stability of model.	- A piping system to connect two flashing tanks at Rusal Aughinish. - Around 5% of error between numerical results and estimated plant flows
Mimouni et al. [47] NEPTUNE-CFD	- 6-equation model - Using unphysical heat transfer coefficient - Interphase momentum transfers including drag, added mass and lift forces. - Influences of Nucleation to vapor generation rate, momentum and energy transfer is performed by modified version of Jones' model [42]–[45].. - Always saturated stage of vapor phase	- Critical flow in nozzle of Robert et al. [48] with initially subcooled inlet and flashing outlet. To capture correctly radial vapor profile, model requires experimental information. - Experimental test from Archer [49] with cavitation at downstream of an orifice. An agreement between numerical results and experimental visualizations is observed qualitatively.
Janet et al. [50] CFX 14.5	- Two-fluid model (always saturated vapor phase). - Interphase momentum transfer consists of drag, lift, lubrication, virtual mass and turbulent dispersion force. - Interphase mass transfer depends on interfacial heat transfer - Using bubble number transport equation for nucleation process with source terms including nuclei at wall and coalescence effect of bubbles. - Types of nucleation source term consist of Blinkov et al. [45] RPI model [51]–[53], Riznic model [54], [55], Rohatgi model [56].	- Vertical circular convergent-divergent nozzle from Abuaf et al. [15]. - Good agreement to experiment in terms of critical flow rate and axial profiles but radial vapor fraction is not satisfied.

Pelletingeas et al. [57] STAR-CD	- Mixture model - Rayleigh-Plesset equation for the bubble growth - including surface tension in momentum equation	- A single-hole diesel injector with different needle's lifts. - numerical result and experiment have an agreement in term of discharge coefficient ($\text{error} < 1.3\%$) for fully open injector

Table 4-2: *Flashing Flow Simulation Neglecting Nucleation Proces*

References and code	Numerical model and assumptions	Experimental benchmark and remarks
Laurien and his colleagues [58]–[60] CFX 4.2	- 5-equation model - Neglecting non-drag forces in momentum transfer. - Allowing growth of bubble size by assuming bubble number density. - Always saturated vapor phase	- Cavitation flow in pipes. - Assumptions of model are only reasonable with narrow nucleation zone
Frank [61] CFX	- 5-equation model - Only considering drag force for momentum transfer - Bubble diameter is assumed constant (1mm) - Always saturation state for vapor phase.	- Edward blowdown test
Liao et al. [62] CFX 14.0	- 5-equation model (vapor phase is always saturated). - including drag, lift, lubrication, virtual mass and turbulent dispersion forces in momentum transfer. - Mass transfer mechanism depends on interfacial heat transfer - constant bubble number density for nucleation process.	- Transient pressure release in vertical pipe of Schaffrath [63] is used as benchmark. - Show large deviations in case of lack experimental information of bubble number density. - To improve accuracy of model, poly-disperse simulation should be performed instead of mono-disperse method
Yazdani et al. [64] FLUENT 12.0	- Mixture model with slip phenomenon between two phases - Heat transfer considers affection of phase change phenomenon driven by pressure Singhal et al. [65] and temperature - sonic velocity equation Brennen [66] is used for rate of phase change	- Convergent-divergent motive nozzle of Nakagawa et al. [67]. - An agreement between numerical method and experiment in term of pressure profile along divergent section is shown.

Liao and Lucas [68] CFX 14.5	- Same model as in Liao et al. [62]	- vertical circular convergent-divergent nozzle from Abuaf et al. [15]. - Calculated mass flow rate and experiment show agreement with error in range from -6.8% to +3.4% - cross-section averaged pressure and vapor fraction are agreement to measurements. However, radial distribution of vapor fraction is too uniform and have large deviations near nozzle outlet. - Need more experimental information to determine coefficients for flashing model including bubble number density and heat transfer coefficient
Liao and Lucas [69] CFX	- Same model as Liao et al. [62] considering both wall nucleation model by Blinkov et al. [45] and bulk nucleation model by Rohatgi model [56]	- An overview of previous works with assumptions of both mono-disperse approach and poly-disperse approach.

Summary

In general, the flashing flow inside valves, orifices and nozzles plays a significant role in nuclear power plant and chemical plant safety but knowledge about this phenomenon is not satisfied yet. Experimental data cannot provide enough flow local quantities to support a comprehensive understanding of phase change process inside devices. Besides, the lack of published experimental data also leads to difficulties in validation and development of sizing equations for throttling devices. Particularly in case of flashing flow, there are existing models to predict flow coefficient, C_V, for control valves, nozzles and orifices without validation due to lack of information. As a result, development of reliable CFD models for flashing flow inside throttling devices is necessary to understand more completely the physical behaviors of flow inside these geometries and to provide enough data for validation of existing sizing equations. Moreover, basing on knowledge and reliable data of flashing flow, development of sizing equations is performed to improve the accuracy of the flow coefficient prediction for industrial applications.

5. FLUID DYNAMICS

In this chapter, a general review about CFD model is presented, reference in Versteeg and Malalasekera [70]. Firstly, governing equations of fluid dynamics is shown including mass, momentum and energy conservation equations. Basing on this background, models for turbulence, two-phase flow and phase change phenomenon are presented.

5.1. Governing equations

Mass conservation equation

For compressible fluid flow, mass conservation is shown in Eq. 5-1

$$\frac{\partial \rho}{\partial t} + div(\rho \vec{u}) = 0 \tag{5-1}$$

Momentum conservation equation

Using Newton's second law give momentum conservation equation in x-, y- and z- components.

x- component of momentum conservation equation

$$\rho \frac{Du}{Dt} = \frac{\partial(-p + \tau_{xx})}{\partial x} + \frac{\partial \tau_{yx}}{\partial y} + \frac{\partial \tau_{zx}}{\partial z} + S_{Mx} \tag{5-2}$$

y- component of momentum conservation equation

$$\rho \frac{Dv}{Dt} = \frac{\partial \tau_{xy}}{\partial x} + \frac{\partial(-p + \tau_{yy})}{\partial y} + \frac{\partial \tau_{zy}}{\partial z} + S_{My} \tag{5-3}$$

z- component of momentum conservation equation

$$\rho \frac{Dw}{Dt} = \frac{\partial \tau_{xz}}{\partial x} + \frac{\partial \tau_{yz}}{\partial y} + \frac{\partial(-p + \tau_{zz})}{\partial z} + S_{Mz} \tag{5-4}$$

where S_{Mx}, S_{My} and S_{Mz} are body forces.

Energy conservation equation

Basing on the first law of thermodynamic, energy conservation equation gives

$$\rho \frac{DE}{Dt} = -div(p\vec{u}) + \left[\frac{\partial(u\tau_{xx})}{\partial x} + \frac{\partial(u\tau_{yx})}{\partial y} + \frac{\partial(u\tau_{zx})}{\partial z} + \frac{\partial(v\tau_{xy})}{\partial x} + \frac{\partial(v\tau_{yy})}{\partial y} + \frac{\partial(v\tau_{zy})}{\partial z} + \frac{\partial(w\tau_{xz})}{\partial x} + \frac{\partial(w\tau_{yz})}{\partial y} + \frac{\partial(w\tau_{zz})}{\partial z} + div(k\ grad(T)) + S_E \tag{5-5}$$

From expression of total energy $E = i + \frac{1}{2}(u^2 + v^2 + w^2)$ with E is specific total energy, i is specific internal energy and $\frac{1}{2}(u^2 + v^2 + w^2)$ is specific kinetic energy, kinetic energy conservation equation can be extracted as in Eq. 5-6

$$\rho\frac{D\left[\frac{1}{2}(u^2+v^2+w^2)\right]}{Dt}=-\vec{u}\cdot grad(p)+u\left(\frac{\partial(\tau_{xx})}{\partial x}+\frac{\partial(\tau_{yx})}{\partial y}+\frac{\partial(\tau_{zx})}{\partial z}\right)$$
$$+v\left(\frac{\partial(\tau_{xy})}{\partial x}+\frac{\partial(\tau_{yy})}{\partial y}+\frac{\partial(\tau_{zy})}{\partial z}\right) \quad (5\text{-}6)$$
$$+w\left(\frac{\partial(w\tau_{xz})}{\partial x}+\frac{\partial(w\tau_{yz})}{\partial y}+\frac{\partial(w\tau_{zz})}{\partial z}\right)$$
$$+\vec{u}\cdot\vec{S}_M$$

Finally, subtracting Eq. 5-6 from Eq. 5-5 with definition of source term $S_i=S_E-\vec{u}\cdot\vec{S}_M$ derives internal energy conservation equation as Eq. 5-7

$$\rho\frac{Di}{Dt}=-p\,div(\vec{u})+div\big(k\,grad(T)\big)+\tau_{xx}\frac{\partial u}{\partial x}+\tau_{yx}\frac{\partial u}{\partial y}+\tau_{zx}\frac{\partial u}{\partial z}+\tau_{xy}\frac{\partial v}{\partial x}$$
$$+\tau_{yy}\frac{\partial v}{\partial y}+\tau_{zy}\frac{\partial v}{\partial z}+\tau_{xz}\frac{\partial w}{\partial x}+\tau_{yz}\frac{\partial w}{\partial y}+\tau_{zz}\frac{\partial w}{\partial z}+S_i \quad (5\text{-}7)$$

Defining c as specific heat, expression Eq. 5-7 reduces to Eq. 5-8 in case of incompressible flow ($i=cT,\ div(\vec{u})=0$)

$$\rho c\frac{DT}{Dt}=div\big(k\,grad(T)\big)+\tau_{xx}\frac{\partial u}{\partial x}+\tau_{yx}\frac{\partial u}{\partial y}+\tau_{zx}\frac{\partial u}{\partial z}+\tau_{xy}\frac{\partial v}{\partial x}$$
$$+\tau_{yy}\frac{\partial v}{\partial y}+\tau_{zy}\frac{\partial v}{\partial z}+\tau_{xz}\frac{\partial w}{\partial x}+\tau_{yz}\frac{\partial w}{\partial y}+\tau_{zz}\frac{\partial w}{\partial z}+S_i \quad (5\text{-}8)$$

Eq. 5-9 defining specific total enthalpy as:

$$h=i+p/\rho+\frac{1}{2}(u^2+v^2+w^2)=E+p/\rho \quad (5\text{-}9)$$

The energy balance, Eq. 5-10, is obtained by substitution Eq. 5-9 into Eq. 5-5

$$\rho\frac{Dh}{Dt}+div(ph\vec{u})=div\big(k\,grad(T)\big)+\left[\frac{\partial(u\tau_{xx})}{\partial x}+\frac{\partial(u\tau_{yx})}{\partial y}+\frac{\partial(u\tau_{zx})}{\partial z}\right.$$
$$+\frac{\partial(v\tau_{xy})}{\partial x}+\frac{\partial(v\tau_{yy})}{\partial y}+\frac{\partial(v\tau_{zy})}{\partial z} \quad (5\text{-}10)$$
$$+\frac{\partial(w\tau_{xz})}{\partial x}+\frac{\partial(w\tau_{yz})}{\partial y}+\frac{\partial(w\tau_{zz})}{\partial z}+S_h$$

Mass balance (Eq. 5-1), momentum balance (Eq. 5-2, Eq. 5-3 and Eq. 5-4) and energy balance (Eq. 5-5) describe three-dimension flow field including density, energy and three components of velocity. Equation of state should be introduced as such as in Eq. 5-11

$$p=p(\rho,T)\text{ and }i=i(\rho,T) \quad (5\text{-}11)$$

5.2. Turbulence model

"Turbulence" term describes interaction of eddies appearing in high Reynolds number flow with a wide range of time and length scales. In this study, RANS turbulence models are used with consideration of mean flow and effects of turbulence to capture turbulence fluctuations.

For industrial applications, there are six RANS turbulence models: (i) *k-ε* Standard, (ii) *k-ε* Realizable, (iii) *k-ε* RNG, (iv) *k-ω* Standard, (v) *k-ω* SST and (vi) RSM existing in many commercial codes such as ANSYS-FLUENT, ANSYS-CFX and STARCCM+, etc. The original references of these models are reported in **Table 5-1**. Besides, [71] is proposed for further information about their implementation in the commercial code ANSYS-Fluent. In addition to turbulence models, the near wall treatments should be considered. It should be remarked that *k-ω* Standard, *k-ω* SST models do not require a near wall treatment because their mathematical model already emphasizes on the flow near wall. However, implementations in their ANSYS FLUENT should be considered. Concerning the *k-ω* Standard and the *k-ω* SST, a low-Reynolds implementation may be enabled in ANSYS FLUENT for fully resolver near wall grids. On the other hand, the *k-ε* Standard, *k-ε* Realizable, *k-ε* RNG and RSM models need a near wall modeling. The original references of theory and implementation in ANSYS FLUENT concerning the near wall treatments are reported in **Table 5-2** for further information.

Table 5-1: *References of turbulence models*

Turbulence models	**Reference**
$\boldsymbol{k-\varepsilon\ Standard}$	Launder and Spalding [72]
$\boldsymbol{k-\varepsilon\ Relizable}$	Shih et al. [73]
$\boldsymbol{k-\varepsilon\ RNG}$	Yakhot et al. [74]
$\boldsymbol{RSM}$	Launder et al. [75]
$\boldsymbol{k-\omega\ Standard}$	Wilcox [76]–[79]
$\boldsymbol{k-\omega\ SST}$	Menter [80]–[83]

Table 5-2: *References of wall treatments for turbulence models*

Wall treatment	$k-\varepsilon\ Standard$	$k-\varepsilon\ Relizable$	$k-\varepsilon\ RNG$	RSM
Standard Wall Function	Launder and Spalding [84]			
Non-Equilibrium Wall Function	Kim and Choudhury [85]			
Scalable Wall Function	User guide of ANSYS 16.0 [71]			
Enhanced Wall Treatment	User guide of ANSYS 16.0 [71]			
$k-\omega$ options	$k-\omega\ Standard$	$k-\omega\ SST$		
Standard	User guide of ANSYS 16.0 [71]			
Low-Re Corrections	User guide of ANSYS 16.0 [71]			

5.3. Multi-phase flow model

In this section, two models for two-phase flow simulation are presented: mixture model and two-fluid model (Eulerian model), reference in user guide of ANSYS-FLUENT 16.0 [71]. Mixture model assumes two-phase flow as pseudo single-phase flow for modelling. This model archives higher accuracy with high gas mass fraction flow. Conversely, Eulerian model solves each phase separately and use momentum interaction forces to couple two phases. In general, Eulerian model is better than mixture model to capture all interactions between two phases. However, this model is always more complicated and require more strategies for solution stabilization.

5.3.1. The mixture model for multi-phase flow

The mixture model considers multi-phase flow as a pseudo single-phase flow; the mass, momentum and energy governing equations give:

Mass conservation.

$$\frac{\partial \rho_m}{\partial t} + \nabla \cdot (\rho_m \vec{v}_m) = 0 \qquad 5\text{-}12$$

Momentum conservation.

$$\frac{\partial (\rho_m \vec{v}_m)}{\partial t} + \nabla \cdot (\rho_m \vec{v}_m \vec{v}_m) = -\nabla P + \nabla \cdot [\mu_m (\nabla \vec{v}_m + \nabla \vec{v}_m^T)] + \nabla \cdot \left(\sum_{k=1}^{n} \alpha_k \rho_k \vec{v}_{dr,k} \vec{v}_{dr,k} \right) \qquad 5\text{-}13$$

The third term of 5-13 $\nabla \cdot \left(\sum_{k=1}^{n} \alpha_k \rho_k \vec{v}_{dr,k} \vec{v}_{dr,k} \right)$ is added for relative motion between two phases

Energy conservation.

$$\frac{\partial (\sum_{k=1}^{n} \alpha_k \rho_k E_k)}{\partial t} + \nabla \cdot \sum_{k=1}^{n} \left(\alpha_k \vec{v}_k (\rho_k E_k + P) \right) = \nabla \cdot \left(k_{eff} \nabla T \right) + S_E \qquad 5\text{-}14$$

In the governing equations in Eq. 5-12, Eq. 5-13 and Eq. 5-14, averaged-mass mixture velocity $\vec{v}_m$, mixture density ρ_m, mixture dynamic viscosity μ_m and effective conductivity k_{eff} are defined as:

$$\vec{v}_m = \frac{\sum_{k=1}^{n} \alpha_k \rho_k \vec{v}_k}{\rho_m} \qquad 5\text{-}15$$

$$\rho_m = \sum_{k=1}^{n} \alpha_k \rho_k \qquad 5\text{-}16$$

$$\mu_m = \sum_{k=1}^{n} \alpha_k \mu_k \qquad 5\text{-}17$$

$$k_{eff} = \sum_{k=1}^{n} \alpha_k (k_k + k_t) \qquad 5\text{-}18$$

$$\sum_{k=1}^{n} \alpha_k = 1 \quad (5\text{-}19)$$

turbulence thermal conductivity, k_t, is defined by the turbulence model

S_E is volumetric heat sources. E_k in Eq. 5-14 is defined as:

For compressible phase

$$E_k = h_k - \frac{p}{\rho_k} + \frac{v_k^2}{2} \quad (5\text{-}20)$$

For incompressible phase

$$E_k = h_k \quad (5\text{-}21)$$

h_k is sensible enthalpy for phase k

Secondary phase volume fraction equation

$$\frac{\partial(\alpha_p \rho_p)}{\partial t} + \nabla \cdot (\alpha_p \rho_p \vec{v}_p) = -\nabla \cdot (\alpha_p \rho_p \vec{v}_{dr,p}) + \sum_{q=1}^{n} (\dot{m}_{qp} - \dot{m}_{pq}) \quad (5\text{-}22)$$

where p is secondary phase and q is primary phase. $\dot{m}_{qp}$ describes mass transfer from the p^{th} to the q^{th} phase, and $\dot{m}_{pq}$ describes mass transfer from the q^{th} to the p^{th} phase.

Slip model for relative motion between two phases.

The mechanical non-equilibrium comes from the relative motion between the vapor phase and the liquid phase. In the mixture approach, the slip effect between two phases is formulated by the drift velocity term ($\vec{v}_{dr,k}$) in the momentum equation (see Eq. 5-13). The drift velocity between the two phases reads as follows:

$$\vec{v}_{dr,p} = \vec{v}_{pq} - \sum_{k=1}^{n} c_k \vec{v}_{qk} \quad (5\text{-}23)$$

According to Manninen et al. [86] where $\vec{v}_{pq}$ is defined as follows:

$$\vec{v}_{pq} = \frac{\tau_p}{f_{drag}} \frac{(\rho_p - \rho_m)}{\rho_p} \vec{a} \quad (5\text{-}24)$$

In Eq. 5-24, f_{drag} is the drag function, which is determined as in Naumann and Schiller [87] as follows:

$$f_{drag} = \begin{cases} 1 + 0.15\mathrm{Re}^{0.687} & \mathrm{Re} \leq 1000 \\ 0.0183\mathrm{Re} & \mathrm{Re} > 1000 \end{cases} \quad (5\text{-}25)$$

where Re is the relative Reynolds number.

5.3.2. The Eulerian model for multi-phase flow

Conversely to the mixture model, the Eulerian model solves governing equations for each phase separately and then considers phase interaction to close model.

Mass conservation for phase q^{th}

$$\frac{\partial(\alpha_q\rho_q)}{\partial t} + \nabla\cdot(\alpha_q\rho_q\vec{v}_q) = \sum_{p=1}^{n}(\dot{m}_{pq} - \dot{m}_{qp}) \quad 5\text{-}26$$

with $\vec{v}_q$ is velocity of phase q^{th}. $\dot{m}_{qp}$ describes mass transfer from the p^{th} to the q^{th} phase, and $\dot{m}_{pq}$ describes mass transfer from the q^{th} to the p^{th} phase.

Momentum conservation for phase q^{th}

$$\frac{\partial(\alpha_q\rho_q\vec{v}_q)}{\partial t} + \nabla\cdot(\alpha_q\rho_q\vec{v}_q\vec{v}_q) = -\alpha_q\nabla P + \nabla\cdot\bar{\bar{\tau}}_q + \alpha_q\rho_q\vec{g} + \sum_{p=1}^{n}(\vec{R}_{pq} + \dot{m}_{pq}\vec{v}_{pq} - \dot{m}_{qp}\vec{v}_{qp}) + (\vec{F}_q + \vec{F}_{\text{lift},q} + \vec{F}_{vm,q}) \quad 5\text{-}27$$

where $\bar{\bar{\tau}}_q$ is the stress tensor of q^{th}

$$\bar{\bar{\tau}}_q = \alpha_q\mu_q(\nabla\vec{v}_q + \nabla\vec{v}_q^T) + \alpha_q\left(\lambda_q - \frac{2}{3}\mu_q\right)\nabla\cdot\vec{v}_q\bar{\bar{I}} \quad 5\text{-}28$$

where μ_q and λ_q describes the shear and bulk viscosity of phase q^{th}, $\vec{F}_q$ is external body force. P is pressure used for all phases. $\vec{F}_{\text{lift},q}$, $\vec{F}_{vm,q}$ and $\vec{R}_{pq}$ are the lift force, the virtual mass force and the interaction force between phases, respectively.

$\vec{v}_{pq}$ describes the interphase velocity defined as:

Case: mass transfer from phase p^{th} to phase q^{th} $(\dot{m}_{pq} > 0)$

$\vec{v}_{pq} = \vec{v}_p$

Case: mass transfer from phase q^{th} to phase p^{th} $(\dot{m}_{pq} < 0)$

$\vec{v}_{pq} = \vec{v}_q$

For force terms, the reader should refer to [71] for details about their implementation and definition in the commercial code ANSYS-Fluent.

Energy conservation for phase q^{th}

$$\frac{\partial(\alpha_q\rho_q h_q)}{\partial t} + \nabla\cdot(\alpha_q\rho_q\vec{v}_q h_q) = -\alpha_q\frac{\partial P}{\partial t} + \bar{\bar{\tau}}_q:\nabla\vec{v}_q - \nabla\cdot\vec{q}_q + S_q + \sum_{p=1}^{n}(Q_{pq} + \dot{m}_{pq}h_{pq} - \dot{m}_{qp}h_{qp}) \quad 5\text{-}29$$

where h_q describes the specific enthalpy of the phase q^{th}, $\vec{q}_q$ and S_q are heat flux and source term, respectively. Q_{pq} is the heat exchange intensity between the phase p^{th} and the phase q^{th} considering local heat balance conditions ($Q_{pq} = -Q_{qp}$ and $Q_{qq} = 0$). h_{pq} is the interphase enthalpy. All terms in energy equation are presented in detail in [71].

5.4. Phase change model

This section will present some numerical models for phase change phenomenon, reference in user guide of ANSYS-FLUENT 16.0 [71]. There are two kinds of model to describe the change of phase from liquid to its vapor consisting of (i) phase change driven by interfacial heat transfer and (ii) phase change driven by pressure. The first one is always used for boiling process (evaporation) where heat transfer at interphase plays a significant role. The latter is applied in cavitation phenomenon where depressurization contributes mainly to phase change process.

5.4.1. Evaporation-condensation model

5.4.1.1. Lee model

The vapor transport equation is used to define mass transfer mechanism as in Eq. 5-30

$$\frac{\partial(\alpha_v \rho_v)}{\partial t} + \nabla \cdot (\alpha_v \rho_v \vec{v}_v) = \dot{m}_{lv} - \dot{m}_{vl} \quad 5\text{-}30$$

where v and l are vapor and liquid, respectively. Velocity vector of vapor phase is $\vec{v}_v$ and vapor density is defined as ρ_v.

In Eq. 5-30, $\dot{m}_{lv}$ and $\dot{m}_{vl}$ define mass transfer rate from liquid to vapor (evaporation) and vapor to liquid (condensation). Clearly, in case of evaporation, R.H.S of Eq. 5-30 is positive and conversely negative in condensation case.

From mechanisms of thermal phase change, mass transfer rates can be defined as:

If $T_l > T_{sat}$ (evaporation):

$$\dot{m}_{lv} = coeff * \alpha_l \rho_l \frac{(T_l - T_{sat})}{T_{sat}} \quad 5\text{-}31$$

If $T_v < T_{sat}$ (condensation):

$$\dot{m}_{vl} = coeff * \alpha_v \rho_v \frac{(T_{sat} - T_v)}{T_{sat}} \quad 5\text{-}32$$

Experimental coefficient, $coeff$, in Eq. 5-31 and Eq. 5-32 is described as a relaxation time coefficient and should be tuned for specific cases.

Influences of mass transfer mechanism to energy equation can be defined by imposing source term of energy equation as product of mass transfer rate and the latent heat.

Formula of Hertz Knudsen [88], [89], defining evaporation-condensation flux, is considered in Eq. 5-33

$$F = \beta \sqrt{\frac{M}{2\pi R T_{\text{sat}}}} (P^* - P_{sat}) \quad 5\text{-}33$$

where M is molar mass. P^* is the partial pressure at interface on the vapor side with value close to saturation pressure, P_{sat}.

Relation between the pressure and temperature at saturation stage can be described by the Clapeyron-Clausius equation given in Eq. 5-34

$$\frac{dP}{dT} = \frac{L}{T(v_v - v_l)} \tag{5-34}$$

In case of P^* and T^* are near to saturation condition, expression Eq. 5-34 can lead to Eq. 5-35

$$(P^* - P_{\text{sat}}) = -\frac{L}{T(v_v - v_l)}(T^* - T_{\text{sat}}) \tag{5-35}$$

Substituting Eq. 5-35 into Hertz Knudsen formula, Eq. 5-33, gives

$$F = \beta\sqrt{\frac{M}{2\pi R T_{\text{sat}}}}L\left(\frac{\rho_v\rho_l}{\rho_l - \rho_v}\right)\frac{(T^* - T_{sat})}{T_{sat}} \tag{5-36}$$

Definition of β is related to the vapor physical characteristics and $\beta = 1$ at near equilibrium stage.

Combination between evaporation-condensation flux, Eq. 5-36, and interfacial area density, Eq. 5-37, gives the phase source term in Eq. 5-38

$$A_i = \frac{6\alpha_v\alpha_l}{d_b} \tag{5-37}$$

$$FA_i = \frac{6}{d_b}\beta\sqrt{\frac{M}{2\pi R T_{\text{sat}}}}L\left(\frac{\alpha_v\rho_v}{\rho_l - \rho_v}\right)\left[\alpha_l\rho_l\frac{(T^* - T_{sat})}{T_{sat}}\right] \tag{5-38}$$

In Eq. 5-38, d_b is the bubble diameter and expression of A_i can be changed by specific cases.

Finally, $coeff$, extracted from Eq. 5-38, is the inverse of the relaxation time $(1/s)$ and given in Eq. 5-39. Equation Eq. 5-38 becomes mass transfer source term for evaporation with a similar form to Eq. 5-31.

$$coeff = \frac{6}{d_b}\beta\sqrt{\frac{M}{2\pi R T_{\text{sat}}}}L\left(\frac{\alpha_v\rho_v}{\rho_l - \rho_v}\right) \tag{5-39}$$

Using the same manner of establishment of evaporation expression leads to condensation expression Eq. 5-32. Generally, $coeff$ should be chosen differently for evaporation and condensation process. Besides, definition of d_b and β should be performed for each specific case basing on experimental information.

Lee model for phase change process can be combined to two-phase models as mixture, Eulerian-Eulerian and VOF model.

5.4.1.2. Thermal phase change model

Thermal phase change model bases on two-resistance method for extracting heat transfer coefficient. This method is only applied for Eulerian multi-phase model in ANSYS FLUENT.

Definitions of heat flow rate from interface to liquid phase and from interface to vapor phase are Eq. 5-40 and Eq. 5-41, respectively.

$$\dot{Q}_l = h_l A_i (T_s - T_l) - \dot{m}_{lv} H_{ls} \quad 5\text{-}40$$

$$\dot{Q}_v = h_v A_i (T_s - T_v) - \dot{m}_{lv} H_{vs} \quad 5\text{-}41$$

where h_l and h_v are heat transfer coefficients of liquid and vapor phase. Vapor and liquid enthalpies are presented as H_{vs} and H_{ls}. Interfacial temperature is T_s at equilibrium state and $T_s = T_{\text{sat}}$ in case of neglecting surface tension effects.

The heat balance at interface leads to Eq. 5-42

$$\dot{Q}_l + \dot{Q}_v = 0 \quad 5\text{-}42$$

From Eq. 5-40, Eq. 5-41 and Eq. 5-42, expression for mass transfer rate from liquid to vapor, Eq. 5-43, is extracted

$$\dot{m}_{lv} = -\frac{h_l A_i (T_{\text{sat}} - T_l) - h_v A_i (T_{\text{sat}} - T_v)}{H_{vs} - H_{ls}} \quad 5\text{-}43$$

Generally, in case of mass transfer, latent heat between the two phases leads to discontinuity of H_{vs} and H_{ls} which need to calculate correctly.

Depending works of Prakash [90], definitions of H_{vs} and H_{ls} are shown in Eq. 5-44 and Eq. 5-45 for evaporation and condensation, respectively.

If $\dot{m}_{lv} \geq 0$ (evaporation)

$$\begin{aligned} H_{ls} &= H_l(T_l) \\ H_{vs} &= H_v(T_{\text{sat}}) \end{aligned} \quad 5\text{-}44$$

If $\dot{m}_{lv} < 0$ (condensation)

$$\begin{aligned} H_{ls} &= H_l(T_{\text{sat}}) \\ H_{vs} &= H_v(T_{\text{v}}) \end{aligned} \quad 5\text{-}45$$

Prakash formula leads to stable state for both physical and numerical aspect. Besides, $H_{vs} - H_{ls}$ results in non-zero (only greater than or equal to latent heat) as presented in Eq. 5-46

$$L = H_v(T_{\text{sat}}) - H_l(T_{\text{sat}}) \quad 5\text{-}46$$

Definition of total enthalpy in case of mass transfer is shown in Eq. 5-47

$$H(T) = H(T_{ref}) + \int_{T_{ref}}^{T} C_p(T) dT \quad 5\text{-}47$$

$H(T_{ref})$ is standard state enthalpy at reference temperature T_{ref}.

In thermal phase change model, heat transfer is governed only by heat transfer at interphase and overall heat balance without using accommodation coefficient as Lee model.

5.4.2. Cavitation model

Process of depressurization of liquid at constant temperature leading to mass transfer from liquid to vapor phase is called cavitation and this phenomenon is encountered frequently when liquid spends a rapid drop of pressure below saturation state in throttling devices. Phase change process inside throttling devices comes from nuclei existing in liquid flow and growing under effects of depressurization.

There are three famous cavitation models mostly used in commercial software

- Singhal et al. model: combined with mixture two-phase model
- Zwart-Gerber-Belamri model: combined with mixture or Eulerian two-phase model
- Schnerr and Sauer model: combined with mixture or Eulerian two-phase model

In all standard cavitation models, assumptions are imposed as follow:

- Existence of both vapor and liquid in a system.
- Cavitation models consider both bubble growth (evaporation) and collapse (condensation).
- The growth of vapor bubbles in a liquid is described by Rayleigh-Plesset equation.
- Considering non-condensable gases is performed by Singhal et al. model assuming as a known constant.
- Definition of fluid properties in cavitation models can be constant or depend on temperature.
- Cavitation models can be used in combination of conventional turbulence models as RANS, RSM.

5.4.2.1. Transport equation of vapor fraction

Vapor transport equation governing evaporation and condensation process is presented in Eq. *5-48*

$$\frac{\partial(\alpha_v \rho_v)}{\partial t} + \nabla \cdot (\alpha_v \rho_v \vec{v}_v) = R_e - R_c \qquad 5\text{-}48$$

Mass source terms respecting to the growth and the collapse process of vapor bubbles are R_e and R_c, respectively.

In many cavitation models, R_e and R_c are modeled by the Rayleigh-Plesset equation.

5.4.2.2. Rayleigh-Plesset equation

Rayleigh-Plesset equation, Eq. 5-49, describes development of bubble radius neglecting relative motion between bubble and surround flowing liquid.

$$r_b \frac{D^2 r_b}{Dt^2} + \frac{3}{2}\left(\frac{Dr_b}{Dt}\right)^2 = \left(\frac{P_B - P}{\rho_l}\right) - \frac{4v_l}{r_b} r_b - \frac{2S}{\rho_l r_b} \qquad 5\text{-}49$$

P_B and P are pressure of bubble at interface and local far-field pressure

Eq. 5-49 is simplified to Eq. 5-50 by neglecting high order terms and surface tension force.

$$\frac{Dr_b}{Dt} = \sqrt{\frac{2}{3}\frac{P_b - P}{\rho_l}} \quad 5\text{-}50$$

Effects of bubble dynamic, via Eq. 5-50, are introduced into cavitation model.

5.4.2.3. Singhal et al. model

This cavitation model is developed by Singhal et al. [91] considering all first-order effects as (i) phase change (ii) bubble dynamic (iii) turbulent pressure fluctuations, and (iv) non-condensable gases. Furthermore, this cavitation model takes into account N-phase flow, multi-phase species flow, relative motion between phases, compressibility and thermal effects of all phases existing in flow.

Singhal et al. model is used in ANSYS FLUENT with mixture model (both slip and non-slip models).

Continuity equations of Liquid, vapor phase and mixture are presented in Eq. 5-51, Eq. 5-52 and Eq. 5-53, respectively.

Liquid phase:

$$\frac{\partial}{\partial t}[(1-\alpha_v)\rho_l] + \nabla \cdot [(1-\alpha_v)\rho_l \vec{v}_m] = -R \quad 5\text{-}51$$

Vapor phase:

$$\frac{\partial(\alpha_v \rho_v)}{\partial t} + \nabla \cdot (\alpha_v \rho_v \vec{v}_m) = R \quad 5\text{-}52$$

Mixture

$$\frac{\partial \rho_m}{\partial t} + \nabla \cdot (\rho_m \vec{v}_m) = 0 \quad 5\text{-}53$$

ρ_m is mixture density and is defined in Eq. 5-54

$$\rho_m = \alpha_v \rho_v + (1-\alpha_v)\rho_v \quad 5\text{-}54$$

Relation between mixture density, ρ_m, and vapor volume fraction, α_v, in Eq. 5-55 can be derived from Eq. 5-51, Eq. 5-52 and Eq. 5-53

$$\frac{D\rho_m}{Dt} = -(\rho_l - \rho_v)\frac{D\alpha_v}{Dt} \quad 5\text{-}55$$

Relation between vapor volume fraction, α_v, the bubble number density, N_b, and the bubble radius, r_b, is given in Eq. 5-56.

$$\alpha_v = N_b \times \left(\frac{4}{3}\pi r_b^3\right) \quad 5\text{-}56$$

Eq. 5-56 is then substituted into Eq. 5-55 gives

$$\frac{D\rho_m}{Dt} = -(\rho_l - \rho_v)(N_b 4\pi)^{\frac{1}{3}}(3\alpha_v)^{\frac{2}{3}}\frac{Dr_b}{Dt} \quad 5\text{-}57$$

Extending term $\frac{Dr_b}{Dt}$ using Eq. 5-50 and deriving evaporation rate R, R_e in Eq. 5-48, gives Eq. 5-58

$$R = (N_b 4\pi)^{\frac{1}{3}}(3\alpha_v)^{\frac{2}{3}}\frac{\rho_v\rho_l}{\rho_m}\left[\frac{2}{3}\left(\frac{P_b - P}{\rho_l}\right)\right]^{\frac{1}{2}} \quad 5\text{-}58$$

In Eq. 5-58, bubble number density, N_b, is provided by experimental data. In case of lack information for estimating N_b, Eq. 5-58 can be rewritten using bubble radius instead of N_b as given in Eq. 5-59.

$$R = \frac{3\alpha_v}{r_b}\frac{\rho_v\rho_l}{\rho_m}\left[\frac{2}{3}\left(\frac{P_b - P}{\rho_l}\right)\right]^{\frac{1}{2}} \quad 5\text{-}59$$

Eq. 5-59 shows evaporation rate as a function of both ρ_m, ρ_v and ρ_l. This expression describes accurately phase change process from liquid to vapor because Eq. 5-59 is derived directly from equations of volume fraction.

Practically, local far-field pressure P is the same to pressure at cell center and the bubble pressure P_b is equal to the saturation vapor pressure P_v.

Finally, vapor mass fraction transport equation , combining expression Eq. 5-59 for cavitation model, is proposed by Singhal et al. [65]:

$$\frac{\partial}{\partial t}(\dot{x}_v\rho_m) + \nabla\cdot(\dot{x}_v\rho_m\vec{v}_v) = \nabla(\Gamma\nabla\dot{x}_v) + R_e - R_c \quad 5\text{-}60$$

where $\dot{x}_v$ is vapor mass fraction and Γ is diffusion coefficient.

Mass transfer rates R_e and R_c can be presented as following:

If $P \le P_v$

$$R_e = F_{vap}\frac{max\left(1.0,\sqrt{k}\right)\left(1-\dot{x}_v-\dot{x}_g\right)}{\sigma}\rho_v\rho_l\left[\frac{2}{3}\left(\frac{P_v - P}{\rho_l}\right)\right]^{\frac{1}{2}} \quad 5\text{-}61$$

If $P > P_v$

$$R_c = F_{cond}\frac{max\left(1.0,\sqrt{k}\right)\dot{x}_v}{\sigma}\rho_l\rho_l\left[\frac{2}{3}\left(\frac{P_v - P}{\rho_l}\right)\right]^{\frac{1}{2}} \quad 5\text{-}62$$

$\dot{x}_G$ is non-condensable gas mass fraction and σ is liquid surface tension coefficient.

Saturation vapor pressure is proposed in expression Eq. 5-62 considering effects of local turbulent pressure fluctuations

$$P_v = P_{\text{sat}} + \frac{1}{2}(0.39\rho k) \quad 5\text{-}63$$

F_{vap} and F_{cond} are experimental coefficients and suggested values of 0.02 and 0.01, respectively.

5.4.2.4. Zwart-Gerber-Belamri Model

In this model, bubble number density, N_b, assuming the same size for all bubbles, is used to calculate the total interphase mass transfer rate model per unit volume, R. Expression for R is proposed in Eq. 5-64 by Zwart et al. [92]

$$R = N_b \times \left(4\pi r_b^2 \rho_v \frac{Dr_b}{Dt}\right) \quad 5\text{-}64$$

Using Eq. 5-56 to extend N_b and Eq. 5-50 to extend $\frac{Dr_b}{Dt}$ in Eq. 5-64 gives

$$R = \frac{3\alpha\rho_v}{r_b}\left[\frac{2}{3}\left(\frac{P_b - P}{\rho_l}\right)\right]^{\frac{1}{2}} \quad 5\text{-}65$$

The only difference between Singhal et al. model, Eq. 5-59, and Zwart-Gerber-Belamri model, Eq. 5-65, is dependency of R on density. In Zwart-Gerber-Belamri model, R is only a function of ρ_v, ρ_l while Singhal et al. model establishes R as a function of both ρ_v, ρ_l and ρ_m.

Finally, mass transfer rate for evaporation and condensation is given in Eq. 5-66 and Eq. 5-67 with some modifications to consider relation between vapor fraction and bubble number density.

If $P \leq P_v$

$$R_e = F_{vap}\frac{3\alpha_{nuc}(1-\alpha_v)}{r_b}\left[\frac{2}{3}\left(\frac{P_v - P}{\rho_l}\right)\right]^{\frac{1}{2}} \quad 5\text{-}66$$

If $P > P_v$

$$R_c = F_{cond}\frac{3\alpha\rho_v}{r_b}\left[\frac{2}{3}\left(\frac{P_v - P}{\rho_l}\right)\right]^{\frac{1}{2}} \quad 5\text{-}67$$

where $r_b = 10^{-6}m$, $\alpha_{nuc} = 5 \times 10^{-4}$ is nucleation site volume fraction, F_{vap} and F_{cond} are experimental coefficients and suggested values of 50 and 0.001, respectively.

5.4.2.5. Schnerr and Sauer Model

Using a similar approach as Singhal et al. model, Schnerr and Sauer [93] established vapor transport equation, Eq. 5-68, to derive exact expression for mass transfer rate from liquid to vapor.

$$\frac{\partial(\alpha_v\rho_v)}{\partial t} + \nabla\cdot(\alpha_v\rho_v\vec{v}_m) = \frac{\rho_v\rho_l}{\rho_m}\frac{D\alpha}{Dt} \quad 5\text{-}68$$

with mass source is extracted from Eq. 5-68 as

$$R = \frac{\rho_v\rho_l}{\rho_m}\frac{D\alpha}{Dt} \quad 5\text{-}69$$

Expression for relation between vapor volume fraction, α_v, the number bubble density, N_b, is given in Eq. 5-70. It is noticed that this expression is different from Singhal et al. and Zwart-Gerber-Belamri.

$$\alpha_v = \frac{N_b \frac{4}{3}\pi r_b^3}{1 + N_b \frac{4}{3}\pi r_b^3} \quad \text{5-70}$$

Finally, using the same method as Singhal et al. to derive mass transfer rate from liquid to vapor in Eq. 5-71

$$R = \frac{3\alpha_v(1-\alpha_v)}{r_b}\frac{\rho_l\rho_v}{\rho_m}\left[\frac{2}{3}\left(\frac{P_v - P}{\rho_l}\right)\right]^{\frac{1}{2}} \quad \text{5-71}$$

$$r_b = \left(\frac{\alpha}{1-\alpha}\frac{3}{4\pi}\frac{1}{N_b}\right)^{\frac{1}{3}} \quad \text{5-72}$$

In Eq. 5-71, bubble number density, N_b, must be determined. In case of lack information, $N_b = constant$ is accepted with assumption of no bubbles created or destroyed.

It is similar the other approaches, general expression for evaporation and condensation is given as

If $P \leq P_v$ (evaporation)

$$R_e = \frac{3\alpha_v(1-\alpha_v)}{r_b}\frac{\rho_l\rho_v}{\rho_m}\left[\frac{2}{3}\left(\frac{P_v - P}{\rho_l}\right)\right]^{\frac{1}{2}} \quad \text{5-73}$$

If $P > P_v$ (condensation)

$$R_e = \frac{3\alpha_v(1-\alpha_v)}{r_b}\frac{\rho_l\rho_v}{\rho_m}\left[\frac{2}{3}\left(\frac{P - P_v}{\rho_l}\right)\right]^{\frac{1}{2}} \quad \text{5-74}$$

6. PROPOSED COMPUTATIONAL FLUID DYNAMICS (CFD) MODEL AND VALIDATION

This chapter is devoted to a presentation of a proposed CFD model for flashing flow. After that, validation of the results and sensitivity analysis on turbulence quantities and semi-emperical coefficients are performed.

6.1. Multi-phase flow model

In this thesis, the mixture model has been applied to model two-phase flow. Within the mixture approach, a slip model is used to couple the two phases (liquid and vapour); the mass, momentum and energy governing equations. Details of the mixture model considering relative motion between the two phases are presented in section 5.3.1

6.2. Phase change model

In this work, the Lee model, detailed in section 5.4.1.1, is modified to become the phase change model driven by pressure. In addition, the thermal non-equilibrium effect is inserted into the present phase change model by "*artificial coefficients*" as defined in the following of section.

The first step is to define the vapor transport equation, which is solved along with the other governing equations:

$$\frac{\partial(\alpha_v \rho_v)}{\partial t} + \nabla \cdot (\alpha_v \rho_v \vec{v}_m) = \dot{m} \qquad 6\text{-}1$$

The change of phase source terms is derived from Hertz [88] with the evaporation-condensation flux at the interface F similar to Eq. *5-33*

$$F = \beta \sqrt{\frac{M}{2\pi R T_{\text{sat}}}} (P_{\text{sat}} - P^*) \qquad 6\text{-}2$$

where M is molar mass. P^* is the partial pressure at interface on the vapor side with value close to saturation pressure, P_{sat}.Eq. 6-2, can be inserted into the vapor transport equation as a source term, should be modified to take into account the interfacial area density. Particularly in this thesis, the interfacial area density is applied following the proposal of Liao and Lucas [68], as defined in Eq. 6-3:

$$A_i = (6\alpha_v)^{2/3} (\pi N_b)^{1/3} \qquad 6\text{-}3$$

Combining Eq. 6-2 and Eq. 6-3, the source term for the vapor transport equation at the interface is defined as:

$$\dot{m} = F A_i = A_i \beta \sqrt{\frac{M}{2\pi R T_{\text{sat}}}} (P_{\text{sat}} - P^*) \qquad 6\text{-}4$$

In this paper, the formula of the vaporization pressure, P_v as defined in Hinze [94], is used to account for local turbulence effects. It reads as follows:

$$P_v = P_{\text{sat}} + 0.195\rho k \quad (6\text{-}5)$$

It should be noticed that, Eq. 6-5 is also used in some cavitation models presented in section 5.4.2

Finally, considering Eq. 6-5 along with Eq. 6-4, the source term for the mass flux at the interface is as follows:

$$\dot{m} = FA_i = A_i\beta\sqrt{\frac{M}{2\pi RT_{\text{sat}}}}(P_v - P^*) \quad (6\text{-}6)$$

6.3. Turbulence model

The turbulence behavior has been treated using RANS approaches. In particular, six RANS turbulence models have been tested and compared: (i) *k-ε* Standard, (ii) *k-ε* Realizable, (iii) *k-ε* RNG, (iv) *k-ω* Standard, (v) *k-ω* SST and (vi) RSM. The reader should refer to section 5.2 for further information concerning RANS approaches and the near wall treatments.

6.4. CFD validation

6.4.1. Experimental benchmark

For flow without phase change, the experimental data provided by Charless in Charless [31], **Figure 6.1**, inside a convergent-divergent nozzle are used as reference.

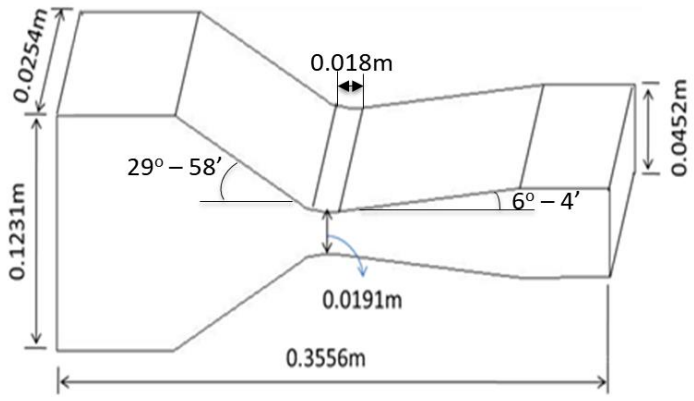

Figure 6.1: *Geometrical details of the convergent-divergent nozzle in Charless* [31]

The tested conditions are two-phase air/water flow presented in **Table 6-1**:

Table 6-1: *Operating conditions and case code of Air/liquid flow are available in Charless* [31]

Air/Water flow	Upstream inlet pressure (Pa)	Mixture inlet temperature (K)	Inlet air mass fraction [-]
AW1	359492.64	302.66	0.915
AW2	350529.46	302.72	0.894
AW3	376660.59	290.11	0.901
AW4	330258.87	290.17	0.882
AW5	328466.23	290.00	0.899
AW6	344048.38	289.22	0.908

For the case of flashing flow , the experimental data, proposed in Abuaf et al. [15], have been used. The considered benchmark deals with a vertical circular convergent-divergent nozzle, with initially sub-cooled water at the nozzle inlet. **Figure 6.2** shows the dimensions of the nozzle. The operating conditions of the experiment (i.e., pressure, temperature and mass flow rates) are listed in **Table 6-2**. The experimental setup includes the steady flow of water which is throttled through the nozzle and is built to measure net rates of vaporization with non-equilibrium effects. On the wall inside the converging-diverging nozzle, 49 taps and two available windows for observation at inlet and outlet are set up to measure global and local quantities including: mass flow rate, averaged vapor fraction, pressure, distributions along nozzle, flashing inception point and 27 radial positions to measure transverse vapor distribution.

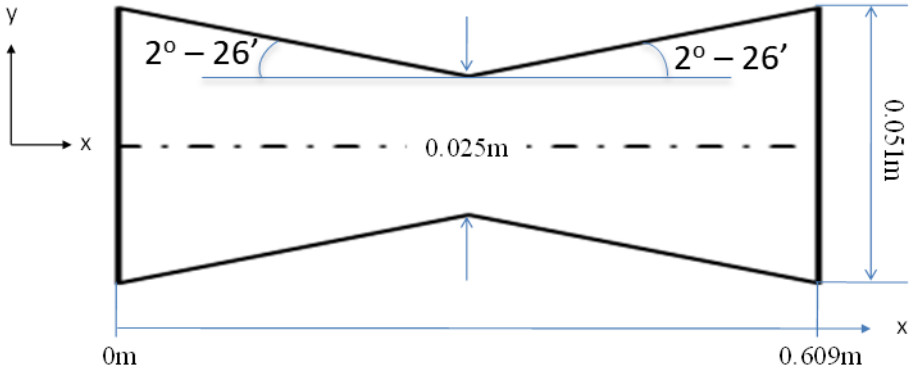

Figure 6.2: *Vertical circular convergent-divergent nozzle in Abuaf et al. [15]*

Table 6-2: *Operating conditions and case code names of flashing flow in Abuaf et al. [15]*

Case code name	Upstream pressure [Pa]	Inlet temperature [K]	Outlet pressure [Pa]	Flashing inception pressure [Pa]	Saturation pressure [Pa]	Mass flow rate [kg/s]
BNL284	530000	422.35	456000	404700	466000	7.3
BNL309	555900	422.25	402500	393500	464800	8.8
BNL273	573500	421.85	442100	419200	459800	8.7
BNL268	575200	422.05	443000	405700	462300	8.7
BNL304	577700	422.15	441000	399700	463500	8.8
BNL278	688600	421.95	434100	425700	461000	11.7
BNL296	764900	421.95	432600	417000	461000	13.1

6.4.2. Validation of mixture model without phase change phenomenon

6.4.2.1. Numerical domain and boundary conditions

In this validation, the experimental benchmark for air/water flow of Charless [31], presented in **Figure 6.1** and **Table 6-1**, is used.

The computational mesh and boundary conditions are shown in **Figure 6.3** and **Table 6-3**. The mesh is based on quadratic cells with skewness quality below 0.52. Mesh sensitivity analysis has been performed; particularly, a coarse mesh (15751 elements) and a finer one (25457 elements) were compared. The discrepancies of numerical results in terms of mass flow rate are below 2% between the two meshes. Therefore, the coarse mesh can be adopted. Standard $k-\varepsilon$ turbulence model is chosen in this validation with boundary condition values for k and ε at inlet are adopted to be $0.1 m^2 s^{-2}$ and $0.1 m^2 s^{-3}$, respectively.

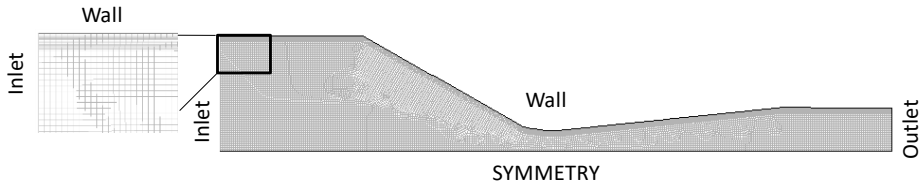

Figure 6.3: *Computational grid and boundary conditions corresponding to experiment of Charless* [31]

Table 6-3: *boundary conditions corresponding to experiment of Charless* [31]

Boundary	Flow boundary	Turbulence boundary
Inlet	Total pressure	Turbulence intensity and hydraulic diameter
Outlet	Static pressure	
Wall	Adiabatic wall	Wall function
SYMMETRY	SYMMETRY	SYMMETRY

6.4.2.2. Numerical set-up

In this study, the commercial code ANSYS Fluent rel.16.0 is used for modeling. The PISO method for solving the pressure-velocity coupling is used. The Green-Gauss Cell Based solver for gradient discretization, second order upwind for spatial discretization of all other quantities, except volume fraction for which a first order upwind scheme for the purpose of solution stabilization are specified. A convergence criterion has been applied in the order of 10^{-6} for all variables and mass balance between inlet and outlet around 2%.

6.4.2.3. Numerical results

The comparison between the computed mass flow rate and experimental data for all available operating conditions are performed (shown in ***Figure 6.4*** and ***Table 6-4***) with an average and maximum relative error equal to 3.9% and 5.9% (case AW2), respectively.

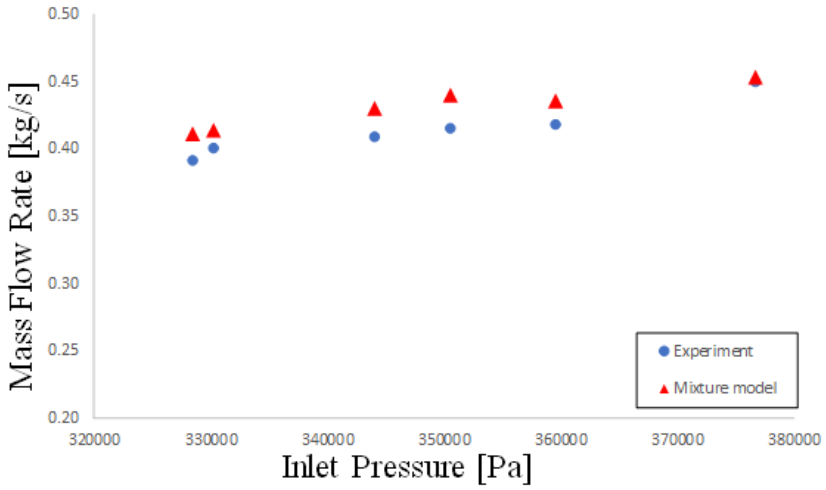

Figure 6.4: *Comparison between experimental mass flow rate Charless* [31] *and CFD mass flow rate*

Table 6-4: *Comparison of Experimental Mass Flow Rate in Charless* [31] *and CFD Mass Flow Rate*

Air/Water flow	Experimental Mass Flow Rate (kg/s)	CFD Mass Flow Rate (kg/s)	Relative error
AW1	0.417895	0.435	4.1%
AW2	0.414737	0.4395	5.9%
AW3	0.449474	0.453	0.07%
AW4	0.4	0.4135	3.4%
AW5	0.390526	0.4105	5.1%
AW6	0.408421	0.4295	5.2%

It should be noticed that the trend of mass flow rate is very clear showing that the increase of mass flow rate corresponds to the increase of pressure difference between inlet and outlet. Besides, Numerical results show an over-prediction compared to experimental data. This can be explained by the simplification of mixture model that only considers relative motions between two phases. Generally, the momentum interaction between two phases is a key factor for accuracy in this simulation, thus, a more complete model such as the Eulerian model, which accounts for interaction forces between two phases, should be considered.

The velocity magnitude field and static pressure field for case AW3 are presented in **Figure 6.5** and ***Figure 6.6***. Results are appropriate to physical behaviour of flow inside nozzle when maximum velocity magnitude corresponds to minimum pressure at convergent part of nozzle.

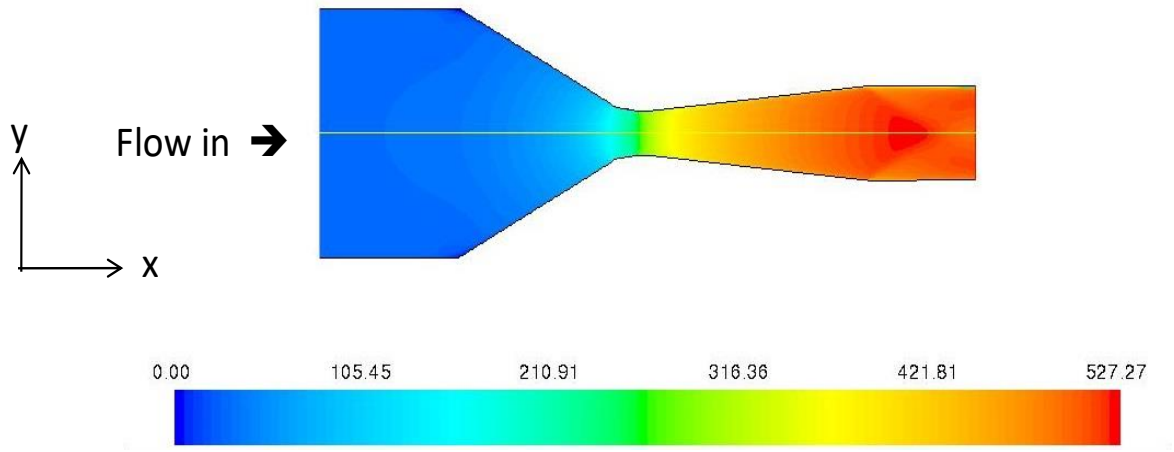

Figure 6.5: *Velocity magnitude field of AW3*

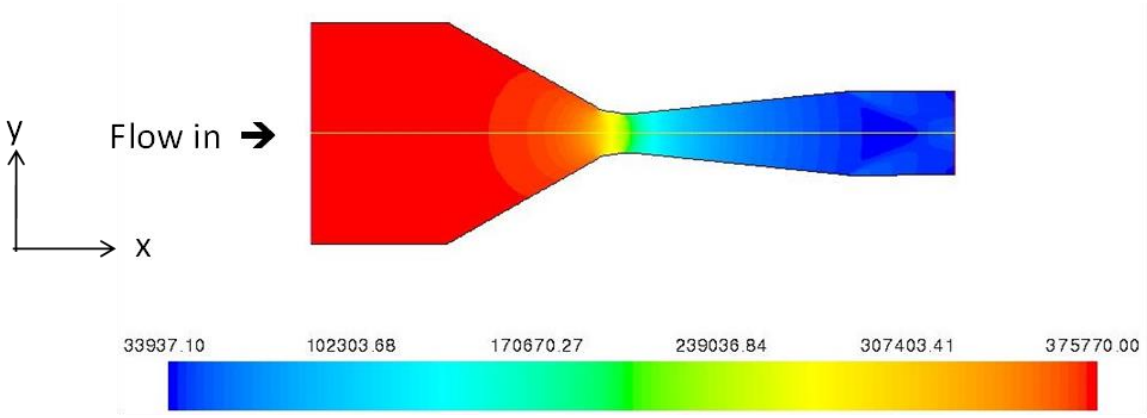

Figure 6.6: *Static pressure field of AW3*

Presenting the results of the velocity field and static pressure field help to understand the behavior of the vena-contracta inside the nozzle. Case AW3 shows the vena-contracta point, corresponding to the minimum static pressure point, is located in the divergent part of nozzle and the distance is far from the throat. It also reveals that the flow goes through throat without any fluctuation. This information will be provided to calculate the recovery factor, F_L, which involves the pressure recovery going through vena-contracta.

6.4.3. Validation of mixture model with phase change phenomenon

6.4.3.1. Numerical domain and boundary conditions

The computational domain has been set up with structured quadrilateral elements (maximum skewness below 0.05, minimum orthogonally higher 0.95) and a 2D-axisymmetric approach is taken. **Figure 6.7** and **Table 6-5** show mesh and boundary conditions used for the simulations. It should be noticed that a grid independency study and sensitivity analysis for the turbulence boundary conditions have been discussed in section 6.4.3.3.

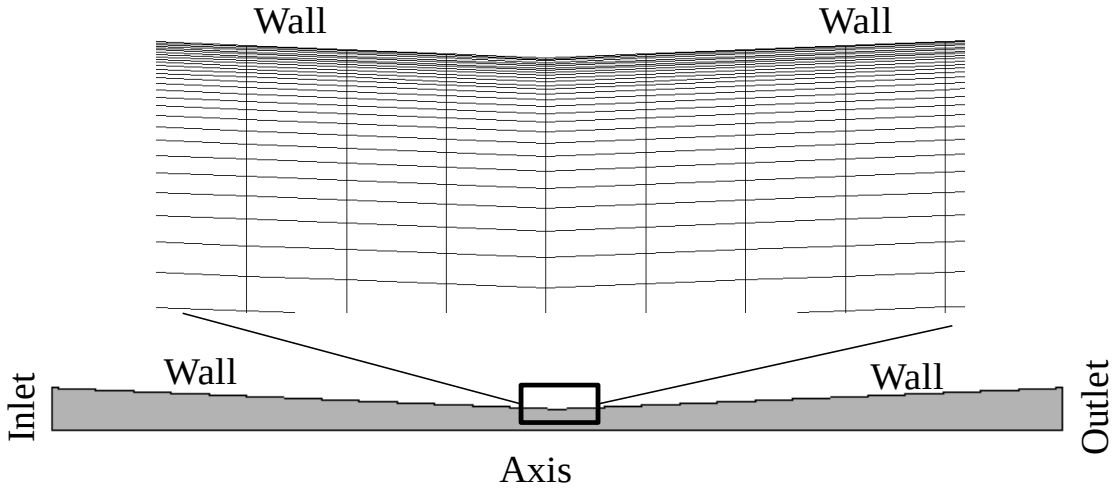

Figure 6.7: *Mesh and boundary condition of convergent-divergent nozzle corresponding to experiment of Abuaf et al. [15]*

Table 6-5: *Boundary conditions corresponding to experiment of Abuaf et al. [15]*

Boundary	Flow boundary	Turbulence boundary
Inlet	Total pressure	Turbulence intensity and hydraulic diameter
Outlet	Static pressure	
Wall	Adiabatic wall	Wall function
Axis	Axis	Axis

6.4.3.2. Numerical set-up

The proposed approach uses PISO for Pressure-Velocity Coupling algorithm and Second Order Implicit scheme for transient formula with spatial discretization of quantities presented in **Table 6-6**. Transient equations are used to establish a steady solution with a steady criteria: mass balance between inlet and outlet are below 0.2% and the residuals for all the other quantities are below 10^{-6}. Bubble number density, maximum of difference between P^* and P_{sat} ($dp = P_{\text{sat}} - P^*$) are fixed to $4 \cdot 10^8$ and 75Pa, respectively. The accommodation coefficient used to tune the boiling delay effect has been in the range from 0.8 to 1.2 for specific test cases. It is worth noting that a vapor fraction of 1e-5 has been imposed at the inlet to initiate the phase change process.

Table 6-6: *Numerical method*

Spatial discretization	Scheme
Gradient	Green-Gauss Cell Based
Pressure	PRESTO!
Density	Second Order Upwind
Momentum	
Volume Fraction	
Turbulence Kinetic Energy	
Specific Dissipation Rate	
Energy	

6.4.3.3. Sensitivity analysis

In this section, sensitivity analysis has been performed concerning (i) grid convergence index (GCI), (ii) RANS modelling approaches, (iii) near-wall treatments, (iv) turbulence inlet parameters and (v) semi-empirical coefficients.

a) Grid convergence index (GCI)

In order to assess the grid independency, a GCI has been analyzed on case of BNL309 with 4 different meshes and a range of y^+ from 6 to 16. The four computational domains consist of (a) 21350, (b) 53184, (c) 109728 and (d) 214650 elements with a factor approximately 2 $\left(\frac{N_{i+1}}{N_i} \approx 2\right)$. Results of the grid independency research are presented in **Table 6-7** including (i) the mass flow rate, (ii) the averaged outlet vapor fraction and (iii) the averaged radial turbulence kinetic energy at the throat for GCI. Finally, a mesh of 109728 elements has been used for the remaining of the analyses.

Table 6-7: *Mesh independency study: Grid Convergence Index*

Mesh elements	Mass flow rate (kg/s)	Outlet averaged vapor fraction	Radial averaged turbulence kinetic energy at throat (m^2/s^2)
21350	8.63	0.765132	0.138114
53184	8.79	0.762243	0.125219
109728	8.82	0.762015	0.123920
214650	8.82	0.762013	0.123901

Table 6-8 presents the influence of the near wall refinement (in terms of y^+) on mass flow rate of BNL309: a negligible influence can be observed. Indeed, a mesh having $y^+ \approx 1$ is similar to the numerical results obtained with the mesh having $y^+ > 1$ in term of mass flow rate. In addition, **Figure 6.8** presents the influence of y^+ on the velocity magnitude at the centerline: all the numerical results show a negligible deviation between $y^+ \approx 1$ and $y^+ > 1$.

Table 6-8: *Effects of y^+ on the Mass Flow Rate in case BNL309*

	$0.6 < y^+ < 1.8$	$1 < y^+ < 3$	$6 < y^+ < 16$
Mass flow rate (kg/s)	8.8	8.8	8.8

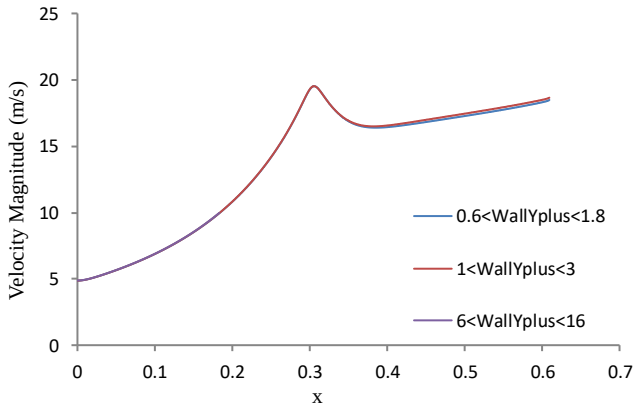

Figure 6.8: *Influence of y^+ on the velocity magnitude at the center line*

b) <u>Screening of turbulence models</u>

The relative errors for case BNL309 between the numerical models and the experimental data in term of mass flow rate are summarized in **Table 6-9**. As previously stated, in this thesis, six turbulence RANS models including (i) *k-ε* Standard, (ii) *k-ε* Realizable, (iii) *k-ε* RNG, (iv) *k-ω* Standard, (v) *k-ω* Standard and (vi) RSM with different wall treatments have been used in conjunction withpresent flashing flow model to analyze the influences of turbulence model to phase change process.

Table 6-9: Mass Flow Rate Relative Error $\left(\frac{\dot{M}_{CFD}-\dot{M}_{experiment}}{\dot{M}_{experiment}}\right)$ of BNL309 in Analysis of Turbulence Models and Wall Treatments

Wall treatment	$k-\epsilon$ ***Standard***	$k-\epsilon$ ***Relizable***	$k-\epsilon$ ***RNG***	***RSM***
Standard Wall Function	-3.9%	+0.1%	-2.5%	-0.1%
Non-Equilibrium Wall Function	-5.9%	-2.1%	-4.7%	-1.2%
Scalable Wall Function	-3.7%	+0.1%	-2.3%	-0.2%
Enhanced Wall Treatment	-4.1%	-1.3%	-3.2%	-3.0%
$k-\omega$ **options**	$k-\omega$ *Standard*	$k-\omega$ *SST*		
Standard	+1.7%	+0.2%		
Low-Re Corrections	+4.0%	+2.0%		

Six RANS models with wall treatments have presented acceptable relative error (range of relative error <6%). In particular, $k-\varepsilon$ Standard has given larger errors, ranging from -3.9% to -5.9% (under-estimation) compared with the other RANS turbulence models. A better agreement to the experimental data has been observed with $k-\varepsilon$ Realizable and $k-\omega\ SST$ models with a range of errors is in (+0.1% to-1.3%) and (+0.2% to -2%), respectively. In addition, a local analysis of transverse vapor distribution with influences of turbulence RANS models has been analyzed and presented in **Figure 6.9**; A summary of the results is, finally, given in **Table 6-9**. $k-\varepsilon\ Standard$ shows higher vapor volume fraction at the center region of the nozzle compared to measurements from point x=0.559m to the outlet of the nozzle corresponding to lower mass flow rate in **Table 6-9**. Nevertheless, there has been no significant difference of transverse vapor profiles with different turbulence RANS models. Finally, $k-\omega$ SST with Standard option gives the best agreement to measurements in both global and local quantities. For this reason, $k-\omega$ SST with Standard option has been used for the other analyses.

Section A (x=0.306m)

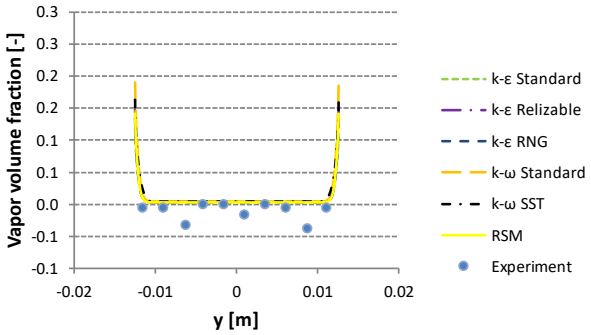

Section B (x=0.319m)

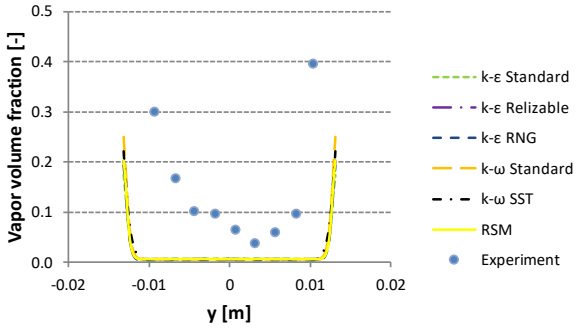

Section C (x=0.332m)

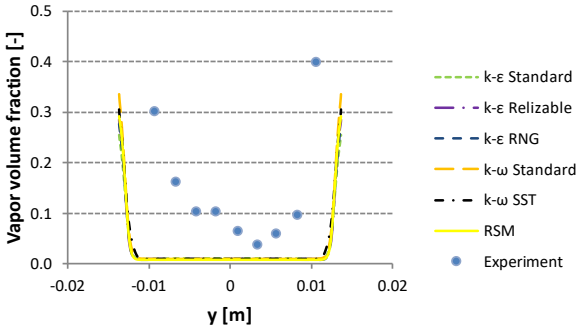

Section D (x=0.344m)

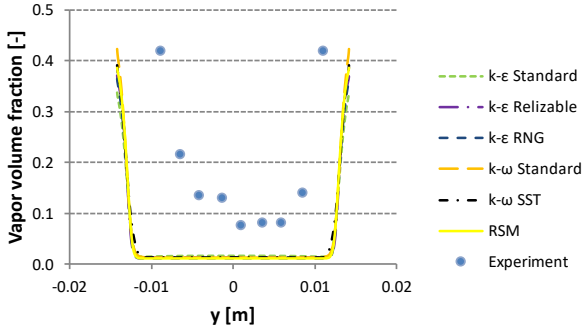

Section E (x=0.357m)

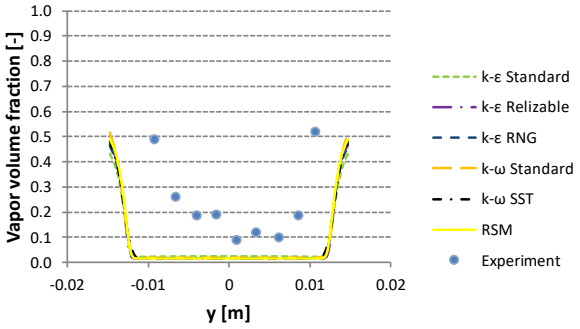

Section F (x=0.382m)

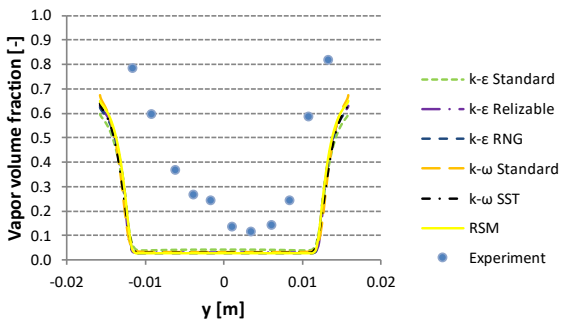

Section G (x=0.407m)

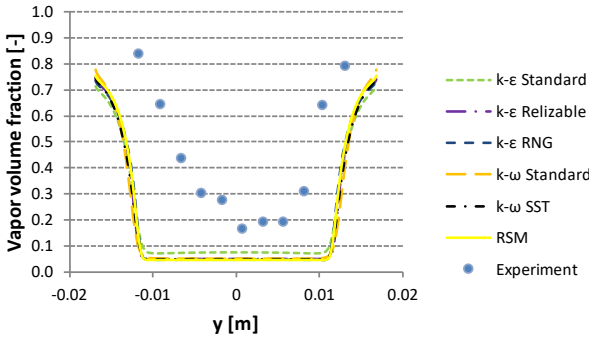

Section H (x=0.433m)

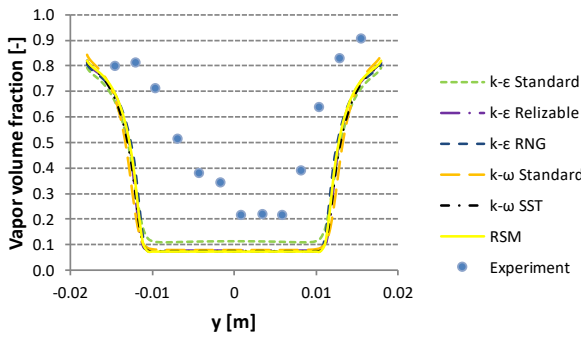

Section I (x=0.458m)

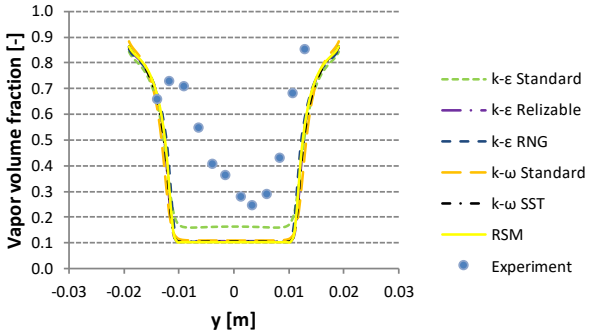

Section J (x=0.483m)

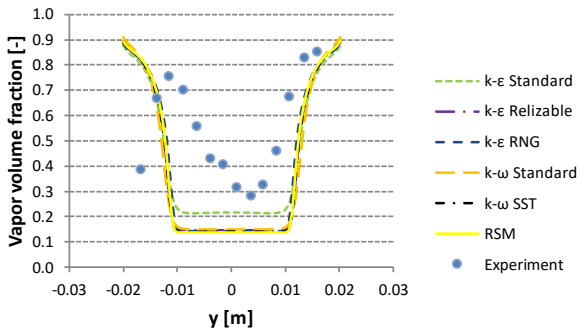

Section K (x=0.508m)

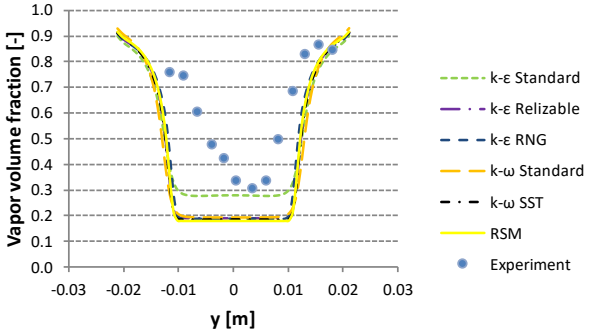

Section L (x=0.534m)

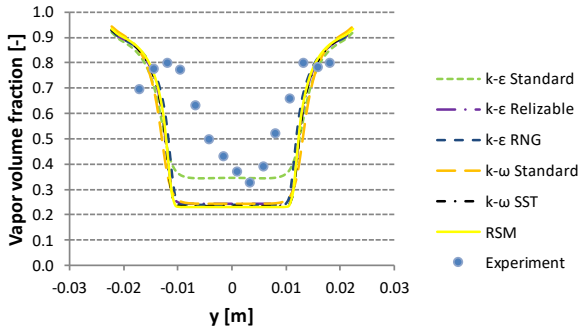

Section M (x=0.559m) Section N (x=0.577m)

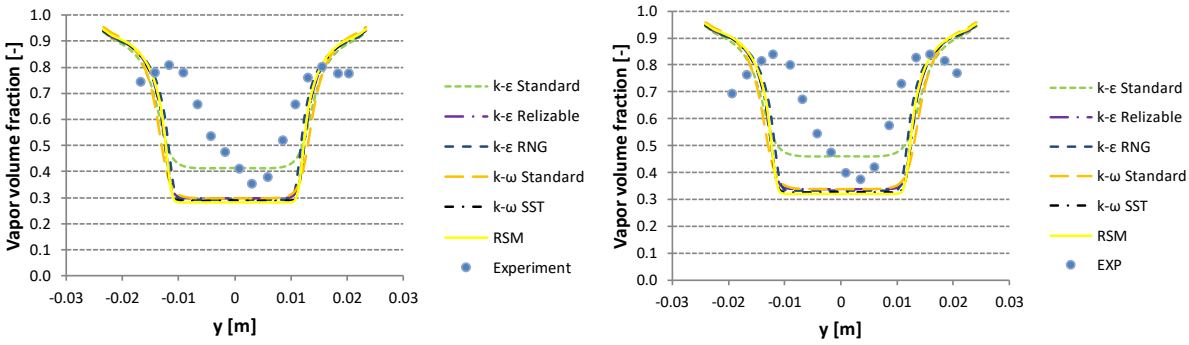

Figure 6.9: *Section description and Radial vapor profile with effects of turbulence RANS models*

c) *Turbulence inlet intensity*

The turbulence boundary conditions at the inlet have been imposed by: (i) the hydraulic diameter and (ii) the turbulence intensity. The hydraulic diameter has been equal to 0.051m according to the real geometry. Conversely, the turbulence intensity has been analyzed in the range from 1% to 5% on case BNL309. **Figure 6.10** and **Table 6-10** shows the impact of the turbulent intensity at the inlet on (i) the mass flow rate, (ii) the averaged vapor volume fraction along the nozzle and (iii) the vapor volume fraction profile at x=0.577m. The numerical results show high sensitivity to the turbulence inlet boundary condition and from a theoretical point of view, an analysis on uncertainty of turbulence inlet should be performed. Turbulence inlet intensity of 1% has been used in other calculations.

a) vapor fraction along center line

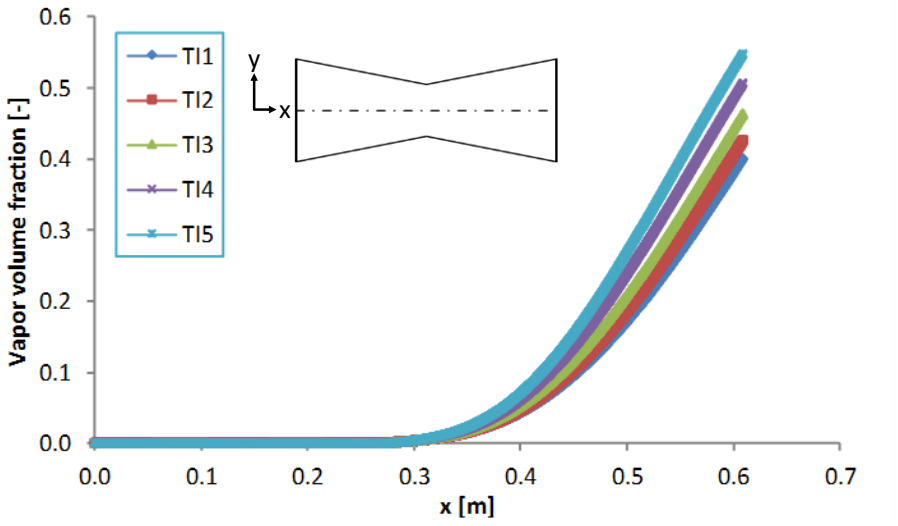

b) radial vapor profile at x=0.577m

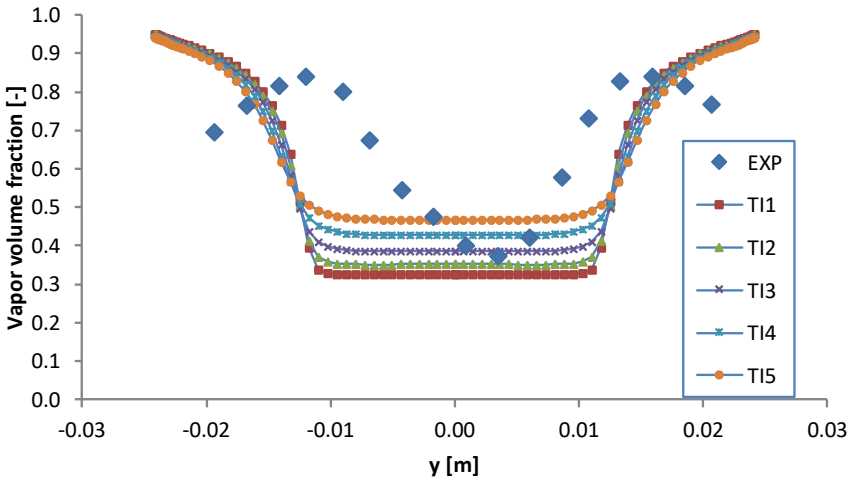

Figure 6.10: *Influence of turbulence inlet intensity to numerical results*

Table 6-10: *Sensitivity of turbulence inlet intensity to mass flow rate in case of BNL309*

Turbulence Inlet Intensity	**1%**	**2%**	**3%**	**4%**	**5%**
Mass Flow Rate (kg/s)	8.82	8.78	8.76	8.70	8.64
Relative Error compared to experimental data	0.2%	-0.2%	-0.4%	-1.1%	-1.8%

d) Artificial coefficients for thermal non-equilibrium effect

The boiling delay effect has been modelled and controlled by the artificial coefficients including the accommodation coefficient, β, and difference between saturation pressure and vapour partial pressure at the interface on the vapor side, dp, (details presented in section 6.2). The influence of these coefficients on the flashing flow model has been presented in ***Figure 6.11***. there is a clear trend of increase the averaged vapor fraction corresponding to an increase in the artificial coefficients. The static pressure line shows an increase near nozzle throat when increasing the artificial coefficients.

a) Vapor profile with artificial coefficients

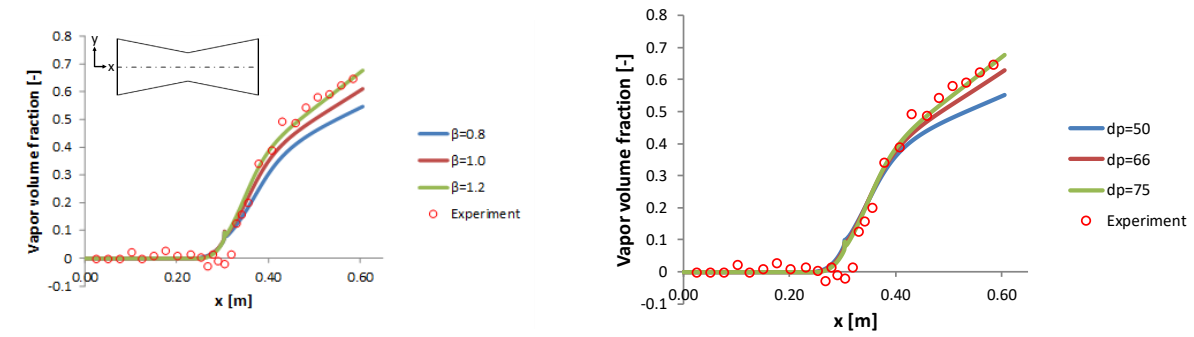

b) Static pressure with artificial coefficients

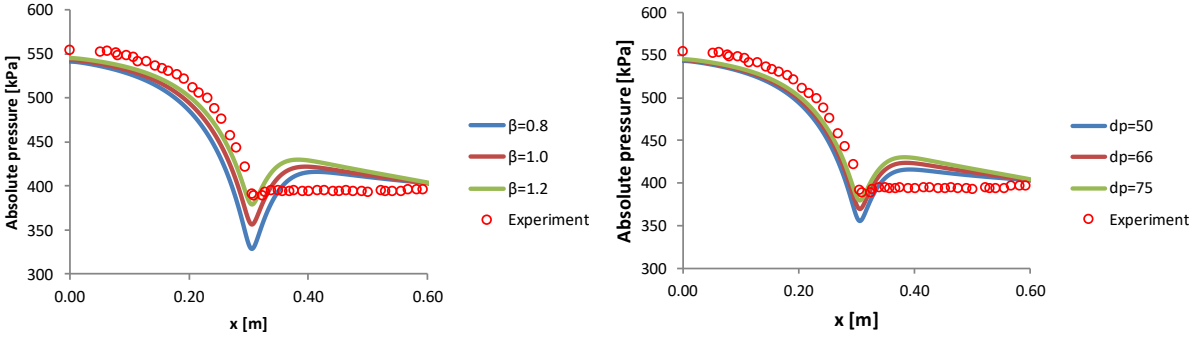

Figure 6.11: *Artificial coefficients sensitivity in BNL309*

6.4.3.4. Numerical results

In this section, a comparison is performed between the present model, the phase change model driven by interfacial heat transfer in Liao and Lucas [68] and the experimental data of Abuaf et al. [15] for both global and local quantities.

The present model is different from the model of Liao and Lucas [68] which requires experimental data for the bubble number density from Wu et al. [95] to tune the boiling delay effect. In the proposed CFD model, the nucleation stage has been neglected and the boiling delay effect has been controlled by the accommodation coefficient. The bubble number density, N_b, in this study is fixed to $4 \cdot 10^8$ for all tested cases.

a) <u>Global results</u>

Various operating conditions of the experimental benchmarking case have been performed here, comparing mass flow rate, vapour volume fraction and absolute pressure.

In **Table 6-11**, the CFD mass flow rate has been compared to measurements for all available operating conditions, showing a minimum and maximum relative error equal to 0.2% and 6.8%, respectively (please notice that the accommodation coefficient is approximately one for all cases).

Table 6-11: *Comparison of Experimental Mass Flow Rate in Abuaf et al.* [15] *and CFD Mass Flow Rate*

Cases	Accommodation coefficient β	Experimental Mass Flow Rate (kg/s)	CFD Mass Flow Rate (kg/s)	Relative error
BNL284	0.8	7.3	7.7	+5.4%
BNL309	1.2	8.8	8.8	+0.2%
BNL273	1.05	8.7	9.3	+6.8%
BNL268	1.0	8.7	9.2	+5.7%
BNL304	1.11	8.8	9.1	+3.4%
BNL278	1.15	11.7	12.3	+5.1%
BNL296	1.18	13.1	13.9	+6.1%

A more specific comparison has been performed in terms of averaged vapor volume fraction and absolute pressure along the convergent-divergent nozzle in **Figure 6.12** for all tested cases. The results show the general agreement of the present model to experiment of Abuaf et al. [15] and the capability to capture the position of flashing inception (Please notice that this position is near the nozzle throat at x=0.3045m). Moreover, for most of operating conditions (BNL268, BNL273, BNL284, BNL304 and BNL309) the averaged vapor volume fraction along the convergent-divergent nozzle has been well predicted, differently from Liao and Lucas [68] that shows an over-prediction of the value for all conditions and an under-prediction for the case BNL278 and BNL296.

For the absolute pressure, a slight difference at the divergent section of the convergent-divergent nozzle has been witnessed. This is due to neglecting the effects of pressure drop across the interface and due to the restrictions of the mixture model when ignoring the other interfacial forces such as lift, drag, wall lubrication and turbulent dispersion force. Nevertheless, general trends of both averaged vapor volume fraction and absolute pressure along convergent-divergent nozzle show an agreement to experiment.

BNL268

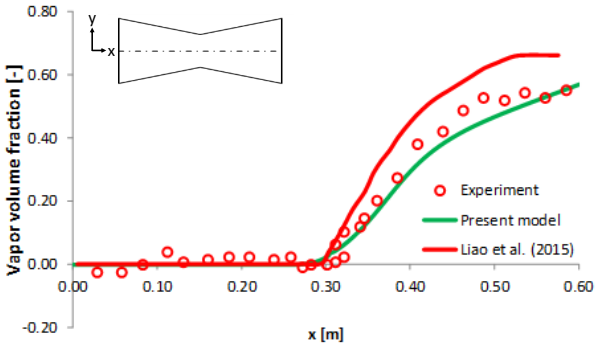

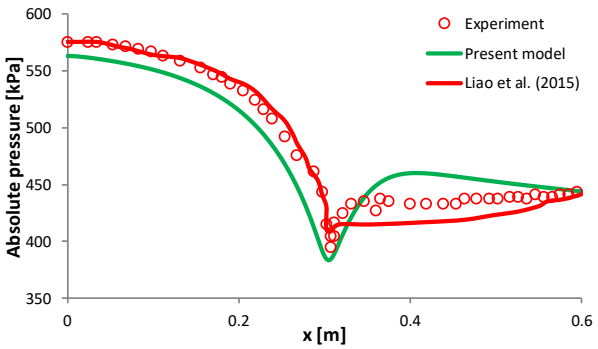

BNL273

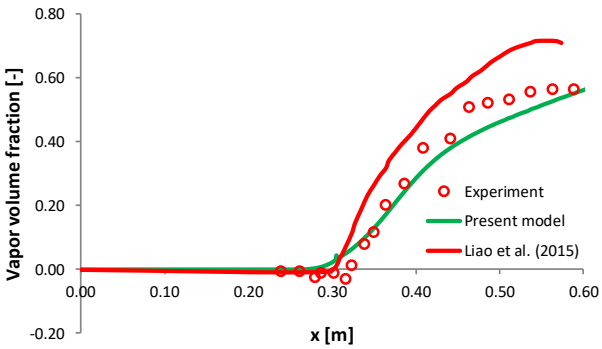

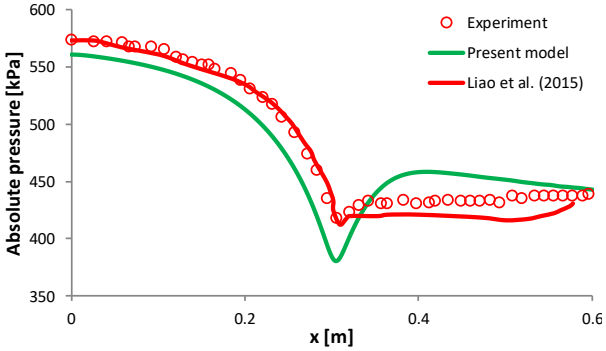

BNL278

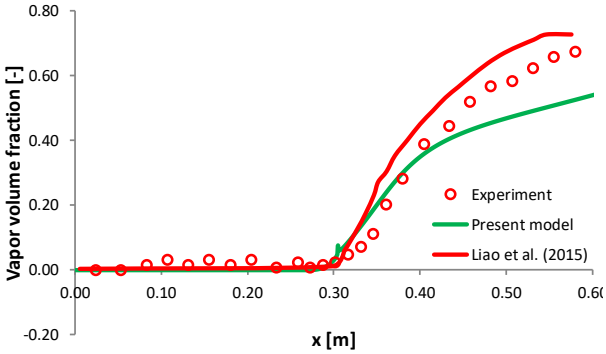

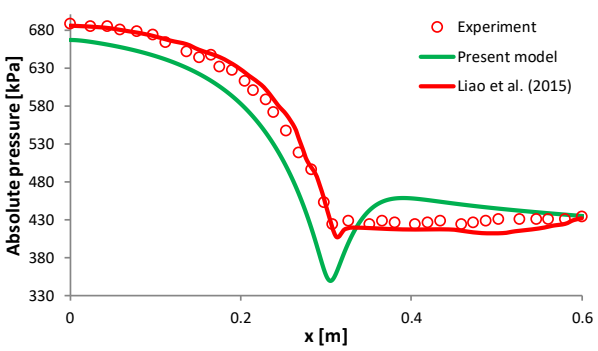

BNL284

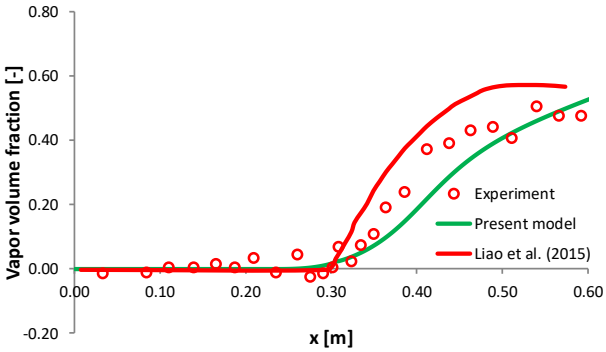

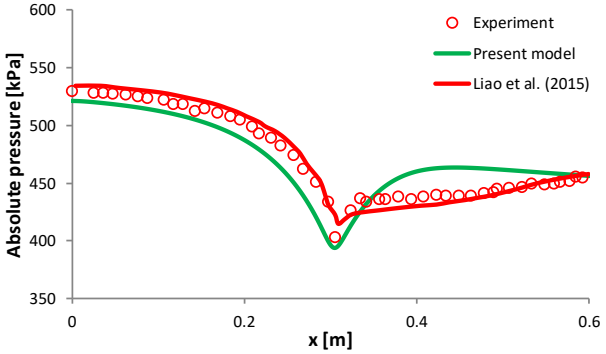

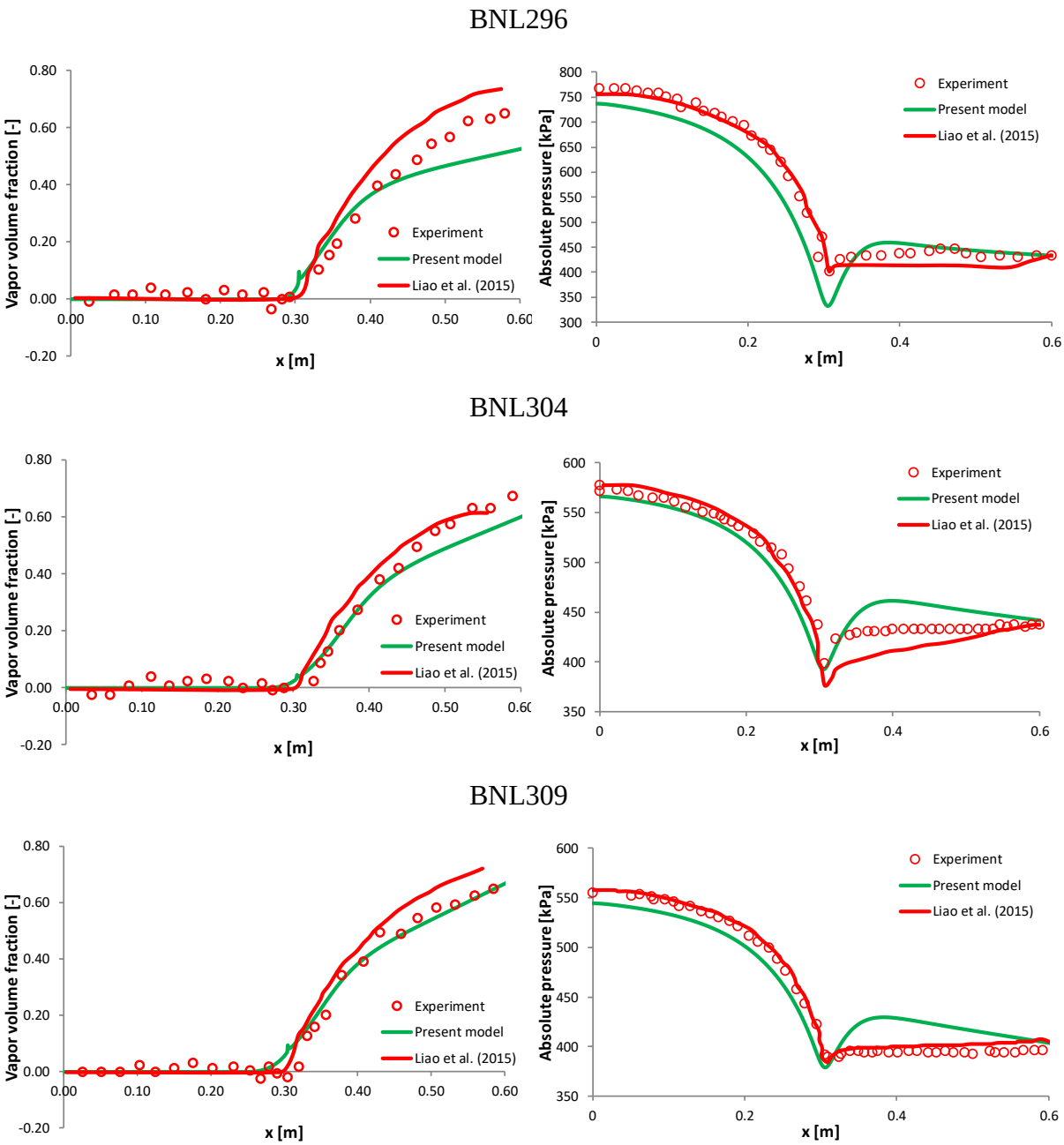

Figure 6.12: *Averaged vapor fraction and absolute pressure along nozzle compared to experimental data in Abuaf et al.* [15] *and Liao and Lucas* [68]

A further comparison with the numerical results of Janet et al. [50] has been carried out. Janet et al. [50] simulated the effects of nucleation and bubble coalescence by using a source term extracted from 1-D physical modelling. In **Figure 6.13a,** the present flashing model has been compared with the CFD results obtained by Janet et al. [50] using various nucleation models, including (i) Blinkov model [45], (ii) RPI model [51]–[53], (iii) RPI model with optimal parameters and(iv) Riznic model [54], [55] for case BNL309. RPI model (default version) and Riznic models show under-estimation in terms of the static pressure near the nozzle throat, and all the models give a good accuracy compared with the experimental data for the averaged vapor volume fraction along nozzle. In **Figure 6.13b** and **Figure 6.13c,** a comparison in terms of the static pressure and averaged vapor fraction is performed for the present flashing model,

Blinkov model and Blinkov model considering the coalescence effect. All models show good agreement with the measurements.

For all analysed global quantities, the proposed CFD flashing model gives good prediction with respect to measurements and other models, considering the nucleation process, available in the existing literature.

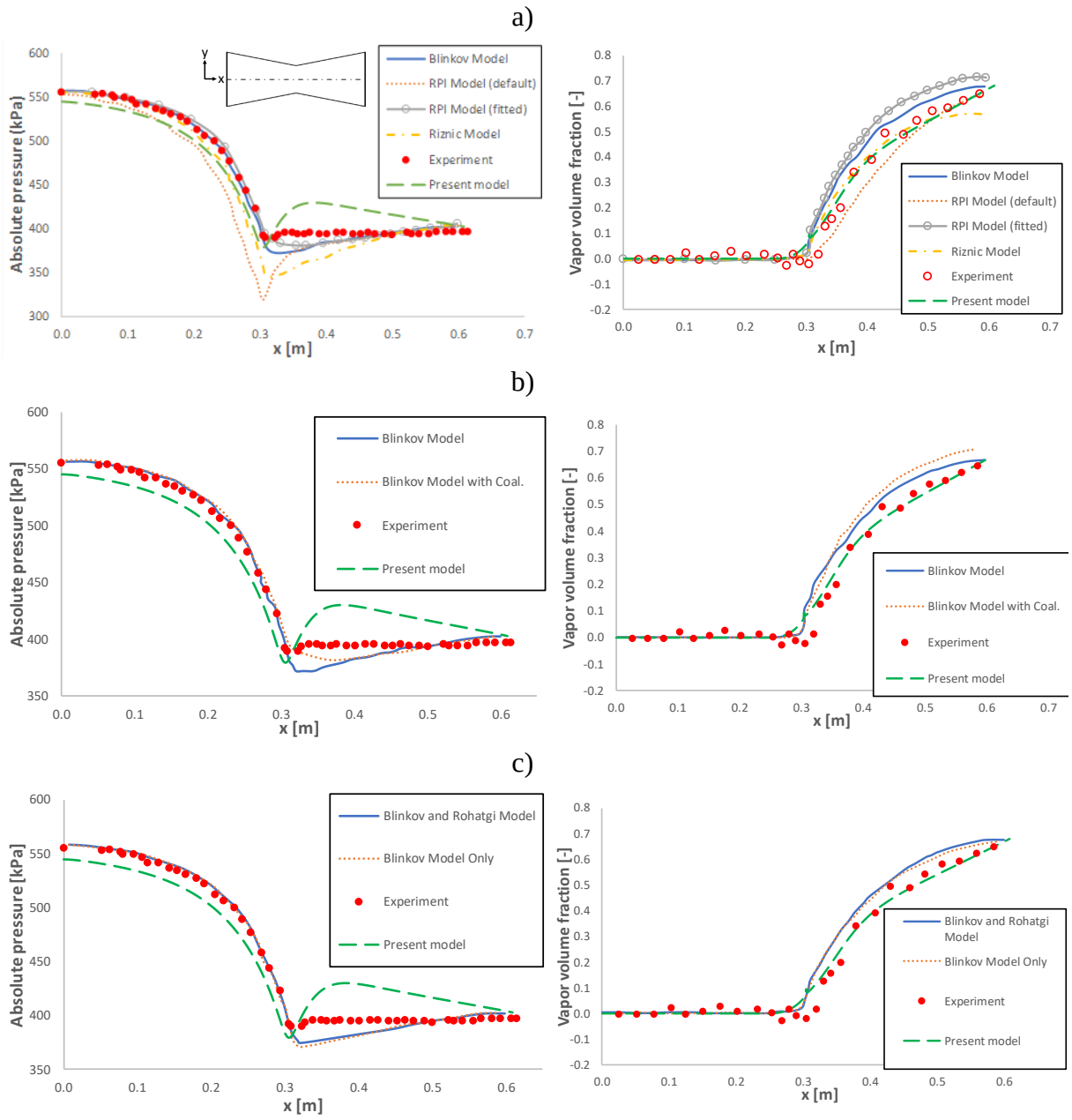

Figure 6.13: *Averaged vapor fraction and absolute pressure along nozzle compared to experimental data Abuaf et al.* [15] *and Janet et al.* [50]

b) Local results

Figure 6.14 and **Figure 6.15** present the transverse vapor volume distribution for BNL309, with 14 positions starting from x=0.306m (near throat) to near the nozzle outlet, at x=0.577m. Results of the present model have been compared to measurements in Abuaf et al. [15] and Liao and Lucas [68] model. At x=0.306 (position A), the experiment shows vapor fraction is equal to zero, whereas the present and Liao models predict a peak near the wall region of the nozzle which implies earlier flashing inception. From x=0.319m to x=0.577m, a peak of vapor fraction near the wall is observed in Liao and Lucas [68] and does not appear in measurements. In addition, in Liao and Lucas [68], vapor volume fraction at the center region also increases faster than experimental data. All the discrepancies described above are explained in Liao and Lucas [68] by unsuitable presumed bubble number density which leads to uncontrollable local behaviors of flashing flow.

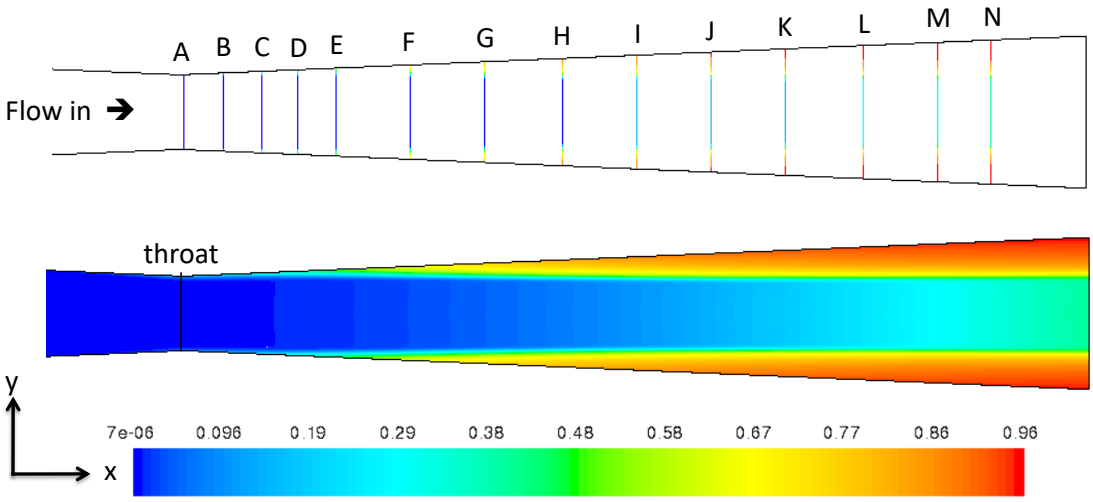

Figure 6.14: *Radial void fraction profile at positions along divergent nozzle*

Section A (x=0.306m)

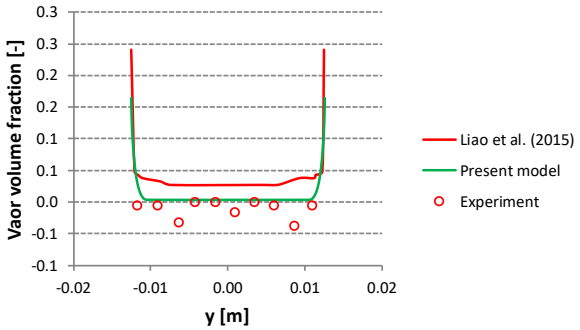

Section B (x=0.319m)

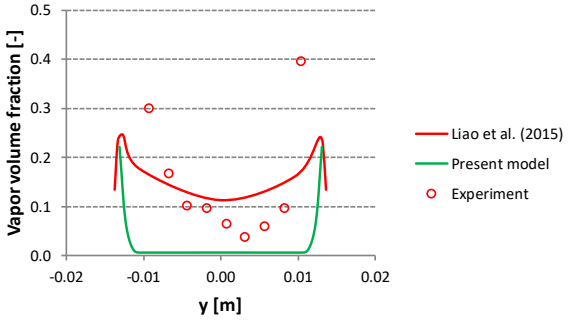

Section C (x=0.332m)

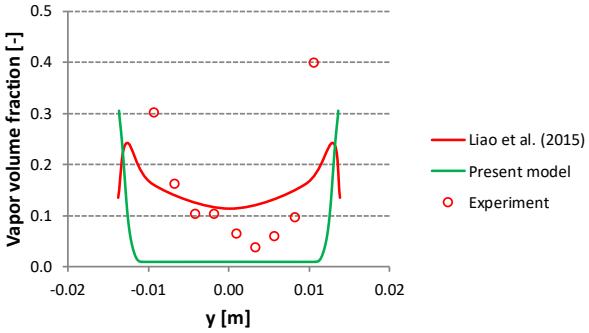

Section D (x=0.344m)

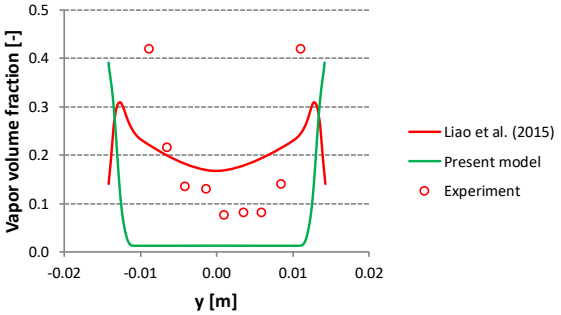

Section E (x=0.357m)

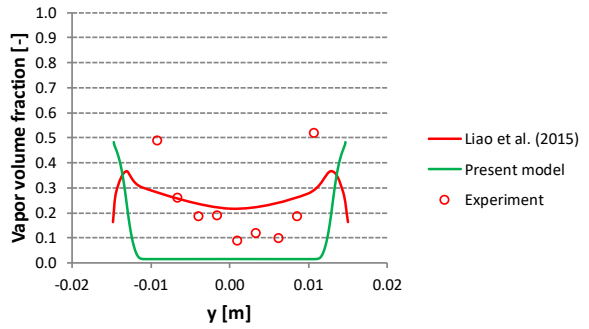

Section F (x=0.382m)

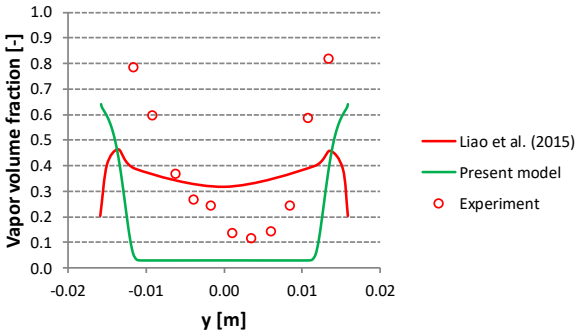

Section G (x=0.407m)

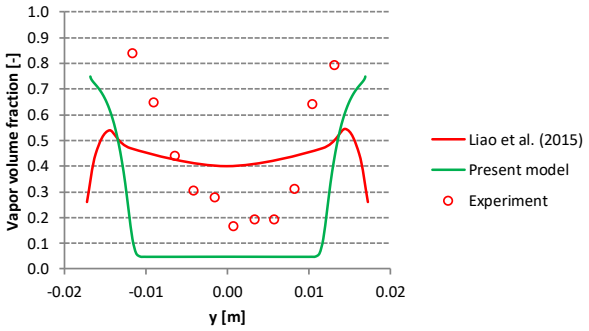

Section H (x=0.433m)

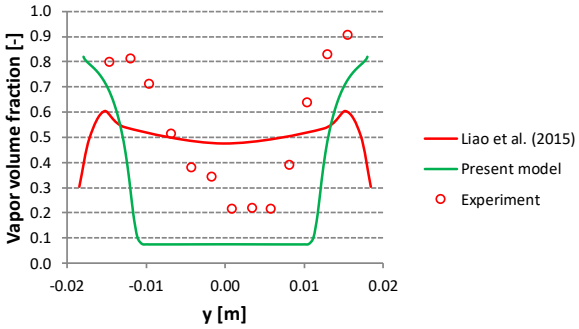

Section I (x=0.458m)

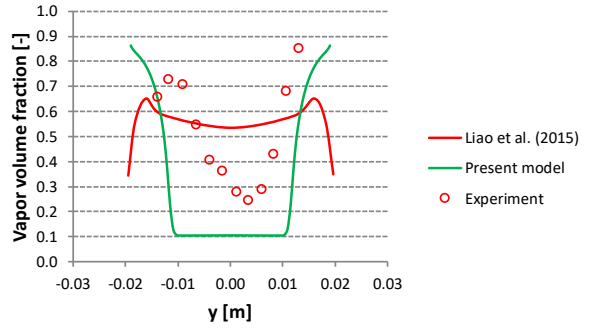

Section J (x=0.483m)

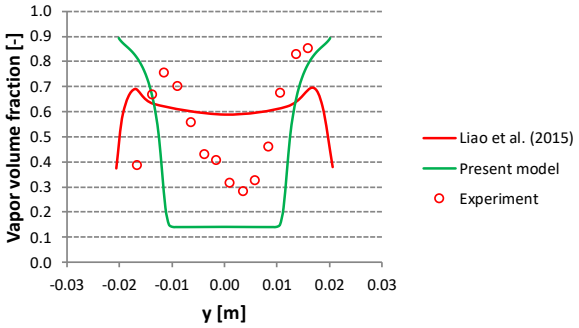

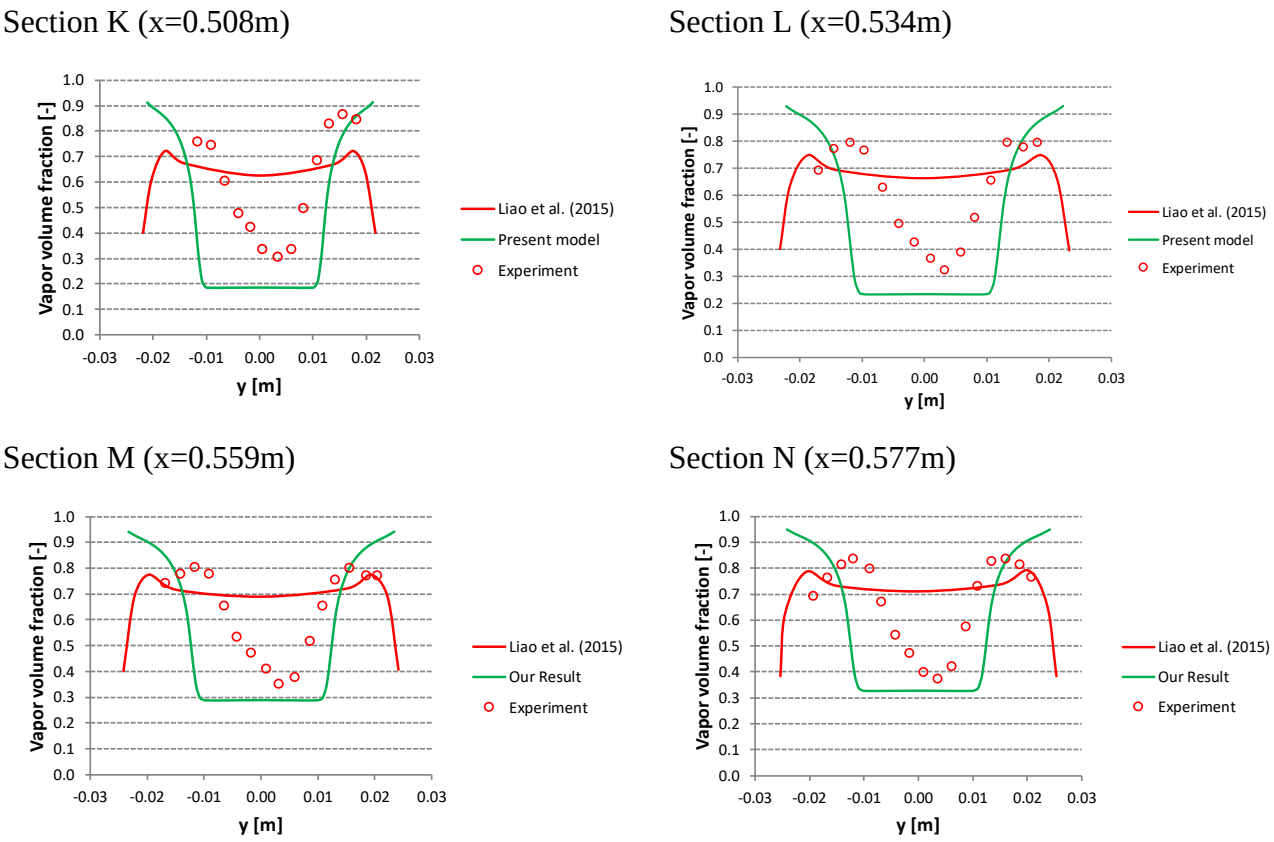

Figure 6.15: *Radial vapor profile of BNL309 compared to experiment Abuaf et al.* [15] *and Liao and Lucas* [68]

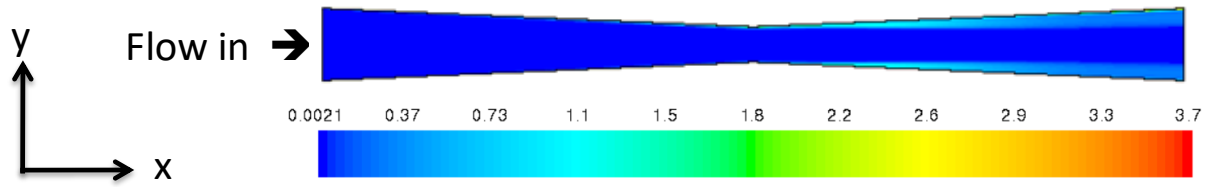

Figure 6.16: *Turbulence kinetic energy field*

The phase change model driven by pressure (present model) is able to better reproduce influences of the local near wall turbulence effects, **Figure 6.16**, to phase change process. **Figure 6.15** shows a better agreement to experiment in the section from x=0.319m to x=0.577m compared to Liao and Lucas [68]. However, local predicted results still present some discrepancies compared to measurements. Indeed, the vapor region thickness near the wall is under-predicted. This can be explained by assumptions within the flashing model which neglects bubble coalescence and migration phenomenon, which have effects of extending the vapor region near the wall. In addition, the migration of bubbles is observed from section H to N in the experimental data, with the vapor volume fraction peak moving from the wall into the bulk region which cannot be captured by the present flashing model, as shown in **Figure 6.15**.

To better reproduce local behavior, the present phase change model should include the impacts of bubble dynamics such as nuclei transport, break-up of bubbles and effects of the phase change process on the momentum and energy conservation equations. Additionally, inter-phase

momentum transfers between vapor and water phase in terms of drag, lift, wall lubrication, virtual mass and turbulent dispersion force should be considered to improve the accuracy of the model, as in Janet et al. [50] and Liao and Lucas [68].

A more complex model from Janet et al. [50] has been compared to the present modeling approach. In Janet et al. [50], the transport equation of the bubble number density, with source terms established from a 1-D nucleation model and coalescence phenomenon, is solved along with governing equations to take into account the nucleation process. Results of Janet et al. [50] show a general under-prediction to the experimental data, especially in the bulk region of the nozzle. The main reason for discrepancies comes from neglecting bulk nucleation effects in the modeling approach. This is different to the present flashing model which is able to capture the development of bulk nucleation by the evaluation of the pressure difference $dp = P_{\mathrm{sat}} - P^{*}$.

Janet et al. [50] developed an original model combining Blinkov and Rohatgi models and included coalescence phenomenon. **Figure 6.17** and **Figure 6.18** show good agreement in term of transverse vapor distribution at x=0.59m among combined model of Blinkov and Rohatgi, the present flashing model and the experiment. The other models still show under-prediction to the experimental data.

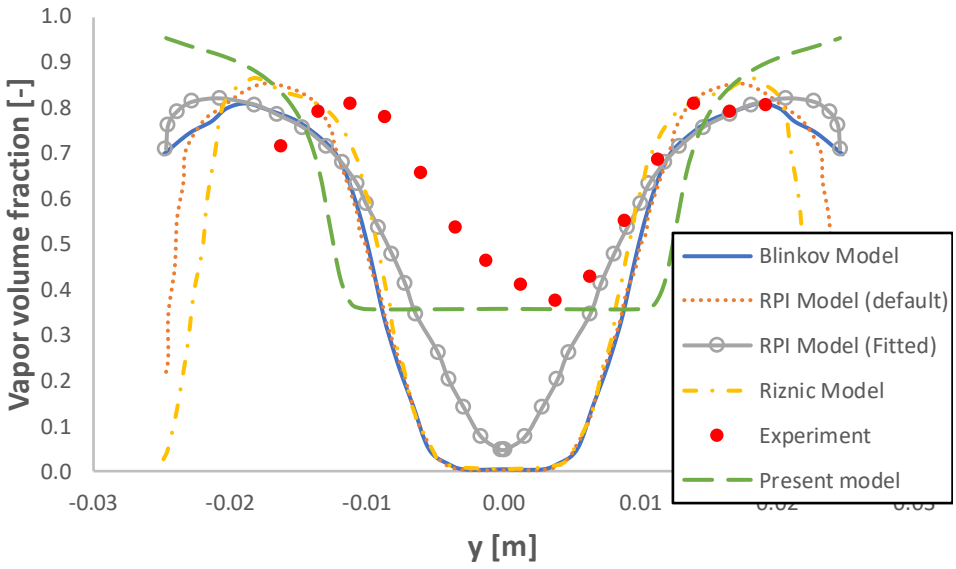

Figure 6.17: *radial vapor fraction in comparison with results of Janet et al.* [50]- *x=0.59m*

a) x=0.59m

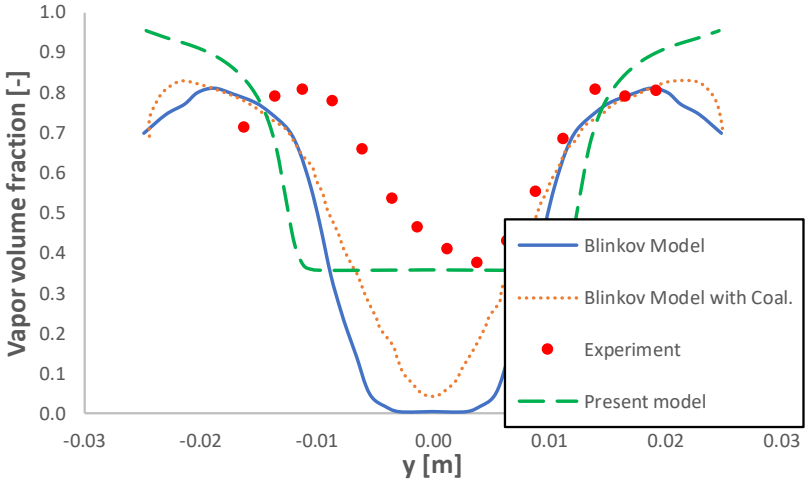

b) x=0.59m

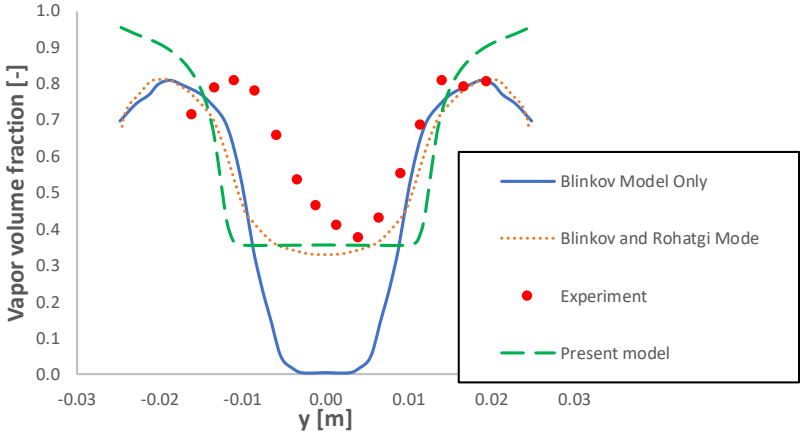

Figure 6.18: *Radial vapor fraction in comparison with results of Janet et al.* [50]

7. PROPOSED SIZING EQUATION AND VALIDATION

In case of liquid mixed with its own vapor flowing through a throttling device, additional complexity arises compared to frozen flow due to heat and mass transfer between the phases. For this reason, there is no formula in standards (IEC, ISO, etc.) for sizing control valves for liquid/vapor mixtures flow. However, some models without confirmation of accuracy are published including SUM, EQUIVALENCE model in Driskell [3], OMEGA model in Leung [7] and HNE-DS in Diener and Schmidt [5].

In this project, a proposed sizing equation is proposed by only modifying omega parameter, ω, in Diener and Schmidt [5] which is the most important factor for phase change phenomenon with non-equilibrium effect inside devices. New omega parameter, ω_{PM}, requires information of the outlet mass averaged specific volume. Practically, this approach is more suitable for control valves when information on the outlet condition is always available.

7.1. Proposed formula for prediction of flow coefficient C_V

Formula to calculate C_V is proposed by Diener and Schmidt [5]

$$C_V = 1.16K_V = 1.16\sqrt{\frac{\Delta p_0}{\Delta p}}\frac{1}{\sqrt{\rho_0\rho_1}}\dot{M}\frac{1}{Y_{MP}} \tag{7-1}$$

where $\dot{M}$ is the measured mass flow rate, $\Delta p_0 = 1\ bar$ and ΔP is the reference and measured pressure drop, respectively. ρ_1 is the density of mixture at inlet calculated by $\rho = 1/V$ with V is mixture specific volume. $\rho_0 = 999.2\ [\mathrm{kg/m^3}]$ is the reference density.

Y_{MP} is the multi-phase expansion factor considering all phase change and slip effects defined in Eq. 7-2.

$$Y_{MP} = \frac{\sqrt{\omega_{PM} ln\left(\frac{1}{\eta}\right) + (\omega_{PM} - 1)(1-\eta)}}{\omega_{PM}\left(\frac{1}{\eta} - 1\right) + 1}\phi\frac{F_L}{\sqrt{x}} \tag{7-2}$$

$\eta = P_2/P_1$ is the pressure ratio between upstream and downstream. F_L and $x = \Delta P/P_1$ are the recovery factor and pressure differential ratio factor, respectively.

Depending on the expansion law used to derive the omega parameter for the present model, ω_{PM}, is calculated by Eq. 7-3

$$\omega_{PM} = \frac{\frac{V_2}{V_1} - 1}{\frac{P_1}{P_2} - 1} \tag{7-3}$$

where P is the absolute pressure and specific volume is referred as $V = 1/\rho$. Subscripts 1 and 2 are upstream and downstream of the valve.

In Diener and Schmidt [5], a correction is considered for relative motion between the two phases, named the slip correction factor ϕ. This factor is proposed as

$$\frac{G_{id,slip}}{G_{id}} = \sqrt{\frac{V_1}{V_{e,1}}} \Rightarrow G_{id,slip} = \phi G_{id} \text{ with } \phi = \sqrt{\frac{V_1}{V_{e,1}}} \quad 7\text{-}4$$

with G_{id} is the mass flux of a frictionless homogeneous flow through an adiabatic nozzle.

In Eq. 7-4, $V_{e,1}$ is the slip-corrected specific volume at inlet. The development of $V_{e,1}$ is performed by a momentum balance as follows:

$$V_{e,1} = \left(\dot{x}_{V,1}V_{G,1} + K\left(1-\dot{x}_{V,1}\right)V_{L,1}\right)\left[\dot{x}_{V,1} + \frac{\left(1-\dot{x}_{V,1}\right)}{K}\right] \quad 7\text{-}5$$

where $K = \left(\frac{V_{V,1}}{V_{L,1}}\right)^{5/6}$ is slip factor proposed in Simpson et al. [96]

Rearrangement of Eq. 7-5 leads to

$$V_{e,1} = V_{L,1}\left\{1 + \dot{x}_{V,1}\left[\left(\frac{V_{V,1}}{V_{L,1}}\right)^{1/6} - 1\right] \times \left(1 + \dot{x}_{V,1}\left[\left(\frac{V_{V,1}}{V_{L,1}}\right)^{5/6} - 1\right]\right)\right\} \quad 7\text{-}6$$

Finally, slip correction factor ϕ can be extracted as

$$\phi = \sqrt{\frac{V_1}{V_{e,1}}} = \sqrt{\frac{V_1}{V_{L,1}}}\left\{1 + \dot{x}_{V,1}\left[\left(\frac{V_{V,1}}{V_{L,1}}\right)^{1/6} - 1\right] \times \left(1 + \dot{x}_{V,1}\left[\left(\frac{V_{V,1}}{V_{L,1}}\right)^{5/6} - 1\right]\right)\right\}^{-1/2} \quad 7\text{-}7$$

7.2. Algorithm for calculation

Steps for calculating C_V will be performed as below:

Step1: input data and pre-calculation

P_1, P_2: static pressure at inlet and outlet

V_1, V_2: specific volume at inlet and outlet

V_{L1}, V_{L2}: specific volume of liquid phase at inlet and outlet

V_{V1}, V_{V2}: specific volume of vapor phase at inlet and outlet

$\dot{M}$: measured mass flow rate

$\dot{x}_1$: mass fraction of vapor phase at inlet

F_L: recovery factor

Step 2: compression effect of present model ω_{PM}

$$\omega_{PM} = \frac{\frac{V_2}{V_1} - 1}{\frac{P_1}{P_2} - 1} \quad 7\text{-}8$$

Step 3: calculation of critical pressure

In case $\omega_{PM} \leq 2$, Tyco [97] suggests an explicit solution

$$\eta_{crit} = [1 + (1.0446 - 0.0093431\omega_{PM}^{0.5})\omega_{PM}^{-0.56261}]^{(-0.70356+0.014685ln(\omega_{PM}))} \quad 7\text{-}9$$

In case $\omega_{PM} > 2$, Epstein et al. [98] proposes

$$\eta_{crit} = 0.55 + 0.217ln(\omega_{PM}) - 0.046\big(ln(\omega_{PM})\big)^2 + 0.004\big(ln(\omega_{PM})\big)^3 \quad 7\text{-}10$$

Calculation of critical pressure ratio ($\eta_{crit} = P_{crit}/P_1$) is very important to detect a choked flow condition. Finally, the correct pressure at downstream, $P_{correct}$, will be defined following critical pressure ratio

$\eta_2 > \eta_{crit}$: $P_{correct} = P_2$ Normal flow (unchoked flow)
$\eta_2 \leq \eta_{crit}$: $P_{correct} = P_{crit}$ Limit flow (choked flow)

$\eta_2 = P_2/P_1$ is downstream pressure ratio

Step 4: re-calculate ω_{PM} with $P_{correct}$

$$\omega_{PM} = \frac{\frac{V_2}{V_1} - 1}{\frac{P_1}{P_{correct}} - 1} \quad 7\text{-}11$$

Step 5: Slip correction

$$\phi = \sqrt{\frac{\frac{V_1}{V_{L,1}}}{\left\{1 + \dot{x}_1\left[\left(\frac{V_{V,1}}{V_{L,1}}\right)^{\frac{1}{6}} - 1\right]\right\}\left\{1 + \dot{x}_1\left[\left(\frac{V_{V,1}}{V_{L,1}}\right)^{\frac{5}{6}} - 1\right]\right\}}} \quad 7\text{-}12$$

Step 6: Expansion factor with $\eta = P_{correct}/P_1$ is pressure ratio

$$Y_{MP} = \frac{\sqrt{\omega_{PM} ln\left(\frac{1}{\eta}\right) + (\omega_{PM} - 1)(1 - \eta)}}{\omega_{PM}\left(\frac{1}{\eta} - 1\right) + 1}\phi\frac{F_L}{\sqrt{x}} \quad 7\text{-}13$$

$x = (P_1 - P_{correct})/P_1$ is pressure differential ratio

Step 7: Flow coefficient

$$\mathrm{C_V} = 1.16\mathrm{K_V} = 1.16\sqrt{\frac{\Delta P_0}{\Delta P}}\frac{1}{\sqrt{\rho_0\rho_1}}\dot{M}\frac{1}{Y_{MP}} \quad 7\text{-}14$$

7.3. Validation of sizing equation with air/water flow

In this section, reliable numerical results for air/water flow, validated by the experiment of Charless [31], will be used as input data to the sizing equations. These predictions will then be compared to the reference flow coefficient, C_V, which is calculated by the incompressible flow sizing equation on the same geometry. Please notice that the tolerance of the incompressible flow sizing equation, published in IEC standard [2], is below 5%. **Figure 7.1** and **Table 7-1** reintroduce the geometry and tested operating conditions from Charless [31].

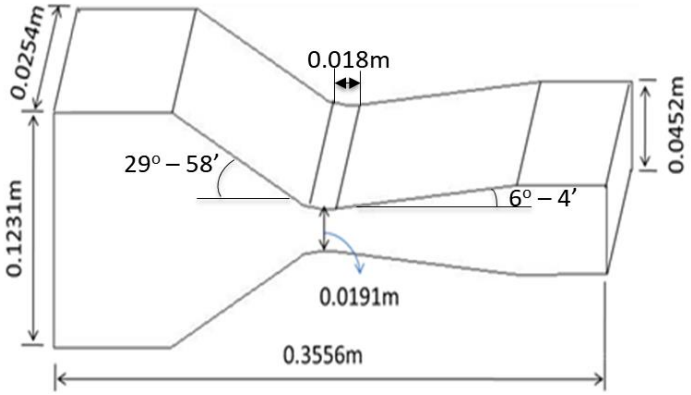

Figure 7.1: *Geometrical details of the convergent-divergent nozzle in Charless* [31]

Table 7-1: *Operating conditions and case code name of Air/liquid flow in Charless* [31]

Air/Water flow	Upstream inlet pressure (Pa)	Mixture inlet temperature (K)	Inlet air mass fraction [-]
AW1	359492.64	302.66	0.915
AW2	350529.46	302.72	0.894
AW3	376660.59	290.11	0.901
AW4	330258.87	290.17	0.882
AW5	328466.23	290.00	0.899
AW6	344048.38	289.22	0.908

For the case of air/water flow without phase change, result of C_V calculated by the present model, SUM and equivalence model are plotted in **Figure 7.2**. The Omega method and HNE-

DS method are not considered here because these methods do not apply to the non-flashing flow.

From **Table 7-2**, present sizing equation shows good prediction when the range of relative error for all cases from -0.01% to 5.67%. Although phase change process does not happen in these cases; however, compression of the air at outlet and slip effect still affect the prediction of the C_V and the present sizing equation shows good ability to capture these effects.

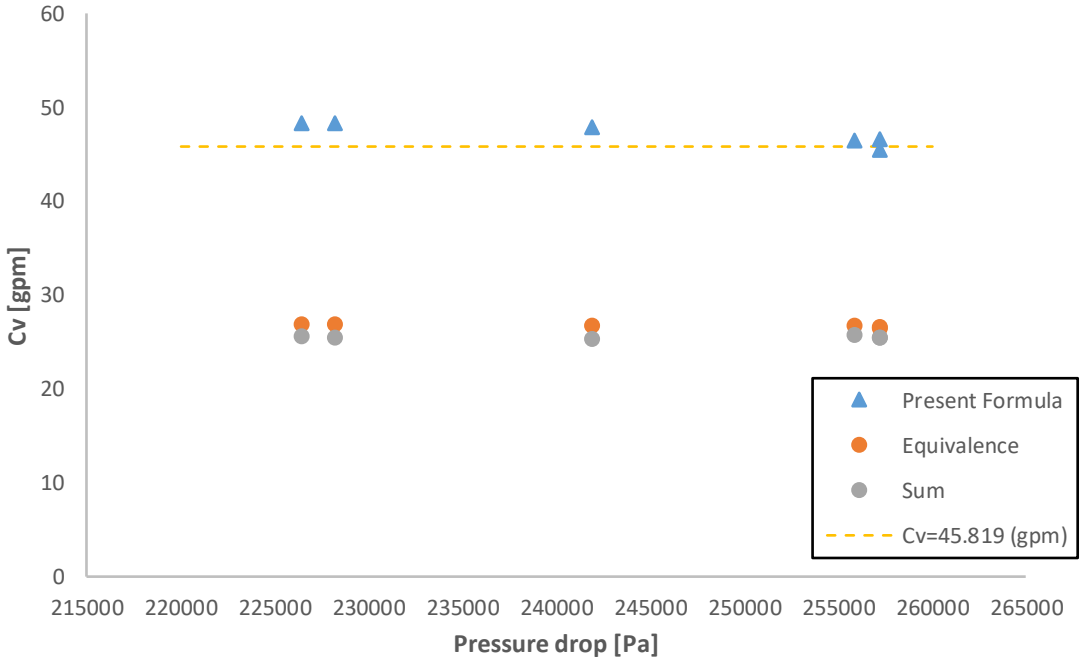

Figure 7.2: *Validation of sizing equations in case of Charless* [31] *Cv=45.819*

Table 7-2: *Relative error of present sizing equation in case of air/water flow*

Case	Pressure drop [bar]	Calculated Cv [gpm]	Reference Cv [gpm]	Error
AW1	2.558	46.52	45.819	+1.52%
AW2	2.572	45.63	45.819	-0.01%
AW3	2.572	46.70	45.819	+1.92%
AW4	2.281	48.36	45.819	+5.54%
AW5	2.264	48.42	45.819	+5.67%
AW6	2.418	47.93	45.819	+4.60%

Results of the EQUIVALENCE sizing equation, which considers two-phase flow mixed perfectly through the throat with the same velocity, show high errors of the order of approximately -41% (under-prediction) compared with the reference C_V value.

Table 7-3: *Relative error of EQUIVALENCE sizing equation in case of air/water flow*

Case	Pressure drop [bar]	Calculated Cv [gpm]	Reference Cv [gpm]	Error
AW1	2.558	27.495	45.819	-41.51%
AW2	2.572	26.563	45.819	-42.02%
AW3	2.572	26.708	45.819	-41.70%
AW4	2.281	27.006	45.819	-41.05%
AW5	2.264	27.006	45.819	-41.05%
AW6	2.418	26.801	45.819	-41.50%

With predictions using the SUM model for the sizing device, under-prediction is shown with error approximately−44%. In this test case of air/water flow without phase change, assumptions of neglecting heat and momentum transfers between two phase are unsuitable.

Table 7-4: *Relative error of SUM sizing equation in case of air/water flow*

Case	Pressure drop [bar]	Calculated Cv [gpm]	Reference Cv [gpm]	Error
AW1	2.558	26.422	45.819	-43.78%
AW2	2.572	25.51	45.819	-44.32%
AW3	2.572	25.543	45.819	-44.25%
AW4	2.281	25.568	45.819	-44.19%
AW5	2.264	25.618	45.819	-44.08%
AW6	2.418	25.4	45.819	-44.56%

Generally, the present model considering outlet information and slip correction factor give the best accuracy compared to the others for the case of air/water flow without phase change. The EQUIVALENCE model shows a better accuracy compared to the SUM model. This is

reasonable because the origin of the EQUIVALENCE model is from compressible sizing equation in IEC standard [1]. So, in cases with high gas mass fraction, this method shows better results.

To evaluate effects of the slip correction factor, the present formula is used with without a slip correction factor in **Figure 7.3** and **Table 7-5**.

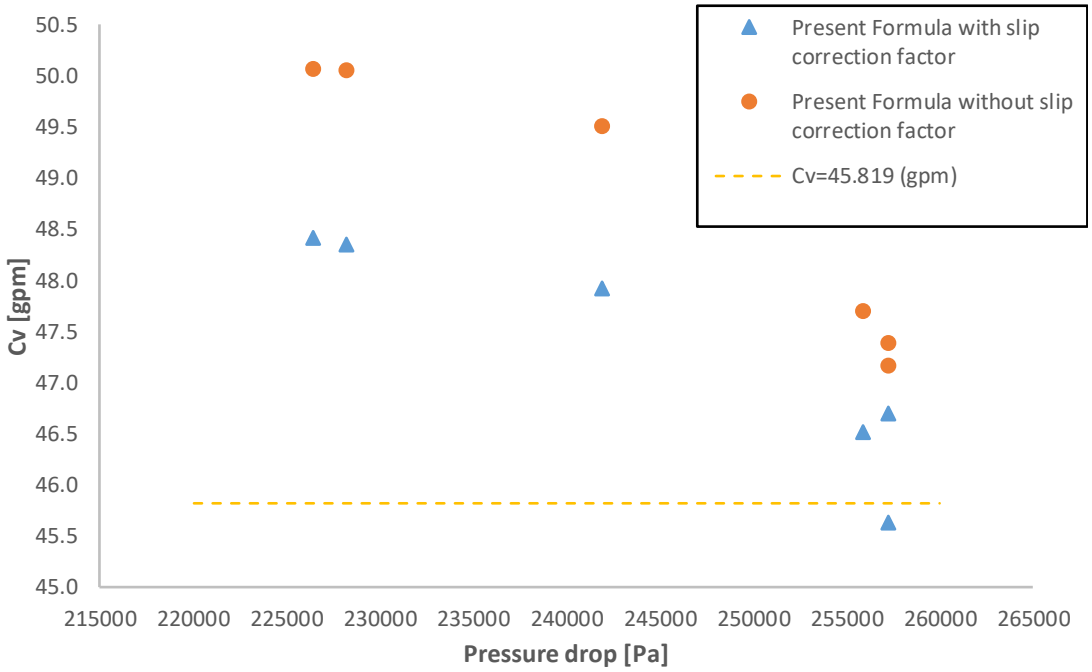

Figure 7.3: *Evaluation of present sizing equation with slip and without slip correction*

Table 7-5: *Evaluation of present sizing equation with slip and without slip correction*

Case	Pressure drop [bar]	Air mass fraction at inlet [-]	Relative error of present formula without slip	Relative error of present formula with slip
AW1	2.558	0.915	+3.96%	+1.52%
AW2	2.572	0.894	+2.86%	-0.01%
AW3	2.572	0.901	+3.31%	+1.92%
AW4	2.281	0.882	+8.47%	+5.54%
AW5	2.264	0.899	+8.50%	+5.67%
AW6	2.418	0.908	+7.47%	+4.60%

It is very clear that the present formula with slip correction factor shows the better accuracy (errors in range from -0.01% to 5.67%) compared to the present formula without slip correction factor (errors from +2.86% to 8.50%). As a result, the slip correction factor is proposed in the present formula for practical use.

7.4. Validation of sizing equation with flashing flow

The sizing equations for flashing flow are validated in this section. Geometry and operating conditions of Abuaf et al. [15], ***Figure 7.4*** and **Table 7-6**, are used here.

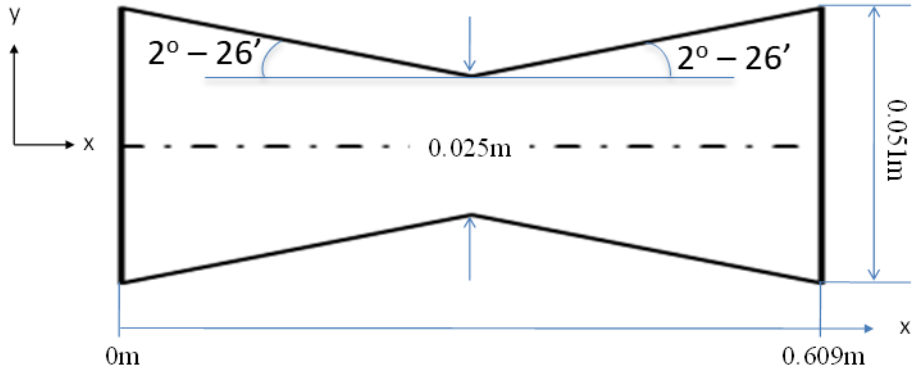

Figure 7.4: *Vertical circular convergent-divergent nozzle in Abuaf et al.* [15]

Table 7-6: *Operating conditions and case code name of flashing flow in Abuaf et al.* [15]

Case code name	Upstream pressure [Pa]	Inlet temperature [K]	Outlet pressure [Pa]	Flashing inception pressure [Pa]	Saturation pressure [Pa]	Mass flow rate [kg/s]
BNL284	530000	422.35	456000	404700	466000	7.3
BNL309	555900	422.25	402500	393500	464800	8.8
BNL273	573500	421.85	442100	419200	459800	8.7
BNL268	575200	422.05	443000	405700	462300	8.7
BNL304	577700	422.15	441000	399700	463500	8.8
BNL278	688600	421.95	434100	425700	461000	11.7
BNL296	764900	421.95	432600	417000	461000	13.1

The approach is similar to air/water flow when reliable numerical results are used as input data and then sizing results are compared to the reference C_V extracted from incompressible sizing equation of IEC standard [1] with error below 5%.

Figure 7.5 shows sizing results using the present formula, HNE-DS, OMEGA, SUM and EQUIVALENCE method. It should be noticed that the slip correction factor for OMEGA, HNE-DS and the present formula for the case of initially sub-cooled flashing flow is not available because expression for slip correction requires vapor mass fraction at inlet.

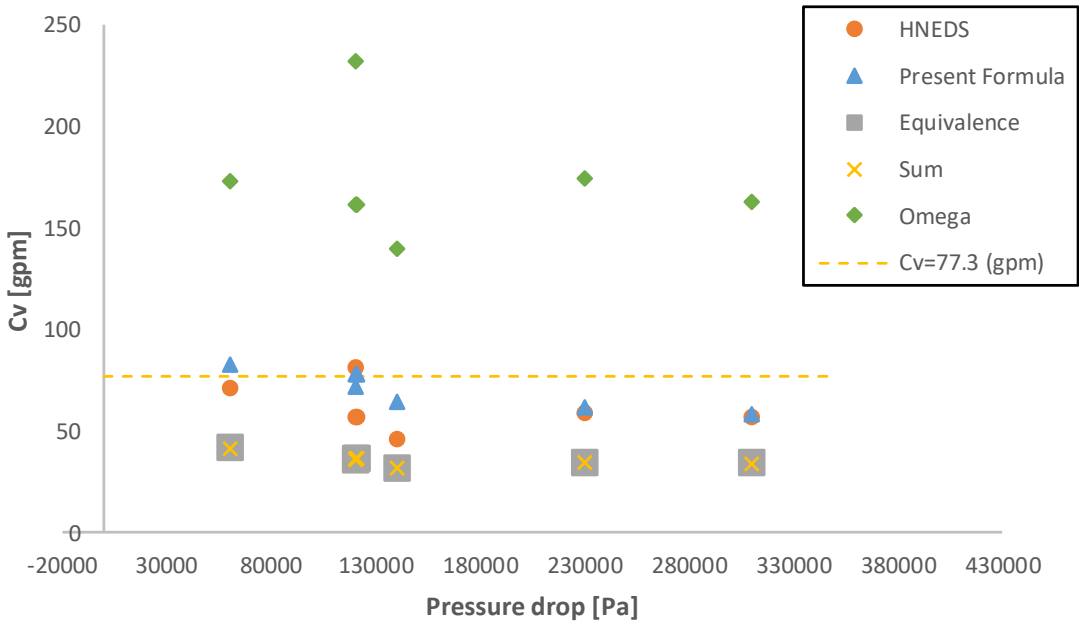

Figure 7.5: *Sizing equations in case of Abuaf et al.* [15] *Cv=77.3*

As shown in **Figure 7.5** and **Table 7-7**, the present model again has a better agreement compared to the other models with a range of error from -23.66% to 7.91%. The trend of error is very clear when pressure drop increases leading to higher discrepancies compared to the reference value due to lack of slip correction factor.

Table 7-7: *Relative error of present sizing equation in case of flashing flow*

Case code name	Pressure drop [bar]	Calculated Cv [gpm]	Reference Cv [gpm]	Error
BNL284	0.6	83.42	77.3	+7.91%
BNL309	1.4	64.94	77.3	-15.98%
BNL273	1.209	78.41	77.3	+1.43%
BNL268	1.2	78.32	77.3	+1.31%
BNL304	1.2	72.21	77.3	-6.5%
BNL278	2.3	62.46	77.3	-19.19%
BNL296	3.1	59.01	77.3	-23.66%

The HNE-DS model shows a range of errors from -39.5% to 6.17% in **Table 7-8** and has a better prediction compared to the OMEGA, SUM and EQUIVALENCE methods. It should be noticed that the HNE-DS method only uses information at the inlet combined with fluid properties and a boiling delay factor to predict the flow coefficient. This is very challenging when flashing process, including nucleation and bubble growth, strongly depends on geometry and operating conditions.

Table 7-8: *Relative error of HNE-DS sizing equation in case of flashing flow*

Case code name	Pressure drop [bar]	Calculated Cv [gpm]	Reference Cv [gpm]	Error
BNL284	0.6	71.52	77.3	-7.47%
BNL309	1.4	46.765	77.3	-39.5%
BNL273	1.209	57.096	77.3	-26.13%
BNL268	1.2	57.056	77.3	-26.18%
BNL304	1.2	82.07	77.3	6.17%
BNL278	2.3	59.743	77.3	-22.71%
BNL296	3.1	57.053	77.3	-26.19%

In this validation, The OMEGA method using equilibrium assumptions shows a significant over-prediction errors ranging from 81.20% to 110.96%, **Table 7-9**. These results also confirm that the effects of boiling delay in HNE-DS should be applied in the sizing equation.

Table 7-9: *Relative error of OMEGA sizing equation in case of flashing flow*

Case code name	Pressure drop [bar]	Calculated Cv [gpm]	Reference Cv [gpm]	Error
BNL284	0.6	173.278	77.3	+124.16%
BNL309	1.4	140.075	77.3	+81.20%
BNL273	1.209	162.166	77.3	+109.78%
BNL268	1.2	162.09	77.3	+109.57%
BNL304	1.2	232.818	77.3	+201.18%
BNL278	2.3	174.862	77.3	+126.21%
BNL296	3.1	163.076	77.3	+110.96%

Errors in the EQUIVALENCE and SUM models in these cases are approximately -50% to -40%, respectively, shown in **Table 7-10** and **Table 7-11**. This result also confirms technical reports about better predictions of SUM model compared to EQUIVALENCE model in the low inlet quality range or for flashing flow of initial sub-cooled liquid.

Table 7-10: *Relative error of EQUIVALENCE sizing equation in case of flashing flow*

Case code name	Pressure drop [bar]	Calculated Cv [gpm]	Reference Cv [gpm]	Error
BNL284	0.6	42.112	77.3	-45.52%
BNL309	1.4	32.143	77.3	-58.41%
BNL273	1.209	36.807	77.3	-52.38%
BNL268	1.2	36.912	77.3	-52.24%
BNL304	1.2	36.155	77.3	-53.22%
BNL278	2.3	35.051	77.3	-54.65%
BNL296	3.1	34.635	77.3	-55.19%

Table 7-11: *Relative error of SUM sizing equation in case of flashing flow*

Case code name	Pressure drop [bar]	Calculated Cv [gpm]	Reference Cv [gpm]	Error
BNL284	0.6	43.899	77.3	-43.09%
BNL309	1.4	38.152	77.3	-50.64%
BNL273	1.209	41.956	77.3	-45.72%
BNL268	1.2	42.510	77.3	-45.00%
BNL304	1.2	40.430	77.3	-47.69%
BNL278	2.3	39.977	77.3	-48.28%
BNL296	3.1	39.412	77.3	-49.01%

Overall, the existing sizing equations for flashing flow (HNE-DS, OMEGA) try to use inlet information combined with vaporization-related fluid properties to predict global information. This approach is very difficult because the phase change process is strongly based on geometry and operating conditions. Besides, in industrial applications of chemical plants, vaporization-

related fluid properties are rarely available leading to the impossibility to use these equations for general purpose. Adding outlet information to formula instead of vaporization-related fluid properties is proposed for better accuracy, especially, in the case of control valves where outlet information is always available.

CONCLUSIONS AND FUTURE WORKS

In this thesis, the main purpose is to understand the behaviors of flashing flow inside throttling devices comprehensively and then make improvements not only for Computational Fluid Dynamics (CFD) flashing model but also equations for predicting flow coefficient of throttling devices for the case of flashing flow.

CFD flashing flow

A CFD flashing flow is proposed with the mixture model, and implemented in the finite-volume commercial solver ANSYS-Fluent rel. 16.0. In order to reproduce evaporation phenomenon, this thesis considers the modified Lee model with phase change process driven by pressure. The numerical results of the flashing model are validated using the available experimental data of two different convergent-divergent nozzles fed with air/water flow and sub-cooled water. The comparison between numerical and experimental results shows a good agreement in terms of mass flow rate (maximum relative error <6%), averaged vapor fraction and static pressure along the nozzle. Moreover, the use of the present model allows better reproduce the local turbulence effects and transverse vapor fraction profiles along the nozzle, compared with flashing models previously used in the literature. A practical guideline is introduced for using flashing model with analysis of (i) impacts of turbulence RANS models; (ii) the influence of turbulence and artificial parameters. In general, the turbulence model with Standard Wall Function shows the best accuracy in terms of mass flow rate and vapor profile. Turbulence intensity at the inlet equal to 1% is suggested. Moreover, this thesis also defines appropriate values for the accommodation coefficient and difference between saturation pressure and vapour partial pressure at the interface on the vapor side corresponding to specific cases of flashing flow in circular convergent-divergent nozzle.

Generally, results of CFD flashing model in this work show an agreement to experiment and an improvement compared to previous works for both global and local qualities. However, there are still discrepancies in transverse vapor distribution between numerical results and experimental data due to the simplicity of the mixture model. In order to improve the better reproduction of local quantities, the two-fluid model is proposed with all the momentum interactions between two phases accounted for.

Sizing equation in case of two-phase flow

For predicting the flow coefficient inside throttling devices, a formula, based on homogeneous non-equilibrium model of Diener and Schmidt (HNE-DS), is developed with addition of outlet information. Validation of new formula is performed by using reliable numerical results for input information and then sizing results are compared to reference flow coefficients. For the case of air/water flow without phase change, the present model is compared to the reference, EQUIVALENCE and SUM model. Results of the proposed sizing equation show a good agreement to the reference with maximum of relative error below 6% for all tested cases and an improvement compared to the SUM and EQUIVALENCE model. The results also confirm the need to use the slip correction factor in the present sizing equation. For the case of flashing flow with phase change, the present sizing equation gives a better improvement

(relative error in the range from -23.66% to 7.91%) compared to the other models including (i) OMEGA (ii) HNE-DS (iii) EQUIVALENCE (iv) SUM. Results of the present model also show higher errors corresponding to the increase of pressure drop and this is due to unsuitable slip correction factor which need to be improved in the future.

Finally, this work also confirms the accuracy of existing methods for sizing two-phase flow. The HNE-DS model shows the best accuracy compared to (i) OMEGA (ii) EQUIVALENCE and (iii) SUM method in case of flashing flow. The EQUIVALENCE model shows better accuracy for the case of high quality at inlet compared to the SUM model. Conversely, using the SUM model for low quality flow at inlet gives a higher agreement to reference values.

NOMENCLATURE FOR FLUID DYNAMICS

Roman characters	
A	Interfacial area density $[\mathrm{m}^{-1}]$
$\vec{a}$	Acceleration vector $[\mathrm{m.s}^{-2}]$
c	Mass fraction
c_p	Specific heat capacity $[\mathrm{J.kg}^{-1}.\mathrm{K}^{-1}]$
E	Internal energy $[\mathrm{kg.m}^2.\mathrm{s}^{-1}]$
f	Drag function
F	Evaporation-condensation flux at flat interface [$kg.m^{-2}.s^{-1}$]
h	Partial expansion energy enthalpy $[\mathrm{J/kg}]$
h_{fg}	Latent heat of vaporization $[\mathrm{J/kg}]$
k	Turbulence kinetic energy $[\mathrm{m}^2.\mathrm{s}^{-2}]$
k_{eff}	Effective thermal conductivity $[\mathrm{W.m}^{-1}.\mathrm{K}^{-1}]$
k_k	Thermal conductivity of k-th phase $[\mathrm{W.m}^{-1}.\mathrm{K}^{-1}]$
k_t	Turbulence thermal conductivity $[\mathrm{W.m}^{-1}.\mathrm{K}^{-1}]$
$\dot{M}$	Mass flow rate $[\mathrm{kg/h}]$
M	Molar mass $[\mathrm{kg/kmol}]$
$\dot{m}$	Rate of mass transfer $[\mathrm{kg.m}^{-3}.\mathrm{s}^{-1}]$
N	Bubble number density
n	Number of phases
P	Pressure [Pa]
P^*	Vapor partial pressure at the interface on the vapor side [Pa]
P_V	Vaporization pressure
R	gas constant $[\mathrm{kJ.kmol}^{-1}.\mathrm{K}^{-1}]$
r	Bubble radius $[m]$
$\dot{r}$	Bubble growth rate $[m/s]$
$\ddot{r}$	Bubble growth acceleration $[m/s]$
s	Entropy $[\mathrm{J.kg}^{-1}.\mathrm{K}^{-1}]$
T	Temperature [K]
t	Time coordinate [s]
$\vec{v}$	Velocity vector $[\mathrm{m.s}^{-1}]$
x	x coordinate [m]

y	y coordinate [m]
y^+	Turbulence parameter
Re	Reynolds number
Greek characters	
α	Vapor volume fraction
β	Accommodation coefficient
ε	Turbulence dissipation rate $[m^2 s^{-3}]$
μ	Dynamic viscosity [Pa. s] or chemical potential [J/kg]
$\Delta\mu$	Chemical potential difference [J/kg]
π	Pi constant
ρ	Density $[kg.\, m^{-3}]$
τ	Particle relaxation time $[s^{-1}]$ or shear stress component
ω	Turbulence eddy frequency $[s^{-1}]$
Subscripts	
b	bubble
c	critical
drag	Drag
dr	Drift
eff	effective
fi	Flashing inception
i	interfacial
in	inlet
k	k-th phase
l	Liquid
m	Mixture
p	Secondary phase
q	Primary phase
Sat	Saturation
t	Turbulence
v	Vapor
x	x-direction (component)
y	y-direction (component)

z	z-direction (component)

NOMENCLATURE FOR SIZING EQUATION

Roman characters	
A_V	Flow coefficient [m^2]
C_V	Flow coefficient [gpm]
F_L	Recovery factor [−]
F_F	Liquid critical pressure ratio factor [−]
F_γ	Specific heat ratio factor ($= \gamma/1.4$)
G_{id}	The mass flux of a frictionless homogeneous flow through an adiabatic nozzle without slip effect between two phases [$kg.s^{-1}m^{-2}$]
$G_{id,slip}$	The mass flux of a frictionless homogeneous flow through an adiabatic nozzle with slip effect between two phases [$kg.s^{-1}m^{-2}$]
K_V	Flow coefficient [m^3/h]
M	Molar mass [kg/kmol]
$\dot{M}$	Mass flow rate [kg/h]
ΔP	Static pressure difference between upstream and downstream [bar]
ΔP_{max}	Critical pressure difference [bar]
P	Static pressure [bar]
T	Temperature [K]
V	Specific volume [m^3/kg]
$\dot{V}$	Volume flow rate [m^3/h]
x	Pressure differential ratio factor ($= \Delta P/P_1$) [−]
x_T	Pressure differential ratio factor in choked condition ($\cong 0.85 \cdot F_L^2$) [−]
$\dot{x}$	Mass fraction
Y	Expansion factor
Y_{DS}	Expansion factor in HNE-DS method
Greek characters	
α	Vapor volume fraction
γ	Specific heat ratio $(= c_p/c_v)$ [−]
η	Pressure ratio [−]
ρ	Density [kg/m^3]

ρ_r	$= \rho/\rho_0$
ϕ	Slip correction factor $[-]$
ω_{PM}	Omega parameter of present model $[-]$
Subscripts	
c	Critical condition
e	Equivalence
G	Gas
L	Liquid
V	Vapor
1	Inlet (upstream)
2	Outlet (downstream)
0	Reference state

Appendix

A. PARAMETERS OF SIZING EQUATIONS

Formulas in this appendix are referenced from IEC standard [1].

A.1. Recovery factor F_L

F_L, given in A-1, shows the transformation from the kinetic energy to pressure energy of the fluid flow in vena contracta.

$$F_L = \sqrt{\frac{P_1 - P_2}{P_1 - P_{VC}}} \qquad A\text{-}1$$

P_{VC} is pressure in vena contracta and always lower than downstream pressure, P_2, leading to F_L is always less than or equal to 1.

An uncomplicated way to determine F_L is the use of expression A-2 in critical conditions:

$$F_L = \frac{1.16 \cdot \dot{V}_{max}}{C_V \cdot \sqrt{P_1 - 0.96 P_V}} \qquad A\text{-}2$$

$\dot{V}_{max}$ is measured critical volume flow rate

If operating fluid is water at $5 \div 40^o C$ ($P_V = 0.02 \div 0.05\ bar$), expression A-2 can be simplified to A-3

$$F_L = \frac{1.16 \cdot \dot{V}_{max}}{C_V \cdot \sqrt{P_1}} \qquad A\text{-}3$$

A.2. Correction coefficients of cavitation x_{FZ} and K_c

In the vena contracta of valves, when pressure is lower than saturation pressure, liquid starts flashing and forming bubbles. If outlet pressure is higher than saturation pressure, bubbles are collapsed or imploded and return to liquid state. In industrial applications, imploded bubbles in cavitation process cause mechanical damage on metal surface.

Coefficients for correcting sizing equation in cavitation flow includes:

(i) x_{FZ} is called “onset cavitation coefficient” and is introduced when incipient cavitation appears. Practically, this parameter does not affect significantly to valve sizing process and it is so complicated to detect value of this correction coefficient precisely.

(ii) K_c is called “critical cavitation coefficient” and is introduced when a deviation from linear higher than 2% is found (shown in **Figure 2.3**). K_c plays a significant role because this is beginning point of mechanical damage on metal surfaces. An approximation of this parameter gives $K_c = 0.8 \cdot F_L^2$

A.3. Liquid critical pressure ratio factor F_F

F_F is used to separate two regions of incompressible liquid flow including (i) Normal flow (ii) Limit flow. Formula of F_F is given in A-4 in case of general fluid

$$F_F = 0.96 - 0.28\sqrt{\frac{P_V}{P_c}} \qquad \textit{A-4}$$

In case of water, Formula can be simplified to A-5

$$F_F = 0.96 - 0.28\sqrt{\frac{P_V}{221.2}} \qquad \textit{A-5}$$

A.4. Expansion factor *Y*

Expansion factor Y is used to calculate expansion effect of compressible fluids. With standard test conditions, there are three hypotheses, confirmed by experiment, to extract Y:

- Y can be described by a linear function of $x = \Delta P/P_1$
- Y is a function of exponent of adiabatic transformation $\gamma = \Delta P/P_1$
- Y varies depending geometry of valve

The first hypothesis gives $Y = 1 - ax$ with a is constant.

Relation between $\sqrt{x}$, Y and $\dot{M}$ can be described by $\dot{M} \div Y\sqrt{x} = \sqrt{x} - a^2\sqrt{x^3}$

At limit flow:

$$\frac{d\dot{M}}{dx} = \frac{1}{2\sqrt{x}} - \frac{3a\sqrt{x}}{2} = 0$$

Solving above equation gives $x = 1/3a$ and $Y = 1 - \frac{1}{3a} \cdot a = 2/3$

Finally, range of Y can be detected with $Y = 1$ at $x = 0$ and $Y = 2/3$ at maximum flow rate.

Considering the third hypothesis by adding x_T into formula of Y leading to A-6.

$$Y = 1 - \frac{x}{3x_T} \qquad \textit{A-6}$$

It is clear that x_T will change with different throttling devices and it satisfies the third hypothesis.

A correction factor named specific heat ratio factor, $F_\gamma = \gamma/1.4$, is introduced to satisfy the second hypothesis giving final formula in A-7.

$$Y = 1 - \frac{x}{3F_\gamma x_T} \qquad \textit{A-7}$$

From A-7, $x = F_\gamma x_T$ at maximum flow rate corresponds to $Y = 2/3 = 0.667$

B. SENSITIVITY OF ARTIFICAL COEFFICIENTS

In Appendix B, the influence of these coefficients to flashing flow has been performed in **Figure B.1**, **Figure B.2**, **Figure B.3**, **Figure B.4** for cases (BNL284, BNL273, BNL268, BNL304). Experimental data is referenced in Abuaf et al. [15]. A clear increase and decrease trend in the averaged vapor fraction and the static pressure is observed when varying coefficients.

a) Vapor profile with artificial coefficients

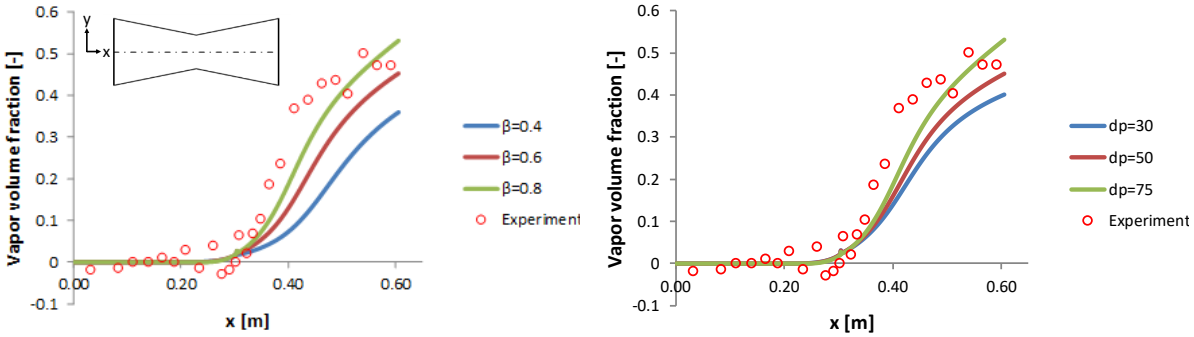

b) Static pressure with artificial coefficients

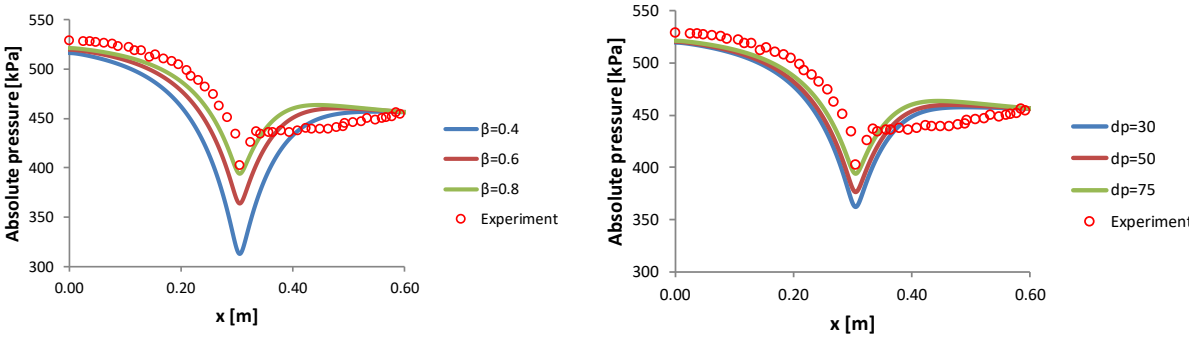

Figure B.1: *Artificial coefficients sensitivity for BNL284*

a) Vapor profile with artificial coefficients

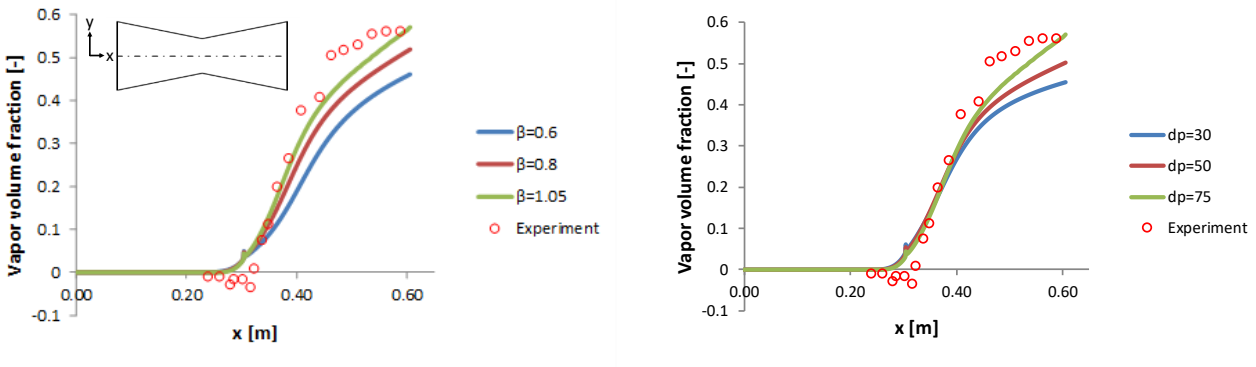

b) Static pressure with artificial coefficients

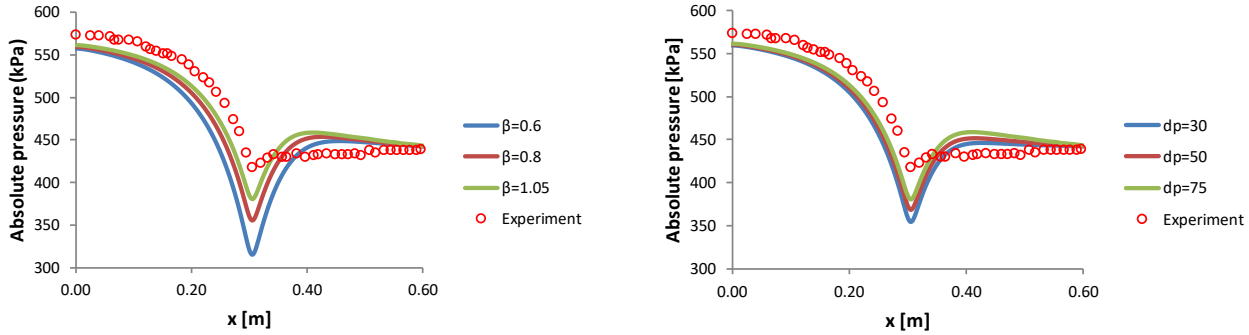

Figure B.2: *Artificial coefficients sensitivity for BNL273*

a) Vapor profile with artificial coefficients

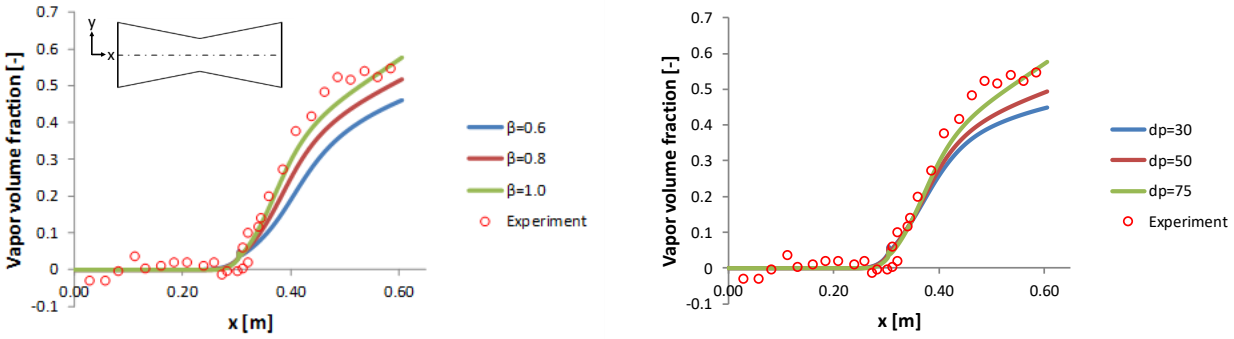

b) Static pressure with artificial coefficients

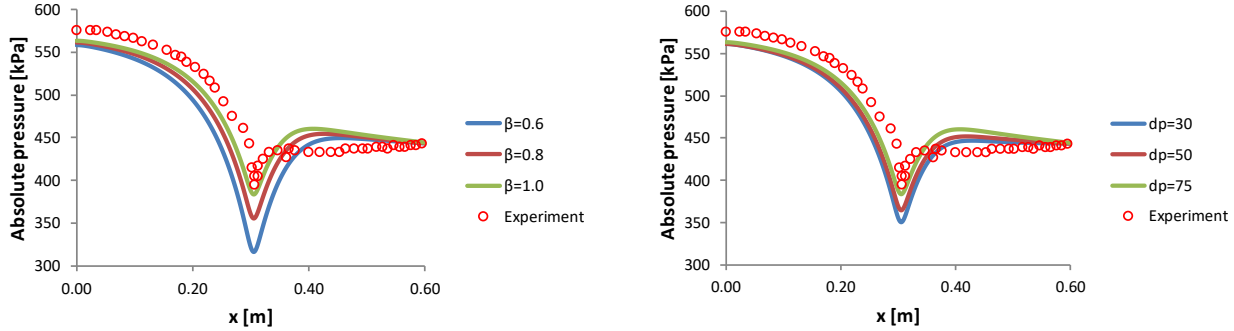

Figure B.3: *Artificial coefficients sensitivity for BNL268*

a) Vapor profile with artificial coefficients

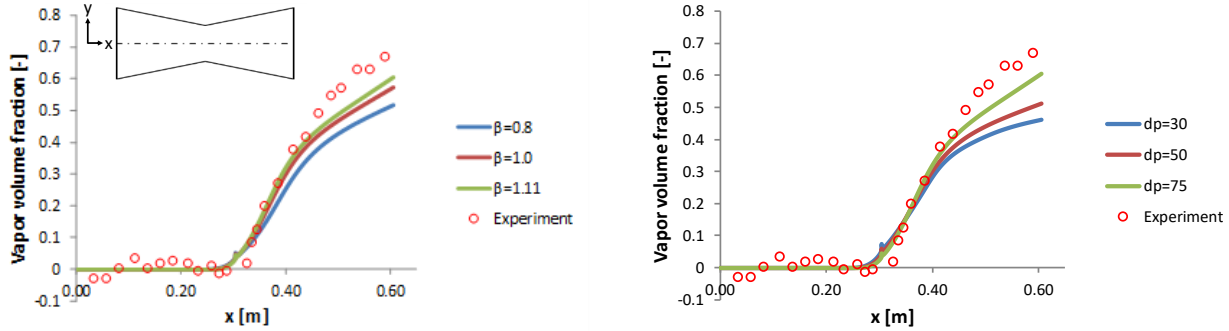

b) Static pressure with artificial coefficients

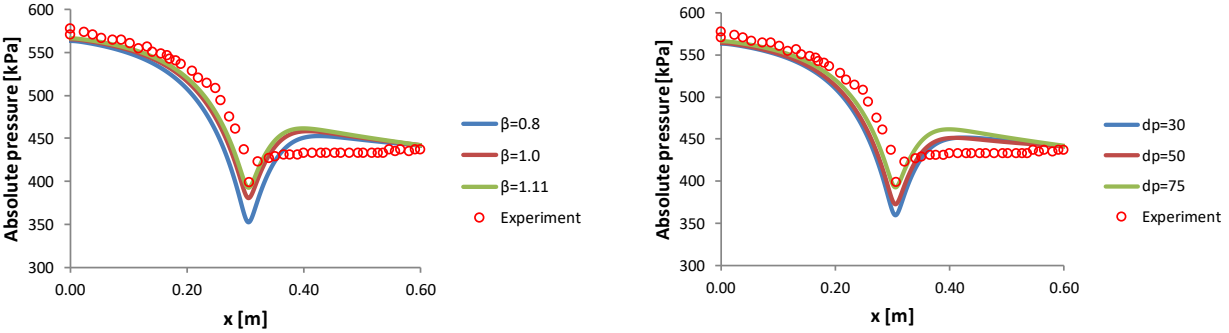

Figure B.4: *Artificial coefficients sensitivity for BNL304*

REFERENCES

[1] IEC 60534-2-1, *Sizing equations for fluid flow under installed conditions*. 1998.

[2] IEC 60534-2-3, *Test procedures*. 1997.

[3] L. Driskell, *Control valve sizing with ISA formulas*. Instrumentation Techonology, 1974.

[4] Parcol, *Control valves for industrial process 4th edition*. 2005.

[5] R. Diener and J. Schmidt, "Sizing of throttling devices for gas liquid two-phase flow, Part 2: control valves, orifices and nozzles," *Process Saf Prog*, vol. 24, no. 1, pp. 29–37, 2005.

[6] ISO/FDIS 4126-10, *Safety devices for protection against excessive pressure*. 2010.

[7] J. C. Leung, "Easily size relief devices and piping for two-phase flow," *Chem. Eng. Prog.*, vol. 92, p. 28–50., 1996.

[8] P. Saha, *A Review of Two-phase Steam–Water Critical Flow Models with Emphasis on Thermal Non-equilibrium*. U.S. Nuclear Regulatory Commission, Washington, DC, 1978.

[9] G. B. Wallis, "Critical two-phase flow," *Int. J. Multiph. Flow*, vol. 6, pp. 97–112, 1980.

[10] H. J. Richter, "Separated two-phase flow model: application to critical two-phase flow," *Int. J. Multiph. Flow*, vol. 9, no. 5, pp. 511–530, 1983.

[11] G. Pinhasi, A. Ullmann, A. Dayan, and T. Israel, "MODELING OF FLASHING TWO-PHASE FLOW Gad A . Pinhasi Department of Chemical Engineering and Biotechnology," *Rev. Chem. Eng.*, vol. 21, no. 3–4, pp. 133–264, 2005.

[12] X. Xi, L. Hong, J. Ming, X. Maozhao, and Y. Hongchao, "A new flash boiling model for single droplet," *Int. J. Heat Mass Transf.*, vol. 107, pp. 1129–1137, 2017.

[13] M. Reocreux, "Contribution to the Study of Critical Flow Rates in Two-phase Water Vapour Flow," Scientific and Medical University of Grenoble, France, 1978.

[14] V. E. Schrock, E. S. Starkman, and R. A. Brown, "Flashing Flow of Initially Subcooled Water in Convergent-Divergent," *J. Heat Transfer*, vol. 99, no. 2, pp. 263–268, 1977.

[15] N. Abuaf, B. J. C. Wu, G. A. Zimmer, and P. Saha, *A Study of Nonequilibrium Flashing of Water in a Convergingdiverging Nozzle: Volume 1*. Experimental. U.S. Nuclear Regulatory Commission, Washington, DC, 1981.

[16] L. Araneo and R. Donde', "Flash boiling in a multihole G-DI injector – Effects of the fuel distillation curve," *Fuel*, vol. 191, pp. 500–510, 2017.

[17] M. J. Moran and Howard N. Sapiro, *Fundamentals of Engineering Thermodynamics*. John Wiley & Sons, Inc, 2006.

[18] O. Miyatake, I. Tanaka, and N. Lior, "A simple universal equation for bubble growth in pure liquids and binary solutions with a non-volatile solute," *Int. J. Heat Mass Transf.*, vol. 40, pp. 1577–1584, 1997.

[19] R. D. Oza and Sinnamon, J.F., "An experimental and analytical study of flashing boiling fuel injection," *SAE Pap.*, p. 830590, 1983.

[20] M. Blander and J. L. L. Katz, "Bubble nucleation in liquids," *AIChE J.*, vol. 21, no. 5, pp. 833– 848, 1975.

[21] A. J. Page and R. P. Sear, "Heterogeneous nucleation in and out of pores," *Phys. Rev. Lett.*, vol. 97, no. 6, p. 65701, 2006.

[22] J. Li and G. P. Peterson, "Microscale heterogeneous boiling on smooth surfaces— from bubble nucleation to bubble dynamics," *Int. J. Heat Mass Transf.*, vol. 48, no. 21, pp. 4316–4332, 2005.

[23] H. J. Jo, M. Kaviany, and S. H. Kim, "Heterogeneous bubble nucleation on ideally-smooth horizontal heated surface," *Int. J. Heat Mass Transf.*, vol. 71, pp. 149–157, 2014.

[24] G. V. Lau, P. A. Hunt, and E. A. Müller, "Water droplet excess free energy determined by cluster mitosis using guided molecular dynamics," *J. Chem. Phys.*, vol. 143, no. 24, p. 244709, 2015.

[25] R. Barbone, "Explosive Boiling of a Depressurized Volatile Liquid," McGill University, Montreal,

Quebec, Canada, 1994.

[26] C. E. Brennen, *Cavitation and Bubble Dynamics*. Oxford University Press, 1995.

[27] L. Rayleigh VIII, "On the pressure developed in a liquid during the collapse of a spherical cavity," *Lond. Edin. Dublin Philos. Mag. J. Sci.*, vol. 34, no. 200, pp. 94–98, 1917.

[28] E. Sher, T. Bar-Kohany, and A. Rashkovan, "Flash-boiling atomization," *Prog. Energy Combust. Sci.*, vol. 34, no. 4, pp. 417–439, 2008.

[29] S. R. De Groot and P. Mazur, *Non-equilibrium Thermodynamics*. Courier Corporation, 2013.

[30] M. L. Roesle and F. A. Kulacki, "Boiling of small droplets," *Int. J. Heat Mass Transf.*, vol. 53, no. 23, pp. 5587–5595, 2010.

[31] G. Charless, "An Analytical and Experimental Study of the Flow of Air-Water and Steam-Water Mixtures in a Converging-Diverging Nozzle," Cornell University, 1968.

[32] G. Giacchetta, M. Leporini, B. Marchetti, and A. Terenzi, "Numerical study of choked two-phase flow of hydrocarbons fluids through orifices," *J. Loss Prev. Process Ind.*, vol. 27, pp. 13–20, 2014.

[33] J. C. Leung, "A generalized correlation for one-component homogeneous equilibrium flashing choked flow," *Am. Inst. Chem. Eng.*, vol. 32, p. 1622, 1986.

[34] J. C. Leung, "Two-phase flow discharge in nozzles and pipes e a unified approach," *J. Loss Prev. Process Ind.*, vol. 3, pp. 27–32, 1990.

[35] J. C. Leung, "The omega method for discharge rate evaluation," in *International symposium on runaway reactions and pressure relief design*, 1995, pp. 367–393.

[36] American Petroleum Institute, *Sizing, selection and installation of pressure relieving devices in refineries, part 1*. 2008.

[37] R. Darby, "Evaluation of two-phase flow models for flashing flow in nozzles," *Process Saf. Prog.*, vol. 1, pp. 32–39, 2000.

[38] R. Darby, P. Meiller, and Stockton, J. R., "Select the best model for two-phase relief sizing," *Chem. Eng. Prog.*, pp. 56–64, 2001.

[39] R. E. Henry and H. K. Fauske, "The two-phase critical flow of one component mixtures in nozzles, orifices, and short tubes," *J. Heat Transfer*, vol. 93, pp. 179–187, 1971.

[40] R. Diener and J. Schmidt, "Sizing of throttling devices for gas liquid two-phase flow, Part 1: safety valves," *Process Saf Prog*, vol. 23, no. 4, pp. 335–344, 2004.

[41] S. Maksic and D. Mewes, "CFD-calculation of the flashing flow in pipes and nozzles," *ASME Jt. US-European Fluids Egineering Conf.*, no. 1, pp. 511–516, 2002.

[42] O. C. Jones and N. Zuber, "Bubble growth in variable pressure fields," *J. Heat Transf.*, vol. 100, pp. 453–459, 1978.

[43] T. S. Shin and O. C. Jones, "An active cavity model for flashing," *Nucl. Eng. Des.*, vol. 95, pp. 185–196, 1986.

[44] T. S. Shin and O. C. Jones, "Nucleation and flashing in nozzles – 1," *Int. J. Multiph. Flow*, vol. 19, pp. 943–964, 1993.

[45] V. N. Blinkov, O. C. Jones, and B. I. Nigmatulin, "Nucleation and flashing in nozzles-2. Comparison with experiments using a five-equation model for vapor void development," *Int. J. Multiph. Flow*, vol. 19, no. 6, pp. 965–986, 1993.

[46] C. A. Marsh and A. P. O'Mahony, "Three-dimensional modelling of industrial flashing flows," *Prog. Comput. Fluid Dyn. an Int. J.*, vol. 9, no. 6–7, pp. 393–398, 2009.

[47] S. Mimouni, M. Boucker, J. Laviéville, A. Guelfi, and D. Bestion, "Modelling and computation of cavitation and boiling bubbly flows with the NEPTUNE_CFD code," *Nucl. Eng. Des.*, vol. 238, no. 3, pp. 680–692, 2008.

[48] M. Robert, M. Farvacque, M. Parent, and B. Faydide, "CATHARE 2 V2.5: a fully validated CATHARE version for various application," in *Proceedings of the 10th International Topical Meeting on Nuclear Reactor Thermal-Hydraulics (NURETH 10), Seoul, Korea.*, 2003.

[49] A. Archer, “A predictive model for cavitation erosion downstream orifices,” in *Proceedings of ASME, Montreal*, 2002.

[50] J. P. Janet, Y. Liao, and D. Lucas, “Heterogeneous nucleation in CFD simulation of flashing flows in converging – diverging nozzles,” *Int. J. Multiph. Flow*, vol. 74, pp. 106–117, 2015.

[51] M. Lemmert and J. Chawla, “Influence of flow velocity on surface boiling heat transfer coefficient,” *Heat Transf. Boil*, vol. 237, p. 247, 1977.

[52] N. Kurul and M. Podowski, “On the modeling of multidimensional effects in boiling channels,” in *ANS Proceedings of the 27th National Heat Transfer Conference. Springer-Verlag, Minneapolis*, 1991, pp. 28–31.

[53] R. Cole, “Bubble frequencies and departure volumes at subatmospheric pressures,” *AIChE J.*, vol. 13, pp. 779–783, 1967.

[54] G. Kocamustafaogullari and M. Ishii, “Interfacial area and nucleation site density in boiling systems,” *Int. J. Heat Mass Transf.*, vol. 26, 1983.

[55] J. R. Riznic and M. Ishii, “Bubble number density and vapor generation in flashing flow,” *Int. J. Heat Mass Transf.*, vol. 32, no. 10, pp. 1821–1833, 1989.

[56] U. Rohatgi and E. Reshotko, “Non-equilibrium one-dimensional two-phase flow in variable area channels,” in *Non-Equilibrium Two-Phase Flows; Proceedings of the Winter Annual Meeting, Houston, Tex., November 30–December 5, 1975, Meeting Sponsored by the American Society of Mechanical Engineers, New York, vol. 1. American Society of Mechanical Engineers*, 1975, pp. 47–54.

[57] A. Pelletingeas, L. Dufresne, and P. Seers, “Characterization of Flow Structures in a Diesel Injector for Different Needle Lifts and a Fluctuating Injection Pressure,” *J. Fluids Eng.*, vol. 138, no. 8, p. 81105, 2016.

[58] T. Giese, E. Laurien, and Schwarz W., “Experimental and Numerical Investigation of Gravity-Driven Pipe Flow With Cavitation,” in *ASME. International Conference on Nuclear Engineering, 10th International Conference on Nuclear Engineering*, 2002, pp. 15–21.

[59] E. Laurien and Giese, T., “Exploration of the two-fluid model of two-phase flow towards boiling, cavitation and stratification,” in *Proc. 3rd ICCHMT, Banff, Canada, 26–30 May*, 2003.

[60] E. Laurien, “Influence of the model bubble diameter on three-dimensional numerical simulations of thermal cavitation in pipe elbows,” in *Proc. 3rd Inter-national Symposium on Two-Phase Modelling and Experimentation, Pisa, Italy, September 22–25.*, 2004.

[61] T. Frank, “Simulation of flashing and steam condensation in subcooled liquid using ANSYS CFX,” in *Proc. 5th FZD & ANSYS MPF Workshop, 25–27 April.*, 2007.

[62] Y. Liao, D. Lucas, E. Krepper, and R. Rzehak, “Flashing evaporation under different pressure levels,” *Nucl. Eng. Des.*, vol. 265, pp. 801–813, 2013.

[63] A. Schaffrath *et al.*, “TOPFLOW—A new multipurpose thermal hydraulic test facility for the investigation of steady state and transient two-phase flow phenomena,” *Kerntechnik*, vol. 66, pp. 209–212, 2001.

[64] M. Yazdani, A. a. Alahyari, and T. D. Radcliff, “Numerical Modeling and Validation of Supersonic Two-Phase Flow of CO 2 in Converging-Diverging Nozzles,” *J. Fluids Eng.*, vol. 136, no. 1, p. 14503, 2013.

[65] A. K. Singhal, M. M. Athavale, H. Li, and Y. Jiang, “Mathematical Basis and Validation of the Full Cavitation Model,” *ASME J. Fluids Eng.*, vol. 124, no. 3, pp. 617–624, 2002.

[66] C. E. Brennen, *Fundamentals of Multiphase Flow*. Cambridge University Press, New York., 2005.

[67] M. Nakagawa, M. S. Berana, and A. Kishine, “Supersonic Two-Phase Flow of CO2 Through Converging-Diverging Nozzles for the Ejector Refrigeration Cycles,” *Int. J. Refrig.*, vol. 32, no. 6, pp. 1195–1202, 2009.

[68] Y. Liao and D. Lucas, “3D CFD simulation of flashing flows in a converging-diverging nozzle,” *Nucl. Eng. Des.*, vol. 292, pp. 149–163, 2015.

[69] Y. Liao and D. Lucas, “Possibilities and Limitations of CFD Simulation for Flashing Flow Scenarios in

Nuclear Applications," *Energies*, vol. 10, no. 1, p. 139, 2017.

[70] H. K. Versteeg and W. Malalasekera, *An introduction to computational fluid dynamics -- The finite volume method*. Pearson Education Limited, 2007.

[71] User's guide of ANSYS FLUENT rel. 16, "User's guide of ANSYS FLUENT rel. 16," 2016.

[72] B. E. Launder and D. B. Spalding, *Lectures in Mathematical Models of Turbulence*. Academic Press, London, England, 1972.

[73] T.-H. Shih, W. W. Liou, A. Shabbir, Z. Yang, and J. Zhu, "A New k-ε Eddy-Viscosity Model for High Reynolds Number Turbulent Flows - Model Development and Validation," *Comput. Fluids*, vol. 24, no. 3, pp. 227–238, 1995.

[74] V. Yakhot, S. A. Orszag, S. Thangam, T. B. Gatski, and C. G. Speziale, "Development of Turbulence Models for Shear Flows by a Double Expansion Technique," *Phys. Fluids A*, vol. 4, no. 7, pp. 1510–1520, 1992.

[75] B. E. Launder, G. J. Reece, and W. Rodi, "Progress in the Development of a Reynolds-stress Turbulence Closure," *J. Fluid Mech.*, vol. 68, no. 3, pp. 537–566, 1975.

[76] D. C. Wilcox, *Turbulence Modelling for CFD*. DCW Industries Inc., La Canada, CA, 1993.

[77] D. C. Wilcox, "Reassessment of the Scale-determining Equation for Advanced, Turbulence Models," *AIAA J.*, vol. 26, no. 11, pp. 1299–1310, 1988.

[78] D. C. Wilcox, "Comparison of Two-equation Turbulence Models for Boundary Layers with Pressure Gradients," *AIAA J.*, vol. 31, no. 8, pp. 1414–1421, 1993.

[79] D. C. Wilcox, "Simulating Transition with a Two-equation Turbulence Model," *AIAA J.*, vol. 32, pp. 247–255, 1994.

[80] F. R. Menter, *Improved Two-equation k–ω Turbulence Models for Aerodynamic Flows*. 1992.

[81] F. R. Menter, M. Kuntz, and R. Langtry, "Ten Years of Industrial Experience with the SST Turbulence Model," in *Proceedings of the Fourth International Symposium on Turbulence, Heat and Mass Transfer, Begell House, Redding, CT.*, 2003.

[82] F. Menter, "Two-equation Eddy-viscosity Turbulence Model for Engineering Applications," *AIAA J.*, vol. 32, pp. 1598–1605, 1994.

[83] F. R. Menter, "Performance of Popular Turbulence Models for Attached and Separated Adverse Pressure Gradient Flow," *AIAA J.*, vol. 30, pp. 2066–2072, 1992.

[84] B. E. Launder and D. B. Spalding, "The Numerical Computation of Turbulent Flows," *Comput. Methods Appl. Mech. Eng.*, vol. 3, pp. 269–289, 1974.

[85] S.-E. Kim and D. Choudhury, "A Near-Wall Treatment Using Wall Functions Sensitized to Pressure Gradient," in *ASME FED Vol. 217, Separated and Complex Flows*, 1995.

[86] M. Manninen, V. Taivassalo, and S. Kallio, "VTT Publications," 1996.

[87] Z. Naumann and L. Schiller, "A drag coefficient correlation," *Z Ver Deutsch Ing*, vol. 77, pp. 318–323, 1935.

[88] H. Hertz, "On the Evaporation of Liquids, Especially Mercury, in Vacuo," *Ann. der Phys.*, vol. 17, p. 177, 1882.

[89] M. Knudsen, "Maximum Rate of Vaporization of Mercury," *Ann. der Phys.*, vol. 47, p. 697, 1915.

[90] C. Prakash, "Two phase model for binary liquid-solid phase change: Parts I and II," *Numer. Heat Transf.*, vol. 18, no. 2, pp. 131–167, 1990.

[91] A. K. Singhal, H. Y. Li, M. M. Athavale, and Y. Jiang, "Mathematical Basis and Validation of the Full Cavitation Model," in *ASME FEDSM'01, New Orleans, Louisiana*, 2001.

[92] P. J. Zwart, A. G. Gerber, and T. Belamri, "A Two-Phase Flow Model for Predicting Cavitation Dynamics," in *In Fifth International Conference on Multiphase Flow, Yokohama, Japan.*, 2004.

[93] G. H. Schnerr and J. Sauer, "Physical and Numerical Modeling of Unsteady Cavitation Dynamics," in *In Fourth International Conference on Multiphase Flow, New Orleans, USA.*, 2001.

[94] J. O. Hinze, *Turbulence, second ed*. McGraw Hill, New York., 1975.

[95] B. J. C. Wu, N. Abuaf, P. Saha, B. J. C. Wu, G. A. Zimmer, and P. Saha, *A Study of Nonequilibrium Flashing of Water in a Convergingdiverging nozzle: Volume 2. Modeling*, no. June 1981. U.S. Nuclear Regulatory Commission, Washington, DC, 1981.

[96] H. C. Simpson, D. H. Rooney, and E. Grattan, "Two phase flow through gate valves and orifice plates," in *Int Conf on the Physical Modelling of Multi-Phase Flow, Coventry, UK, April 19–20, 1983.*, 1983.

[97] Tyco, *Pressure relief valve engineering handbook*. Technical Publication No. TP-V300, Tyco Flow Control, 2008.

[98] M. Epstein, R. E. Henry, W. Midvidy, and R. Pauls, "One-dimensional modeling of twophase jet expansion and impingement," in *2nd International Topical Meeting Nuclear Reactor Thermal•Hydraulics, American Nuclear Society, Santa Barbara, 1983.*, 1983.